Josephson Junctions with Phase Shifts

Stability Analysis of Fractional Fluxons

Dit proefscrift werd mede mogelijk gemaakt met financiële steun van de
Koninklijke Nederlandse Akademie van Wetenschappen (KNAW).

Cover design: TAKM, DS, & H. Susanto
Druk: Wöhrmann Print Service, Zutphen

ISBN 90-365-2283-8

JOSEPHSON JUNCTIONS WITH PHASE SHIFTS
STABILITY ANALYSIS OF FRACTIONAL FLUXONS

PROEFSCHRIFT

ter verkrijging van
de graad van doctor aan de Universiteit Twente,
op gezag van de rector magnificus,
prof.dr. W. H. M. Zijm,
volgens besluit van het College voor Promoties
in het openbaar te verdedigen
op donderdag 19 januari 2006 om 15.00 uur

door

Hadi Susanto
geboren op 27 januari 1979
te Lumajang, Indonesië

Dit proefschrift is goedgekeurd door de promotor:
prof. dr. S. A. van Gils

Samenstelling van de Promotiecommissie

Voorzitter en Secretaris:

prof. dr. A. J. Mouthaan	Universiteit Twente, Nederland

Promotor:

prof. dr. S. A. van Gils	Universiteit Twente, Nederland

Leden:

prof. dr. A. Doelman	Centrum voor Wiskunde en Informatica, Nederland
prof. dr. J. W. M. Hilgenkamp	Universiteit Twente, Nederland
prof. dr. B. J. Geurts	Universiteit Twente, Nederland
prof. dr. N. F. Pedersen	Danmarks Tekniske Universitet, Denemarken
dr. A. A. Golubov	Universiteit Twente, Nederland
dr. E. Goldobin	Universität Tübingen, Duitsland

” Allah will exalt those who believe among you and those who have knowledge to high ranks.”

(QS Al-Mujaadalah 58:11)

for:

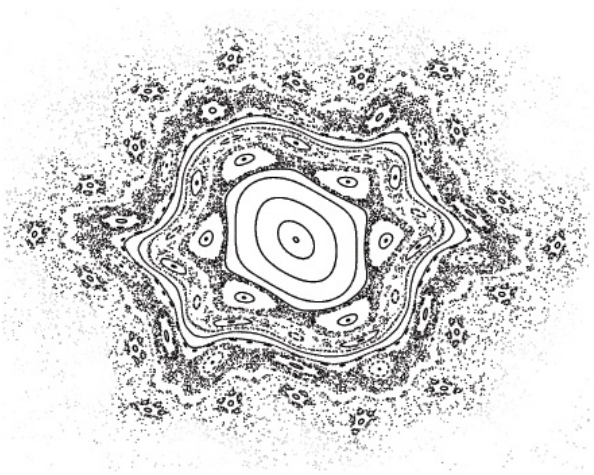

my beloved ones

Contents

1

Josephson junctions and sine-Gordon equations: an Introduction

Chapter 1

1.1 Josephson junctions with phase shift

Heike Kamerlingh-Onnes in 1911 discovered an unmeasurebly small value of electrical resistance of mercury when it was cooled below 4.2 K [1]. He called this phenomenon of no-resistance to an electrical current *superconductivity*. In the subsequent years many more materials were found to be superconducting when cooled down low a certain critical temperature T_c. For his discovery, Kamerlingh-Onnes was awarded the 1913 Nobel Prize in Physics.

A microscopic explanation of superconductivity was not found for nearly half a century. An important contribution to the understanding of this new state of matter was made by Herbert Fröhlich in 1950 [2] and Leon N. Cooper in 1956 [3]. Fröhlich realized that under the right conditions, electrons could experience an attractive interaction mediated by *phonons*. Phonons are quanta of crystal lattice vibrational energy which are analogous to the quanta of light or *photons*. The phonons excert forces that can overcome the electrons' Coulomb repulsion. Afterwards, Cooper showed that given those right conditions, the ground state of a material is unstable with respect to pairs of electrons. Therefore, electrons form so-called *Cooper pairs* that are coupled over a range of hundreds of nanometers, i.e. three orders of magnitude larger than the lattice spacing. The total momentum of this Cooper pair is constant, and the spins of the two electrons forming the Cooper pair are opposite to each other.

A theory of superconductivity was built by John Bardeen, Leon N. Cooper, and Robert J. Schrieffer [4] in 1957 which is named after them, i.e. BCS theory. The BCS theory shows that it is possible for a number of Cooper pairs to form a homogeneous condensate at the same energy level. Below the critical temperature, this condensation is able to move through the lattice relatively unaffected by thermal vibrations and hence experiences no resistance. Bardeen, Cooper, and Schrieffer were then awarded the 1972 Nobel Prize in Physics.

Another discovery was made in 1962 by Brian D. Josephson who predicted that Cooper pairs can tunnel through a nonsuperconducting barrier from one superconductor to another without any voltage across the barrier[5]. He also derived the exact form of the current and voltage relations for the junction. Experiments confirmed his analytical calculations, and Josephson was awarded the 1973 Nobel Prize in Physics for his work. Since then, the *Josephson effects* that describes the flow of a supercurrent through a tunnel barrier, have been a subject of considerable research studies.

In a *Josephson junction*, i.e. a system of superconductors separated by barrier(s), the nonsuperconducting barrier separating the two superconductors must be very thin. If

the barrier is an insulator, it has to be on the order of 30 Å thick or less. If the barrier is another metal (nonsuperconducting), it can be as much as several microns thick. Until a critical current is reached, a supercurrent can flow across the barrier without a voltage difference. This is known as the *DC Josephson effect*. When a constant voltage is applied across the junction, the supercurrent will oscillate in time which is known as the *AC Josephson effect*. The oscillation frequency of this AC voltage is nearly 500 GHz per mV across the junction.

Detecting and measuring the change from one state to the other is at the heart of the many applications for Josephson junctions.

The macroscopic explanation of this process starts with the *wavefunction*[1] that characterizes all Cooper pair that can be expressed as

$$\Psi = n_s^{1/2} \exp(i\theta), \tag{1.1.1}$$

where n_s is twice the density of Cooper pairs and θ is the internal phase of the electrons. If Ψ_1 and Ψ_2 are the wavefunctions of the first and second superconductors, linearly coupled Schrödinger equations give the two basic equations which describe the Josephson effects

$$I_s = I_m \sin\phi, \quad \frac{d\phi}{dt} = \frac{2\pi}{\Phi_0} V. \tag{1.1.2}$$

Here I_m, V, and ϕ are the maximum direct supercurrent through the junction, the electrical voltage across the junction, and the phase difference of the wavefunctions, respectively, and Φ_0, which equals 2.068×10^{-15} Wb, is the magnetic flux quantum. The first and second equation of (1.1.2) are referred to as the aforementioned DC and AC Josephson effect, respectively.

Apart from this discussion on Josephson junctions, an important break-through in the study of superconductivity has been made by Johannes G. Bednorz and Karl A. Müller who received the Nobel Prize in Physics in 1987. Ceramic materials which are expected to be insulators, were discovered in 1986 by Bednorz and Müeller to be superconductors only at a transition temperature of 35 K [6]. The material they studied was lanthanum-barium-copper-oxide $La_{2-x}Ba_xCuO_4$ ceramics. Before the mid 1980s, superconductivity had only been observed in metals and metallic alloys that had been cooled below 23 K. Soon after the discovery of Bednorz and Müller, the superconductive transition temperature was improved rapidly as is shown in Fig. 1.1. This −together with other anomalous properties of ceramic superconductors− has lead to the differentiation of superconductors in two classes: low- and high-critical temperature (T_c) superconductors.

In low-temperature superconductors the electrons pair together so that their total orbital angular momentum is zero −a so-called *s-wave state*. In high-temperature superconductors, on the other hand, the pairs are in a so-called *d-wave state*, a superposition of states in which the angular momentum is non-zero. This *d*-wave symmetry has been

1 Rather than saying that a particle has a specified position and momentum, one instead describes it by a wavefunction which is a function of all coordinates and of time. The quantity $|\Psi|^2$ has an important physical interpretation: it is related to the probability that electrons can be found in a particular region of space at a particular time instant.

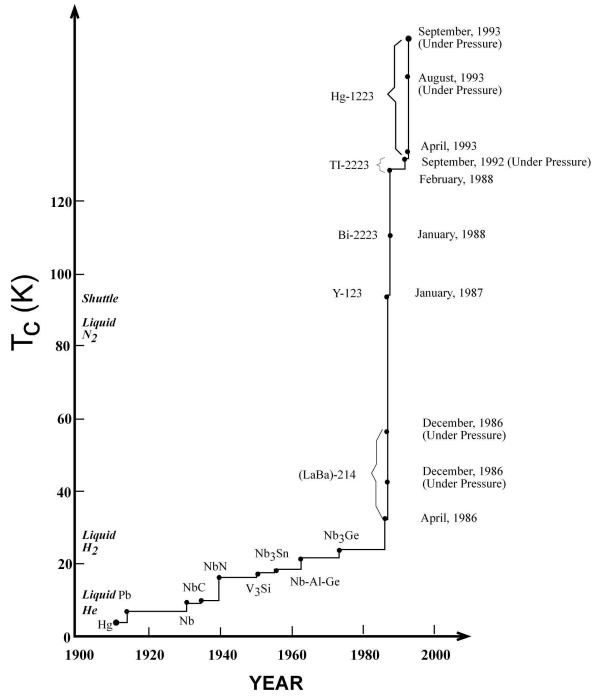

Figure 1.1: *Development of the superconducting transition temperature after the discovery of the phenomenon in 1911. This figure is taken from [7].*

verified only recently by elegant experiments. Theoretically, these superconductors have been recognized to have an unconventional symmetry of the *order parameter*[2].

With this unconventional symmetry of the order parameter, the superconducting phase θ of the wave function (1.1.1) is anisotropic and exhibits π-difference at the perpendicular direction in *the momentum space*.

To know about momentum space, we need to notice that electrons in a crystal display wavelike properties, and can be described using a wave vector $\mathbf{k}$ that has components k_x, k_y, and k_z. We can consider the overall distribution of electrons by representing each electron in $\mathbf{k}$- or momentum-space.

The crystal structure of the family of the high-T_c superconductors has unit cells with the same size along the x- and y-crystal direction but a different size along the z-axis. Along this z-crystal direction, the unit cell has a larger dimension. The superconductivity is then supposed to be localized in the $x - y$ plane, leading to the term *layered superconductor*.

One commonly and widely used material of a layered structure is yttrium-barium-

2 An order parameter is defined to quantify how much 'order' is present in a material (see [10]). In superconductivity, this order parameter is proportional to the wavefunction.

copper-oxide $YBa_2Cu_3O_7$ that is superconductive below 98 K. This material was found by the research group of Maw-Kuen Wu and of Paul C. W. Chu [8]. In Fig. 1.2, we present a sketch of the atomic structure of this material where the unit cell is larger in the vertical direction than in the horizontal ones.

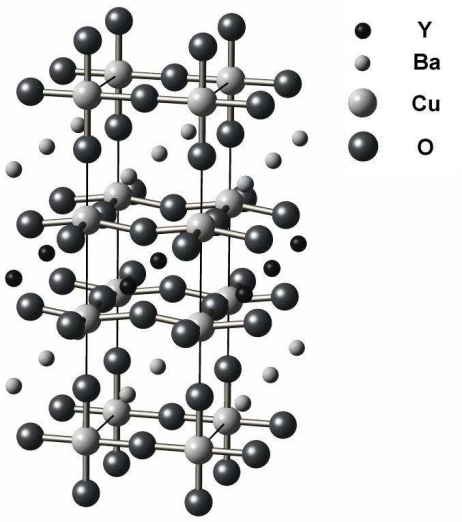

Figure 1.2: *Illustration of the crystal structure of yttrium-barium-copper-oxide ceramics materials. One can notice that the unit cell in the vertical and horizontal direction are not equal. This is why the supercurrent flow in the vertical direction feels resistance and the materials can then be considered to be superconducting layers separated by barriers.*

Using the above description of the momentum space and the layered structure of high-T_c superconductor, the *s*-wave and *d*-wave state in **k**-space is illustrated in the pictures in Fig. 1.3 (see [9]).

If one replaces one of the (*s*-wave) superconductors in Josephson junctions with a *d*-wave superconductor, then there can occur an intrinsic π-phase shift in the Josephson junction, as is depicted in Fig. 1.3(b). If the negative lobe of the order parameter of the *d*-wave superconductor in one side of the junction overlaps with the positive lobe of the order parameter of the *s*-wave superconductor in another side of the junction, then a *π-junction* is formed.

The connection of the two superconductors by such an arrangement does not, by itself, lead to any special phase difference, because the phases of the order parameters on both sides simply arrange themselves to minimize the Josephson energy, $\sim \cos(\phi + \pi)$, by setting the phase difference ϕ equal to π. It merely relates to a phase change in one of the two superconductors, e.g. $\phi_1 \to \phi_1 + \pi$. Hence, whether a junction is a π-junction or not is only a matter of convention. Therefore, to get a π-junction, the junction has to be made in certain way such that there is no way to minimize the energy in all parts of the junction. This condition can be achieved by several ways. One is by making

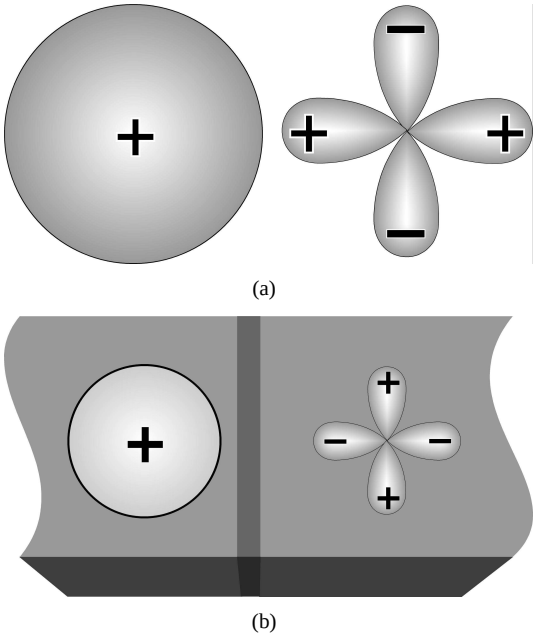

Figure 1.3: *(a) Illustration of the s-wave and d-wave order parameter in the momentum space. (b) Josephson junction between s-wave and d-wave. This corresponds to a π-junction because of the phase-shift of the phase difference by π. The negative lobe of the d-wave superconductor meets the positive one of the s-wave.*

multiply connected superconducting systems (see [11]). In Fig. 1.4, we sketch this configuration of three superconducting segments forming a loop with three junctions.

The arrangement is chosen so that all junctions are π-junctions by our definition. We can now think of the above process ($\phi_1 \to \phi_1 + \pi$) to one of the segments to convert its adjacent junctions into 0-junctions and leaving one π-junction only. There is no further transformation to remove the remaining π-junction without changing one of the two 0-junctions again into a π-junction. Hence there is no way to minimize the energy of all junctions. This means *frustation* for the loop.

Another way of making a π-junction is by constructing a junction such that the wave function of the conventional superconductor overlaps simultaneously with a part of the unconventional superconductor wave function with positive sign as well with a part with negative sign. The best-known junction for this configuration is the corner junction [9, 12, 13] (see Fig. 1.4(b)). In Fig. 1.5(a), we present an optical microscope picture of a zigzag junction which consists of several corner junctions.

Recently, several procedures for making a π-junction have been proposed and confirmed experimentally. One can fabricate junctions which are formed at the boundary between two crystalline films of cuprate superconductors with different orientations [14] or Josephson junctions with a ferromagnetic barrier [15, 16]. The most recent

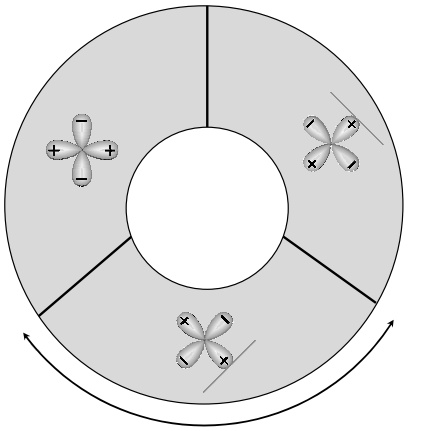

(a)

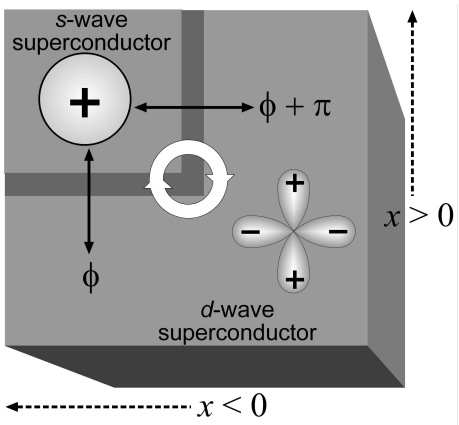

(b)

Figure 1.4: *(a) Superconducting loop with three junctions and (b) a corner junction between s-wave and d-wave superconductor.*

technology is by using a pair of current injectors which are placed close to each other [17] as shown in Fig. 1.5(b). With this latest procedure, one can introduce an arbitrary phase shift to Josephson junctions. For a successful operation, both Δx and Δw (see Fig. 1.5(b)) must be much smaller than the Josephson penetration depth λ_J.

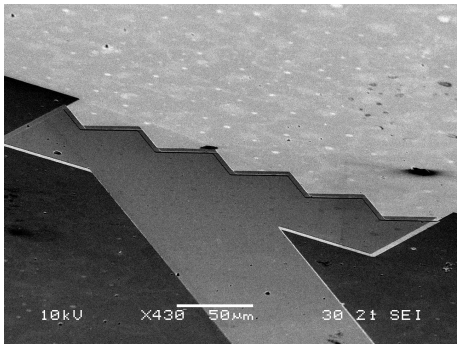

(a)

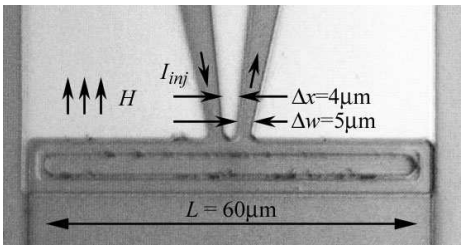

(b)

Figure 1.5: *(a) An optical microscope image of a zigzag junction which consists of several corner junctions. The junction is made by a high-T_c superconductor $YBa_2Cu_3O_{7-\delta}$ and low-T_c superconductor Nb, separated by Au. Courtesy of Ariando. (b) An optical image of an ordinary long Nb-AlO_x-Nb junction with two injectors. This junction can produce a fractional flux quantum. The figure is taken with permission from [17].*

1.2 Sine-Gordon equations

The phase difference between two superconductors forming a Josephson junction satisfies the following sine-Gordon equation (see, e.g. [18]):

$$\phi_{xx} - \phi_{tt} = \sin(\phi + \theta) \tag{1.2.1}$$

for an ideal long Josephson junction or

$$\frac{\phi^{n+1} - 2\phi^n + \phi^{n-1}}{a^2} - \phi^n_{tt} = \sin(\phi^n + \theta^n) \tag{1.2.2}$$

for an array of short Josephson junctions where a is the coupling constant between two consecutive lattices and n numbers the sites. The parameter $\theta(x)$ or θ^n represents the phase shift, which is constant for the continuous and the discrete sine-Gordon equation.

The sine-Gordon equation, Eq. (1.2.1) with $\theta \equiv 0$, was originally considered by Enneper [19] in the differential geometry of surfaces of a constant negative Gaussian curvature.

To name a few applications as physical models, besides the aforementioned description of superconductivity and long Josephson junctions, the sine-Gordon equation also appears in the study of simplified dislocation models where kinks and breathers were first noticed by Seeger and co-workers [20]. Independently, Perring and Skyrme [21] used this equation as a simple one-dimensional model of the scalar field theory modeling a classical particle. One of the simplest macroscopic models describing the dynamics of the discrete sine-Gordon equation, i.e. Eq. (1.2.2) with $\theta^n \equiv 0$, is a system consisting of a chain of pendula with each pendulum being connected to its neighbors by elastic springs [22, 23]. For a rather complete review, the reader is referred to [24, 25].

One of the elementary solutions of the completely integrable sine-Gordon equation which plays a major role in the study of Josephson junctions is the *topological soliton* solution

$$\phi(x,t) = 4\tan^{-1}\exp[\sigma(x-vt)/\sqrt{1-v^2}], \quad \sigma = \pm 1. \tag{1.2.3}$$

Here, we define a *topological charge* as a conserved quantity that is equal to the difference between the phase at $x = +\infty$ and $x = -\infty$. The topological charge of solution (1.2.3) is then $2\pi\sigma$. The solution (1.2.3) is called a *kink* and *antikink* in case $\sigma = +1$ and $\sigma = -1$, respectively. In Josephson junction systems, this (anti)kink represents a vortex of supercurrent that creates a magnetic field with the flux that is equal to the magnetic quantum $\pm\Phi_0 = 2.068 \times 10^{-15}$ Wb. Therefore a sine-Gordon (anti)kink is also called an *(anti)fluxon*. Several expectations on Josephson junctions to be industrially applicable and usable in the future are due to this solitonic solution.

The interesting aspect of a Josephson junction with phase shifts [$\theta \neq 0$ in Eqs. (1.2.1) and (1.2.2)] is the spontaneous appearance of fractional flux quanta. This strengthens the possibility for quantum information processing applications using fractional vortices. This type of ground state by all means has different characteristics from the elementary solutions of Eq. (1.2.1) with $\theta \equiv 0 \pmod{2\pi}$. Nonetheless, only a few theoretical studies have been devoted to an investigation of such a ground state as will be listed below.

Bulaevskii, Kuzii, and Sobyanin [26] were the first who analyzed the Josephson system with magnetic impurities and predicted the possibility for a π-phase shift as well as the presence of spontaneous magnetic flux. After that work, up to the end of the year 2000, there are only few works considering specifically fractional flux quanta from a theoretical and mathematical point of view. To our best knowledge, those articles are [27, 28, 29, 30, 31, 32, 33] for discussions on long 0-π Josephson junctions and [34] for tricrystal grain boundaries. For list of reports on experimental results, the reader is referred to [14] and references therein. Equations (1.2.1) and (1.2.2) then opens a new field with open problems.

1.3 Outline of the thesis

Motivated by the above description, this thesis is made as a contribution toward the understanding of characteristics of fractional fluxons. It is presented as a collection of scientific articles in such a way that the chapters can be read separately.

In Chapter 2, we show and discuss the existence of fractional fluxons in a Josephson system with phase shifts. We exploit phase plane analysis to show existence of the semifluxon states. This method is applicable to the present study because (stable) fractional fluxons in the steady state are independent of time. Using this very basic procedure, we already can answer some important questions addressed by previous authors, such as the presence of a critical bias current above which there is no static semifluxons [29] and the presence of a minimum distance between two consecutive phase shifts needed to have fractional fluxons [31]. Using the phase portrait analysis, it is also shown that there exists some unusual solutions representing different type of fractional fluxons. These types of fractional vortices are predicted to be unstable.

In Chapter 3, we study a 0-π array of short Josephson junctions. We study the case of Josephson systems with one phase shift. A possible implementation of the problem in experiments using the present technology is also mentioned. The main issue of this chapter is the existence and stability of lattice π-kinks. Stability of the solutions obtained in the previous chapter, which are the strong coupling limit of lattice π-kinks, is also discussed.

In Chapter 4, we consider the so-called tricrystal junctions. An infinite long 0-π Josephson junction can be considered as a combination of two semi-infinite 0- and π- junctions. A tricrystal junction is then a combination of three semi-infinite long Josephson junctions having one common point. This type of junctions has promising applications, e.g., as logic device based on the Josephson effect for high-performance computers. In a tricrystal junction system, a fluxon coming toward the common point can be trapped. We also discuss whether the common point can trap more than one fluxon. If one of the junctions is a π-junction, it is shown that a semifluxon is stable for any combination of the Josephson characteristics and it is analyzed whether the system supports a multi-semifluxon state. The minimum number of Josephson junctions forming a star-like multicrystal junction that supports a multiple-semifluxons state is also discussed.

In Chapter 5, we consider a Josephson junction system with phase shifts of κ, with κ is not necessarily π as is the case in the foregoing chapters. This system is not as trivial as it might look, especially because a fractional kink can have a different topological charge from the corresponding fractional antikink. In this chapter we consider a long Josephson junction with one single phase shift and one with periodical phase shifts. For one phase shift, the stability of fractional kinks supported by the system is analyzed. For a periodic structure, the band gap spectrum of fractional kinks is studied.

Bibliography

[1] H. Kamerlingh-Onnes, in *Nobel Lectures, Physics 1901-1921*, (Elsevier Publishing Company, Amsterdam, 1967); available at http://nobelprize.org/physics/laureates/1913/onnes-lecture.pdf

[2] H. Fröhlich, *Theory of the superconducting state. I. The ground state at the absolute zero of temperature*, Phys. Rev. **79**, 845 (1950).

[3] L. N. Cooper, *Bound electron pairs in a degenerate Fermi gas*, Phys. Rev. **104**, 1189 (1956).

[4] J. Baardeen, L. N. Cooper, and J. R. Schrieffer, *Theory of superconductivity*, Phys. Rev. **108**, 1175 (1957).

[5] B. D. Josephson, *Possible new effects in superconductive tunnelling*, Phys. Letts. **1**, 251 (1962).

[6] K. A. Müller and J. G. Bednorz, *Possible high-T_c superconductivity in the Ba-La-Cu system*, Z. Phys. B **64**, 189 (1986).

[7] C.W. Chu, *High-temperature superconducting materials: a decade of impressive advancement of T_c*, IEEE Trans. Appl. Superconductivity **7**, 80 (1997).

[8] M. K. Wu, J. R. Ashburn, C. J. Torng, P. H. Hor, R. L. Meng, L. Gao, Z. J. Huang, Y. Q. Wang, and C. W. Chu, *Superconductivity at 93 K in a new mixed-phase Yb-Ba-Cu-O compound system at ambient pressure*, Phys. Rev. Lett. **58**, 908 (1987).

[9] D. J. Van Harlingen, *Phase-sensitive tests of the symmetry of the pairing state in the high-temperature superconductorsEvidence for $d_{x^2-y^2}$ symmetry*, Rev. Mod. Phys. **67**, 515 (1995).

[10] J. P. Sethna, *1991 Lectures in Complex Systems*, Eds. L. Nagel and D. Stein, Santa Fe Institute Studies in the Sciences of Complexity, Proc. Vol. XV, Addison-Wesley, 1992; available at http://www.lassp.cornell.edu/sethna/OrderParameters/OrderParameter.html

[11] M. Sigrist and T. M. Rice, *Unusual paramagnetic phenomena in granular high-temperature superconductors – A consequence of d-wave pairing?*, Rev. Mod. Phys. **67**, 503 (1995).

[12] H. J. H. Smilde, Ariando, D. H. A. Blank, G. J. Gerritsma, H. Hilgenkamp, and H. Rogalla, *d-Wave-Induced Josephson current counterflow in $YBa_2Cu_3O_7$/Nb zigzag junctions*, Phys. Rev. Lett. **88**, 057004 (2002).

[13] H. Hilgenkamp, Ariando, H. J. H. Smilde, D. H. A. Blank, G. Rijnders, H. Rogalla, J. R. Kirtley, and C. C. Tsuei, *Ordering and manipulation of the magnetic moments in large-scale superconducting π-loop arrays*, Nature **422**, 50 (2003).

[14] C. C. Tsuei and J. R. Kirtley, *Pairing symmetry in cuprate superconductors*, Rev. Mod. Phys. **72**, 969 (2000).

[15] V. V. Ryazanov, V. A. Oboznov, A. Yu. Rusanov, A. V. Veretennikov, A. A. Golubov, and J. Aarts , *Coupling of two superconductors through a ferromagnet: Evidence for a π junction*, Phys. Rev. Lett. **86**, 2427 (2001).

[16] T. Kontos, M. Aprili, J. Lesueur, F. Genêt, B. Stephanidis, and R. Boursier, *Josephson junction through a thin ferromagnetic layer: Negative coupling*, Phys. Rev. Lett. **89**, 137007 (2002).

[17] E. Goldobin, A. Sterck, T. Gaber, D. Koelle, and R. Kleiner, *Dynamics of semi-fluxons in Nb long Josephson 0-π junctions*, Phys. Rev. Lett. **92**, 057005 (2004).

[18] R. P. Feynman, *The Feynman lectures on physics*, Vol. III: Quantum mechanics, (Addison-Wesley, Reading, MA 1965).

[19] A. Enneper, *Ueber asymptotische Linien*, Nachr. Köngl. Gesellsch. d. Wiss. Göttingen, 493 (1870).

[20] A. Kochendörfer and A. Seeger, *Theorie der Versetzungen in eindimensionalen Atomreihen. I. Periodisch angeordnete Versetzungen*, Z. Physik **127**, 533 (1950); A. Seeger and A. Kochendörfer, *Theorie der Versetzungen in eindimensionalen Atomreihen. II. Beliebig Angeordneue und Beschleunigte Versetzungen*, Z. Physik **130**, 321 (1951); A. Seeger, H. Donth, and A. Kochendörfer, *Theorie der Versetzungen in eindimensionalen Atomreihen. III. Versetzungen, Eigenbewegungen und Ihre Wechselwirkung*, Z. Physik **134**, 173 (1953).

[21] J. K. Perring and T. H. R. Skyrme, *A model unified field equation*, Nucl. Phys. **31**, 550 (1962).

[22] A. C. Scott, *A nonlinear Klein-Gordon equation*, Amer. J. Phys. **37**, 52 (1969).

[23] K. Nakajima, T. Yamashita, and Y. Onodera, *Mechanical analogue of active Josephson transmission line*, J. Appl. Phys. **45**, 3141 (1974),

[24] Yu. S. Kivshar and B. A. Malomed, *Dynamics of solitons in nearly integrable systems*, Rev. Mod. Phys. **61**, 763 (1989); *ibid.* **63**, 211 (1991).

[25] O. M. Braun and Yu. S. Kivshar, *The Frenkel-Kontorova Model*, (Springer-Verlag, Berlin, 2004).

[26] L. N. Bulaevskii, V. V. Kuzii, and A. A. Sobyanin, *Superconducting system with weak coupling to the current in the ground state*, JETP Lett. **25**, 290 (1977).

[27] L. N. Bulaevskii, V. V. Kuzii, A. A. Sobyanin, and P. N. Lebedev, *On possibility of the spontaneous magnetic flux in a Josephson junction containing magnetic impurities*, Solid State Commun. **25**, 1053 (1978).

[28] J.H. Xu, J.H. Miller, Jr., and C.S. Ting, *π-vortex state in a long 0-π Josephson junction*, Phys. Rev. B **51**, 11 958 (1995).

[29] A.B. Kuklov, V.S. Boyko, and J. Malinsky, *Instability in the current-biased 0-π Josephson junction*, Phys. Rev. B **51**, 11 965 (1995); *ibid*. **55**, 11878(E) (1997).

[30] M.B. Walker, *Mechanism for magnetic-flux generation in grain boundaries of* $YBa_2Cu_3O_{7-x}$, Phys. Rev. B **54**, 13 269 (1996).

[31] T. Kato and M. Imada, *Vortices and quantum tunneling in current-biased 0-π-0 Josephson junctions of d-wave superconductors*, J. Phys. Soc. Jpn. **66**, 1445 (1997).

[32] R. G. Mints, *Self-generated flux in Josephson junctions with alternating critical current density*, Phys. Rev. B **57**, 3221 (1998).

[33] R. G. Mints and I. Papiashvili, *Self-generated magnetic flux in* $YBa_2Cu_3O_{7-x}$ *grain boundaries*, Phys. Rev. B **62**, 15214 (2000).

[34] V. G. Kogan, J. R. Clem, and J. R. Kirtley, *Josephson vortices at tricrystal boundaries*, Phys. Rev. B **61**, 9122 (2000).

Static semifluxons of a Josephson junction with π-discontinuity points

Chapter 2

We investigate analytically a long Josephson junction with several π-discontinuity points characterized by a jump of π in the phase difference of the junction. The system is described by a perturbed-combined sine-Gordon equation. Via phase-portrait analysis, it is shown how the existence of static semifluxons localized around the discontinuity points is influenced by the applied bias current. In junctions with more than one corner, there is a minimum facet-length for semifluxons to be spontaneously generated. A stability analysis is used to obtain the minimum facet-length for multi-corner junctions.

2.1 Introduction

Superconductors are characterized by the phase coherence of the Cooper pair condensate. Recent technological advances in the control of the phase near a Josephson junction have promoted research on the manipulation and phase biasing of such junctions. Examples are the experimental realization of Superconductor-Ferromagnet-Superconductor (SFS) π-junctions [1], and Superconductor-Normal metal-Superconductor (SNS) junctions in which the charge-carrier population in the conduction channels is controlled [2]. These junctions are characterized by an intrinsic phase-shift of π in the current-phase relation or, in other words, an effective negative critical current.

An alternative branch of phase biasing is offered by the intrinsic anisotropy of unconventional superconductivity. A predominant $d_{x^2-y^2}$ pairing symmetry in high-T_c superconductors [3] enables the possibility to bias parts of the circuit with a phase of π. Examples are the π-SQUID [4, 5], tricrystal rings [3], the corner junction [6], and the zigzag junction [7]. The latter two inspired the analytic investigation in the present work. These structures, of which neighboring facets in a Josephson junction can be considered to have opposite sign of the critical current, present intriguing phenomena such as the intrinsic frustration of the Josephson phase over the junction and the spontaneous generation of fractional magnetic flux near the corners. The fractional fluxes are attached to the discontinuity points and are formed in antiferromagnetic ordering. This ordering has indeed been found experimentally as the ground state of $YBa_2Cu_3O_7$-Nb zigzag junctions [8, 9] as shown in Fig. 2.1.

The presence of a fractional flux, or semifluxon, has been considered before by several authors [8, 10, 11, 12, 13, 14, 15]. In this work we present an analytic investigation of the existence and behavior of these semifluxons in an infinitely long Josephson junction with π-discontinuities. We will introduce the model for these junctions and the method we use to analyze the semifluxons in a Josephson junction with π-discontinuities in Section 2.2. In Section 2.3 the results for one π-discontinuity, the

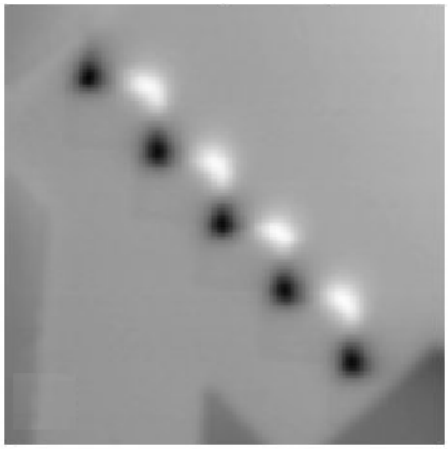

Figure 2.1: *A scanning SQUID microscope image of fractional magnetic flux in a system of $YBa_2Cu_3O_7$-Au-Nb zigzag junctions. The picture is taken from [9] with permission of the authors.*

corner junction, is presented. Section 2.4 discusses the case for two π-discontinuities, in which we compute the minimum facet length between the discontinuity points necessary to be able to spontaneously generate flux. In Section 2.5, it is shown how the model is extrapolated to an increasing number of discontinuities in the infinitely long Josephson junction. We use a stability analysis to discuss the existence of the semifluxons for this case. We conclude the work in Section 2.6.

2.2 Mathematical model and phase-plane analysis

To describe the dynamics of a long Josephson junction with π-discontinuity points a perturbed sine-Gordon equation is used [10]:

$$\phi_{xx} - \phi_{tt} = \sin[\phi + \theta(x)] - \gamma + \alpha\phi_t, \tag{2.2.1}$$

where α is a dimensionless positive damping coefficient related to quasi-particle tunneling across the junction and γ is the applied bias current density, normalized to the junction critical current density J_c. The function $\theta(x)$ takes the value 0 or π, representing the alternating sign of the critical current associated with the presence, or absence, of the additional π-phase shift.

Equation (2.2.1) is written after rescaling where the spatial variable x and time variable t are normalized by the Josephson penetration length λ_J and the inverse plasma frequency ω_p^{-1} respectively.

We consider static semifluxons, hence (2.2.1) reduces to

$$\phi_{xx} = -\frac{\partial U}{\partial \phi}, \tag{2.2.2}$$

where $U = -(1 - \cos[\phi + \theta(x)]) + \gamma\phi$. For physically meaningful solutions, ϕ and ϕ_x are required to be continuous at the discontinuity point.

The first integral of Eq. (2.2.2) is

$$\frac{1}{2}\phi_x^2 = -\cos[\phi + \theta(x)] - \gamma\phi + C, \tag{2.2.3}$$

where C is the constant of integration. If θ would not depend on x, then the integral curves ('orbits') of (2.2.3) form the *phase portrait* in the (ϕ, ϕ_x) phase plane.

Phase-plane analysis is particularly useful for the qualitative analysis of planar differential equations, see for instance [16, 17] for an example involving a perturbed sine-Gordon equation. For a general introduction to phase-plane analysis see for instance [18].

In the present situation however, θ does depend on x, but in a special manner: θ takes only two values. Therefore there are two phase portraits that come into play, one with $\theta = 0$ and another one with $\theta = \pi$. Solutions of (2.2.2) are suitable combinations of orbits on these two phase planes. The position where the switch is made between the two phase planes is determined by the values of x where θ jumps. With this convention in mind we will for simplicity speak about *the* phase portrait of (2.2.2). A similar approach is used by Walker [15] to analyze a particular solution of Eq. (2.2.2) representing semifluxons in the case of $\gamma = 0$. In his paper, Walker analyzes this situation using a combination of the potential functions U, i.e. $U = -(1 - \cos\phi)$ and $U = (1 - \cos\phi)$.

2.3 Junctions with a single π-discontinuity point

In a junction with a single π-discontinuity point, under certain conditions, a semifluxon is expected to be generated [3]. With $\theta(x)$ given by

$$\theta(x) = \begin{cases} 0, & x < 0, \\ \pi, & x > 0, \end{cases} \tag{2.3.1}$$

the parameterization of this semifluxon for $\gamma = 0$ is [10, 12]:

$$\phi(x) = \begin{cases} 4\arctan\exp(x - x_0), & x < 0, \\ 4\arctan\exp(x + x_0) - \pi, & x > 0, \end{cases} \tag{2.3.2}$$

where $x_0 = \ln(\sqrt{2} + 1)$. In the phase plane, the solution (2.3.2) is given by the combination of the curves with arrows in Fig. 2.2. For $x < 0$ we follow the solid curve starting at the origin up to d_1, where $x = 0$. From d_1 we switch flows and follow the dashed curve for $x > 0$ up to $(\phi/\pi, \phi_x) = (1, 0)$. This defines a semifluxon with a π-phase jump: $\phi(\infty) - \phi(-\infty) = \pi$. The intersection of the trajectories for $x < 0$ and for $x > 0$ makes an angle, i.e. *is transversal*, which guarantees the persistence of

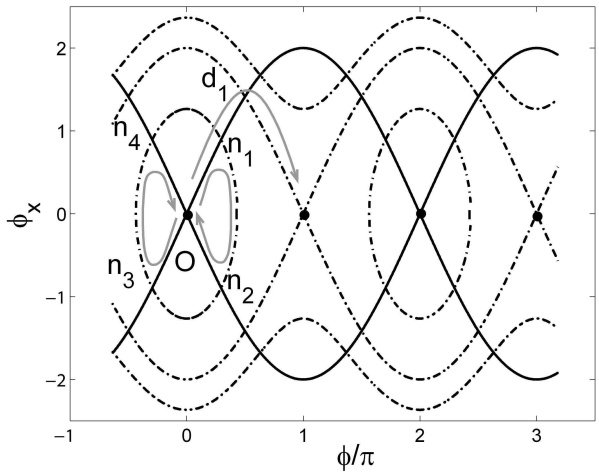

Figure 2.2: *The phase portrait of the system (2.2.2) for $\gamma = 0$. The trajectories for $x < 0$ are indicated with bold lines, the trajectories for $x > 0$ with dashed lines. Any orbit of Eq. (2.2.2) switches at $x = 0$ from bold to dashed. The semifluxon parameterized by (2.3.2) in the phase plane is indicated with arrows with d_1 is the corresponding position of $x = 0$. O is the position of $(0, 0)$. The definition of d_1, $n_1 - n_4$ are in the text.*

the semifluxon when a bias current is applied. Later on it will be shown that this will remain the case up to $\gamma = 2/\pi$.

In the phase plane, equilibria are the points that correspond to the maxima and minima of the potential U, i.e. $(\partial U/\partial\phi = 0, \phi_x = 0)$. When $\gamma = 0$ two adjacent equilibria are connected by heteroclinic connections. Once we set $\gamma \neq 0$, the heteroclinic connections break and form homoclinic connections, i.e. connections between an equilibrium with itself. This opens the possibility for other solutions satisfying Eq. (2.2.2) and boundary condition $\phi(\infty) - \phi(-\infty) = \pi$ than the semifluxon solution described above. As shown in Fig. 2.3, a semifluxon can be constructed by choosing d_2 or d_3 as the point where $x = 0$. With these two discontinuity points, we obtain solutions with an overall phase jump of π, but containing humps as shown in Fig. 2.4. For $\gamma = 0$ these constructions are not possible since the trajectories would pass through an equilibrium.

The semifluxons with humps can be viewed as combinations of semifluxons and 2π-fluxons. The semifluxon with d_2 as the position of $x = 0$ consists of a semifluxon and a fluxon-antifluxon pair, while the semifluxon with d_3 for the corresponding position of $x = 0$ consists of a semifluxon and a fluxon with opposite polarity. Because a fluxon and a semifluxon with opposite (like) polarity are attracting (repelling) each other, we can expect these semifluxons to be unstable. A further study of these semifluxons with humps will be presented elsewhere [1].

When increasing the normalized bias current γ, the homoclinic connections of the

1 see Chapter 3 of this thesis.

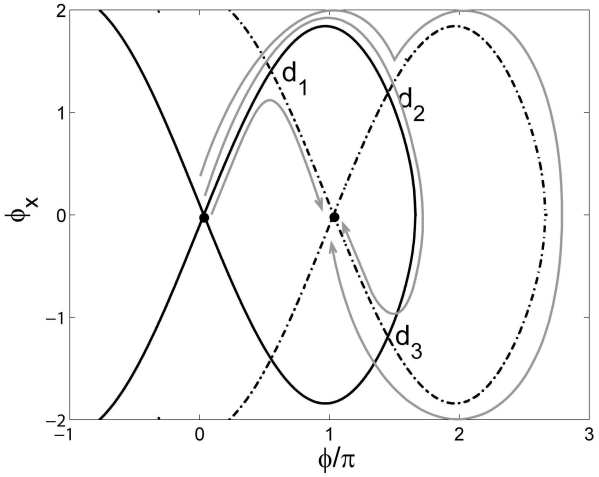

Figure 2.3: *The phase portrait of the system (2.2.2) for $\gamma = 0.1$. For simplicity we only show the stable and unstable manifolds of the fixed points. Instead of d_1, we might also take d_2 or d_3 for the position of $x = 0$.*

two equations will shrink and move apart. Therefore, for a certain value of γ, which we will denote as γ^*, d_2 and d_3 will coincide (see Fig. 2.5). When this happens, the solution with $x = 0$ at d_2 corresponds to a semifluxon and a fluxon-antifluxon pair at infinity. For $\gamma > \gamma^*$, there is no solution with $x = 0$ at d_2 that satisfies Eq. (2.2.2). Hence, only d_1 and d_3 can be used for the position of $x = 0$, in that case.

To deduce the exact expression of γ^*, we consider the boundary conditions for the phase difference and magnetic flux at infinity

$$\lim_{x\to-\infty} \phi(x) = \phi_- = \arcsin(\gamma),$$
$$\lim_{x\to\infty} \phi(x) = \phi_+ = \pi + \arcsin(\gamma),$$
$$\lim_{x\to\pm\infty} \phi_x(x) = 0.$$

From the boundary conditions, the integral constant C of Eq. (2.2.3) is:

$$C = \begin{cases} \cos\phi_- + \gamma\phi_-, & x < 0 \\ -\cos\phi_+ + \gamma\phi_+, & x > 0. \end{cases} \tag{2.3.3}$$

Imposing that $\phi_x(0^-) = \phi_x(0^+)$ and $\phi(0) = \pi + \arcsin\gamma$, we obtain the value of γ which gives the above condition

$$\gamma^* = \frac{2}{\sqrt{4+\pi^2}} \approx 0.54. \tag{2.3.4}$$

When $\gamma > \gamma^*$, the point d_3 moves towards d_1. At a certain value, the points d_1 and d_3 coincide. At that value of γ, the intersection of the trajectories of the system for

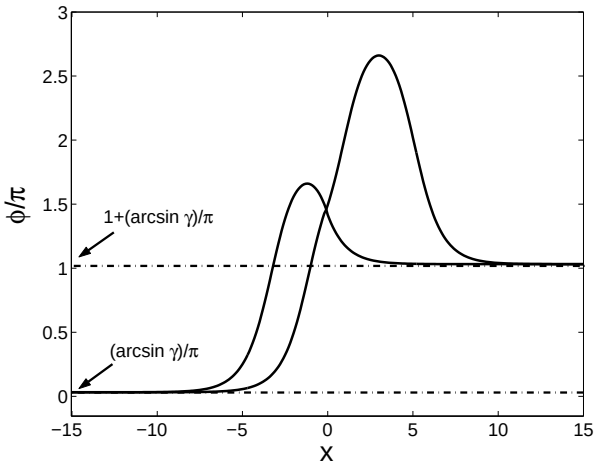

Figure 2.4: *Plot of the phase as a function of x (in units of λ_J) with d_2 and d_3 as discontinuity points. In this picture $\gamma = 0.1$. The solution with higher hump is the phase with d_2 as the discontinuity point. Dash-dot lines are the asymptotes of the solutions.*

$x < 0$ and $x > 0$ is tangential. The heteroclinic flow of the combined phase portrait is 'smooth' (see Fig. 2.6). We then arrive at the edge of the static solution because as the trajectories intersect nontransversally, perturbations make them either nonintersecting or transversally intersecting [19]. We will call the value of γ such that the intersection is nontransversal the *critical current* γ_c. Physically, if we apply a bias current larger than this critical current, there will be no static semifluxon anymore.

A tangential intersection is achieved when at point $d_1 = d_3$,

$$\lim_{x\uparrow 0} \partial\phi_x/\partial\phi = \lim_{x\downarrow 0} \partial\phi_x/\partial\phi.$$

Noticing that $\partial\phi_x/\partial\phi$ is given by

$$\frac{d\phi_x(x)}{dx}\frac{dx}{d\phi(x)}\bigg|_{x=0} = \frac{\phi_{xx}}{\phi_x}\bigg|_{x=0} = \frac{\pm\sin\phi - \gamma}{\phi_x}\bigg|_{x=0},$$

this condition is satisfied when $\sin\phi(0) = 0$, i.e. $\phi(0) \in \{0, \pi\}$.

To obtain the value of ϕ_x at $x = 0$, we use that

$$\int_{-\infty}^{0} \phi_{xx}\phi_x\, dx = \int_{-\infty}^{0} \phi_x \sin\phi - \gamma\phi_x\, dx, \tag{2.3.5}$$

which gives

$$\frac{1}{2}\phi_x(0^-)^2 = -\cos\phi(0^-) + \sqrt{1-\gamma^2} - \gamma(\phi(0^-) - \arcsin\gamma).$$

Here $\phi(0^-)$ is a shorthand for $\lim_{x\uparrow 0}\phi(x)$ and likewise for $\phi_x(0^-)$. Limits from the right are indicated by a '+'.

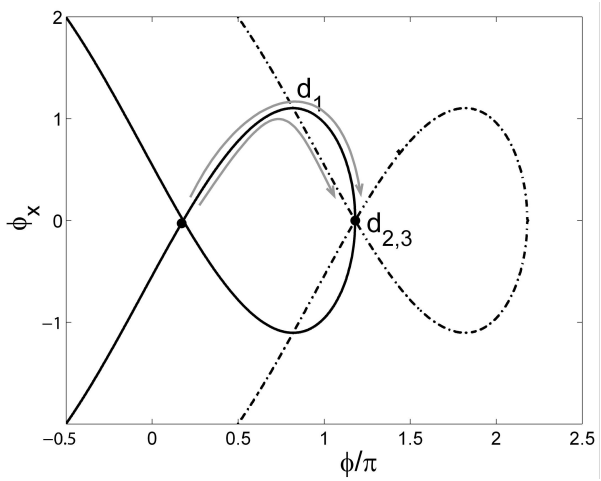

Figure 2.5: *Part of the phase portrait of (2.2.2) for $\gamma = \gamma^*$. At this value of γ d_2 and d_3 coincide.*

The same calculation for $x > 0$ gives

$$-\frac{1}{2}\phi_x(0^+)^2 = -\cos\phi(0^+) - \sqrt{1-\gamma^2} - \gamma(-\phi(0^+) + \pi + \arcsin\gamma).$$

Because $\phi(0^-) = \phi(0^+) = \phi(0)$ and $\phi_x(0^-) = \phi_x(0^+)$, the two above expressions yield the critical current for the existence of static semifluxons:

$$\gamma_c = \frac{2}{\pi} \approx 0.64. \tag{2.3.6}$$

No static solutions exist for γ above γ_c. This result is in agreement with the result of Kuklov, Boyko, and Malinsky [20] that for $\gamma > \gamma_c$ the ϕ-fluxon changes the circulation back and forth while releasing 2π-fluxons. Using phase-plane analysis, we derive the maximum supercurrent from the existence of the static solution while Kuklov et al. derive it from the stability of the solution.

2.4 Junctions with two π-discontinuity points

The analytical discussion on junctions with two π-discontinuity points has been initiated by Kato and Imada [14]. The junctions have a positive critical current for $|x| > a$ and a negative critical current for $|x| < a$. In this system there are two semifluxons with opposite polarity generated at the corners of the junction when a is relatively large. They conjecture that the magnetic flux is sensitive to the ratio $a = d/2\lambda_J$ where d is the distance of the two corners. We call the normalized distance of one corner to the next neighboring corner the normalized facet length, which is $2a$ in our

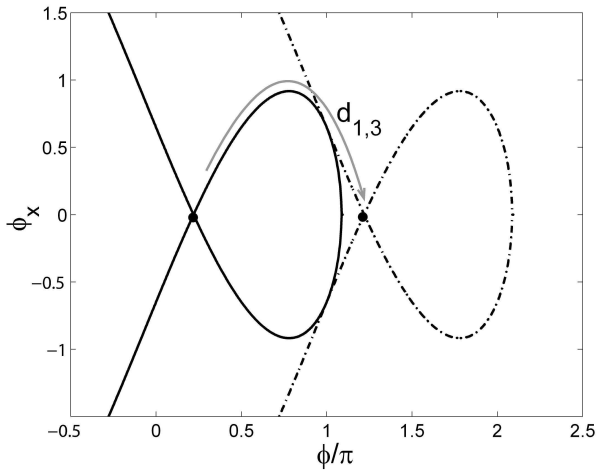

Figure 2.6: *The phase portrait of the system corresponding to the π kink solution for γ the critical current.*

case. Here, we consider the case when the semifluxons generated at the corners have opposite polarity.

Kato and Imada show numerically that the integrated magnetic flux, which is proportional to $\Delta\phi = |\phi(0) - \phi(\infty)|$, depends on a (see Fig. 2.7). When $a \gg 1$, they obtain $\Delta\phi = \pi$. The magnetic flux decreases when the facet length reduces. In the absence of a bias current, for $a \leq a^{(2)}_{min} = \pi/4$, $\Delta\phi = 0$. Here $2a^{(2)}_{min}$ is the minimum facet-length necessary to have a spontaneous flux generation when $\gamma = 0$ (the superscript indicates the number of corners). The minimum facet-length for $\gamma \neq 0$ will be shown to be zero later on. In this section, we will show that the dependence of $\Delta\phi$ on a can be expressed explicitly when looking for the existence of the static semifluxons.

The phase portrait of the system without an applied bias current is given in Fig. 2.2. The semifluxon-antisemifluxon and the antisemifluxon-semifluxon states are represented by the trajectory $O - n_1 - n_2 - O$ and $O - n_3 - n_4 - O$, respectively. As $2a$ is the length of the middle junction, it is the pathlength of $n_1 \rightarrow n_2$ or $n_3 \rightarrow n_4$. If x would be replaced by t, as in the usual pendulum equation, it would be the time needed to go from $n_{1,3}$ to $n_{2,4}$.

Let M_p be the closed trajectory through points n_1 and n_2. This flow represents the periodic motion of the pendulum equation. M_p crosses the ϕ-axes at the points $(\pm\Delta\phi, 0)$. Putting $\gamma = 0$, from Eq. (2.2.3) M_p is implicitly given by the relation

$$\frac{1}{2}\phi_x^2 = \cos\phi - \cos\Delta\phi. \tag{2.4.1}$$

If $n_1 = (\phi^{it}, \phi_x^{it})$, then $\phi^{it} = \arccos(\cos\Delta\phi + \frac{1}{2}{\phi_x^{it}}^2)$.

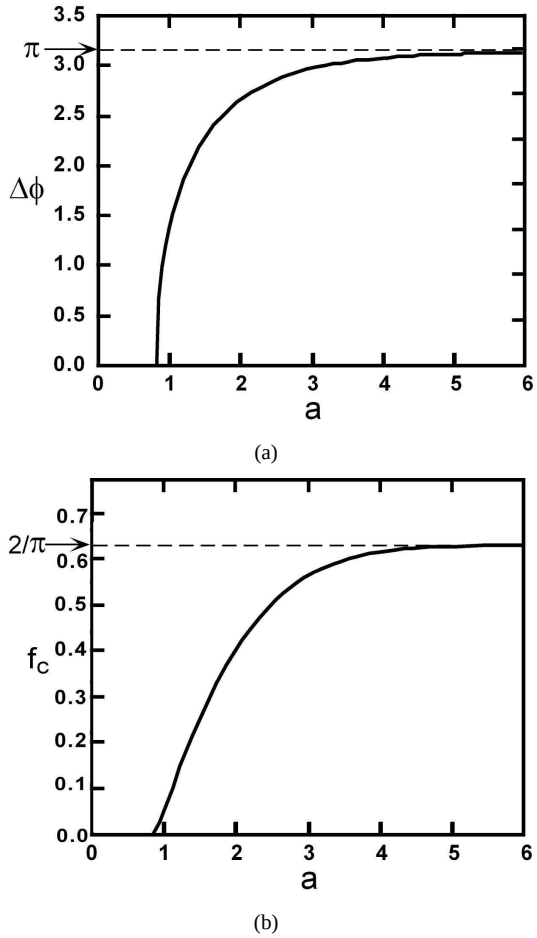

Figure 2.7: *$\Delta\phi$ is drawn as a function of a. The critical current f_c for vortices to change their orientation is also presented. The figure is reproduced with permission from [14].*

The unstable and stable manifolds through n_1 and n_2 are given by

$$\frac{1}{2}\phi_x{}^2 = 1 - \cos\phi. \tag{2.4.2}$$

Hence, ϕ^{it} can be written as

$$\phi^{it} = \arccos\left[(\cos\Delta\phi + 1)/2\right]. \tag{2.4.3}$$

Now, it is straightforward to calculate the pathlength from n_1 to $(\Delta\phi, 0)$ which is ex-

actly a. Using (2.4.1), we get

$$\begin{aligned} a &= \int_{\phi^{it}}^{\Delta\phi} \frac{d\vartheta}{\sqrt{2}(\cos\vartheta - \cos\Delta\phi)^{1/2}} \\ &= \int_{0}^{\Delta\phi} \frac{d\vartheta}{\sqrt{2}(\cos\vartheta - \cos\Delta\phi)^{1/2}} - \int_{0}^{\phi^{it}} \frac{d\vartheta}{\sqrt{2}(\cos\vartheta - \cos\Delta\phi)^{1/2}}. \end{aligned} \tag{2.4.4}$$

Now consider

$$I = \int_{0}^{\phi^{it}} \frac{d\vartheta}{\sqrt{2}(\cos\vartheta - \cos\Delta\phi)^{1/2}}.$$

Using identity $\cos\vartheta = 1 - 2\sin^2(\vartheta/2)$, the integral becomes

$$I = \frac{1}{2}\int_{0}^{\phi^{it}} \frac{d\vartheta}{\sin(\Delta\phi/2)\sqrt{1 - \csc^2(\Delta\phi/2)\sin^2(\vartheta/2)}}.$$

If we let $\sin(\vartheta/2) = \sin(\Delta\phi/2)\sin\Phi$ such that the angle ϑ is transformed to $\Phi = \arcsin(\sin(\vartheta/2)/\sin(\Delta\phi/2))$, the integral then becomes

$$I = \int_{0}^{\Phi^{it}} \frac{d\Phi}{(1 - k^2\sin^2\Phi)^{1/2}} = F(\Phi_{it}, k)$$

with $k = \sin\frac{\Delta\phi}{2}$ and $\Phi^{it} = \arcsin(\sin\frac{\phi^{it}}{2}/\sin\frac{\Delta\phi}{2})$. The function F is the incomplete elliptic integral of the first kind [21]. Hence, we get that

$$a = F(\pi/2, k) - F(\Phi^{it}, k). \tag{2.4.5}$$

This is the explicit relation between $\Delta\phi$ and a when $\gamma = 0$. The plot is shown in Fig. 2.7. With this expression, we can see that

$$\lim_{\Delta\phi\to 0} a = \pi/4$$

because $k \to 0$ and $\Phi^{it} \to \pi/4$. This value is the minimum pathlength from $n_{1,3}$ to $n_{2,4}$ at the limiting point O, which is then the minimum facet-length to have a semifluxon-antisemifluxon or an antisemifluxon-semifluxon at the corners.

An approximation to Eq. (2.4.5) for the facet length a close to the minimum facet length $\pi/4$ has been calculated by Kato and Imada [14] using Hamiltonian energy approximation.

Kato and Imada assume that when $a = \pi/4 + \epsilon$ with $0 < \epsilon \ll 1$, the antisemifluxon-semifluxon state is approximately given by $\phi = C_0\varphi_0$ with

$$\varphi_0(x) = \begin{cases} \sqrt{\dfrac{4}{\pi+4}}\cos x & (|x| < a), \\ \sqrt{\dfrac{4}{\pi+4}}\cos a\, e^{-(|x|-a)} & (|x| > a). \end{cases} \tag{2.4.6}$$

The multiplication constant $\sqrt{4/(\pi+4)}$ is obtained from the normalization condition such that the norm of φ_0 is one. Note that this expression is exact when $\epsilon = 0$. One can also notice that $\Delta\phi = \sqrt{4/(\pi+4)}C_0$.

To determine C_0, they derive an effective Hamiltonian for C_0 by substituting $\phi(x) = C_0\varphi_0(x)$ and (2.4.6) to the Hamiltonian energy

$$H = \int_{-\infty}^{\infty}\left(\frac{1}{2}\phi_x^2 + \cos[\theta(x)](1-\cos\phi) + f\phi\right)\mathrm{d}x. \tag{2.4.7}$$

By assuming that C_0 is small, a simple calculation gives

$$H = -\frac{\lambda_0^2}{2}C_0^2 + \frac{\pi+2}{8(\pi+4)^2}C_0^4 - \sqrt{\frac{32}{\pi+4}}\gamma C_0 \tag{2.4.8}$$

to the fourth order of C_0. Here, $\lambda_0^2 = 4\epsilon/(\pi+4)$.

Finally, by minimizing (2.4.8) as for C_0 and taking $\gamma = 0$ one obtains [14, 22]

$$\Delta\phi = \sqrt{\frac{64}{\pi+2}}(a-\pi/4)^{1/2}.$$

When we start applying a bias current to the junction, a vortex and an antivortex are created at the corners even though the facet length is less than the minimum facet-length for $\gamma = 0$. In other words, the minimum facet-length of the junction is 0 when $\gamma \neq 0$. In the phase portrait, this can be seen from the fact that the equilibria of the system for $x < 0$ do not coincide with the ones for $x > 0$ when $\gamma \neq 0$, see Fig. 2.8. In the presence of the applied bias current, the magnetic flux $\Delta\phi$ is also influenced by γ. There are two different cases of the behavior of the semifluxons under the influence of a bias current. In the following, we will discuss the two cases separately.

2.4.1 Antisemifluxon-semifluxon case

When we start with a pair of antisemifluxon-semifluxon which we will here call a ϕ_2-solution, there is a critical value of the applied bias current to reorient the solution such that it becomes a semifluxon-antisemifluxon, here called a ϕ_1-solution. The flipping-over from the ϕ_2-solution to the ϕ_1-solution has been discussed analytically in [14, 22]. For simplicity f_c is used to denote the critical bias current as in [14]. In Fig. 2.7, f_c is drawn as a function of a. It is natural to expect that one would be able to explain the flipping-over process using phase-plane analysis. A sketch of the phase portrait of the system for $\gamma \neq 0$ is drawn in Fig. 2.8.

When $\gamma \neq 0$, the origin O splits into O_- (an equilibrium of the system for $x < |a|$) and O_+ (an equilibrium of the system for $x > |a|$). The minimum facet-length to have a ϕ_2-solution for $\gamma \neq 0$ now is given by the pathlength of n_3-n_4. These points lie on the unstable and stable manifolds of the system for $x > |a|$. The flipping process happens

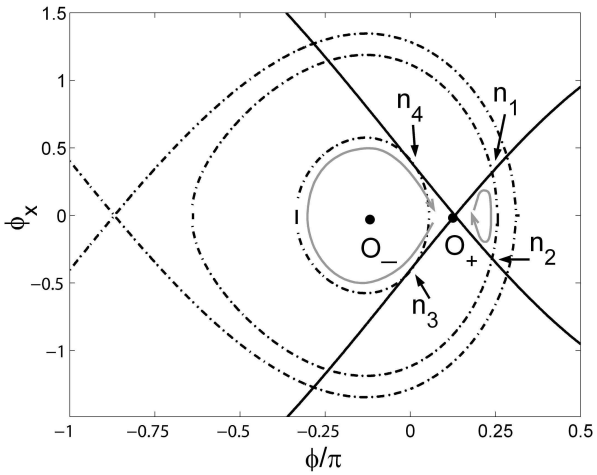

Figure 2.8: *The phase portrait of Eq. (2.2.2) when* $\gamma = 0.4$.

because the minimum facet-length to obtain a ϕ_2-solution for a positive bias current increases when γ increases.

Therefore, given the facet length, increasing γ we arrive at a level of the bias current where the ϕ_2-solution ceases to exist, and the solution will switch to solution of type ϕ_1. In Fig. 2.8, the ϕ_1-solution corresponds to the curve O_+-n_1-n_2-O_+. Hence, $f_c(a)$ also shows the minimum facet-length to have an antisemifluxon-semifluxon state for given positive γ.

One might guess already that the boundary of the existence of this solution is when the circle containing n_3 and n_4 makes nontangential intersection with the separatrices (see Fig. 2.8). But, this is not the case since the arc-length distance from n_3 to n_4 is not a monotonous function of $\Delta\phi$ for a nonzero γ. The arc-length from n_3 to n_4 in the condition illustrated by Fig. 2.8 is not the minimum. Numerical result of the critical current f_c as a function of the facet length a is shown Fig. 2.9. Using Hamiltonian energy approximation, Kato and Imada [14] has calculated an approximation to the curve as

$$f_c = \frac{128}{27(\pi+2)}(a-\pi/4)^{3/2}.$$

This value of f_c is evaluated as the critical value where one of the minima of (2.4.8) disappears.

2.4.2 Semifluxon-antisemifluxon case

When we start with a semifluxon-antisemifluxon state, with a positive current as long as the bias current is less than $2/\pi$, the static semifluxons are attached at the

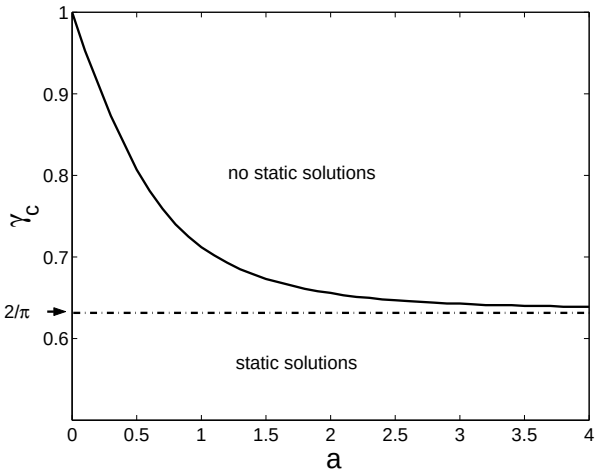

Figure 2.9: *Plot of the critical current γ_c as a function of half facet length a.*

corners for any facet length. If $\gamma > 2/\pi$ there is a limiting value of a, say $a_m(\gamma)$, such that for $a > a_m$ there is no static semivortex-antisemivortex state. a_m depends monotonically on γ which means that we can determine the critical current γ_c for given a. With a certain value of a and $\gamma > \gamma_c$, there is no static vortex-antivortex state. The plot of the relation between a and γ_c is presented in Fig. 2.9.

When the static solutions disappears, the solution becomes time dependent and starts flipping between the two types of semifluxons (the vortex-antivortex and the antivortex-vortex) while releasing 2π-fluxons.

The difference between γ_c and f_c is that the applied bias current of γ_c is the minimum value of the current to pull the two semifluxons apart while f_c is the minimum current to collide the two semifluxons. This can be seen from the Lorentz force induced by the applied bias current. In the limit $a \to \infty$, both γ_c and f_c converge to $2/\pi$.

2.5 Junctions with multiple π-discontinuity points

In [23], Goldobin et al. consider multi-corner junctions. One of the problems they consider is to determine the minimum length such that semifluxon states do exist for $\gamma = 0$. They have shown numerically that the minimum length varies as a function of the number of discontinuity points. In this section, we discuss the question of determining the minimum facet-length $a_{min}^{(N)}$ for semifluxons in a junction with N π-discontinuity points analytically. Recall that $a_{min}^{(N)}$ denotes the minimum facet-length in absence of a bias current. All the facet lengths are assumed to be equal.

One should be able to use existence analysis to determine the minimum facet-length for multi-corner junctions as we did for the case of two-corner ones, but it seems rather difficult. Therefore we use a stability analysis of the constant solution $\phi \equiv 0$. This

constant solution is the trivial state. The idea is mentioned in brief by Kuklov et al. [20] and Kato and Imada [14].

Based on numerical simulations, we assume that once the trivial state is unstable indicated by a zero eigenvalue that moves into the right half-plane, it creates spontaneous semifluxons in an antiferromagnetic order. The damping is assumed to be absent, i.e. $\alpha = 0$, as it does not influence the value of the minimum facet-length.

With the above assumptions the idea of getting the minimum facet-length is by looking at an eigenvalue at zero. The starting equation is

$$\phi_{xx} - \phi_{tt} = \sin[\phi + \theta(x)], \tag{2.5.1}$$

which is Eq. (2.2.1) with $\gamma = \alpha = 0$. Here γ is taken to be zero because we calculate the minimum facet-length in absence of a bias current.

Equation (2.5.1) admits $\phi^0 = k\pi$, $k \in \mathbb{Z}$ as the trivial solutions. We then linearize about ϕ^0 writing $\phi = \phi^0 + v(x,t)$, and retaining the terms linear in v:

$$v_{xx} - v_{tt} = \cos[\theta(x)]v\cos k\pi. \tag{2.5.2}$$

We now make the spectral ansatz $v(x,t) = e^{\lambda t}u(x)$ which gives for u the equation

$$u_{xx} - \lambda^2 u = \cos[\theta(x)]u\cos k\pi. \tag{2.5.3}$$

The real part of λ determines the stability of the trivial solution.

The boundary of the essential spectrum is given by those eigenvalues λ for which there exists a solution to Eq. (2.5.3) of the form $u(x) = e^{i\zeta x}$, with ζ real. It follows that $\lambda = \pm\sqrt{\mp 1 - \zeta^2}$.

Note that from $\lambda = \pm\sqrt{1-\zeta^2}$, there is positive spectrum when $|\zeta| > 1$. This explains that $k\pi$ is an unstable constant solution of the system if $\cos[\theta(\pm\infty)] = \pm 1$.

With the result above, we conclude that there is no stable constant solution if $\cos[\theta(\infty)] \not\equiv \cos[\theta(-\infty)]$. It means there is no minimum facet-length of a long Josephson junction with an odd number of corners. For any facet length, we will always obtain semifluxons as the ground state that are attached at the corners with a total phase jump $|\phi(\infty) - \phi(-\infty)| = \pi$.

Josephson junctions with an even number of π-discontinuity points could have a stable trivial solution. According to our assumption, we need to compute the discrete spectrum. The stability of the trivial solution will depend on the facet length.

If we look at Eq. (2.5.3) (without loosing generality we can take $k = 0$), this equation belongs to the classical scattering problem [24]. This problem has been well discussed in quantum mechanics [25] where $\cos[\theta(x)]$ is the potential function. A discrete eigenvalue is a value of λ^2 for which the corresponding eigenfunction decays exponentially as $x \to \pm\infty$ [24].

As an example, the case of four corner junctions is considered. Notice that the facet length is $2a$. The solution of Eq. (2.5.3) with the above requirement can easily be

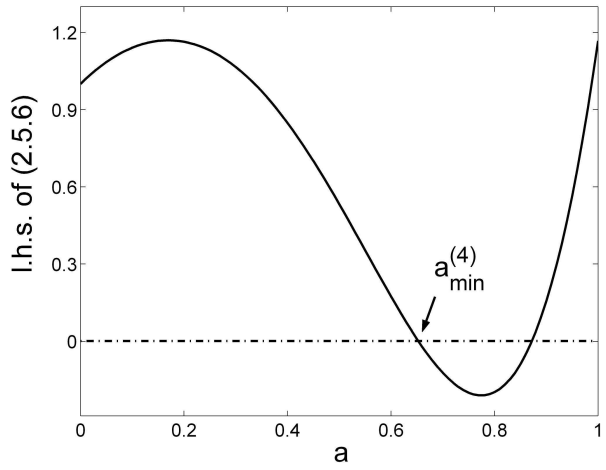

Figure 2.10: *Plot of the left hand side (l.h.s.) of Eq. (2.5.6) as a function of a. The minimum facet-length $a^{(4)}_{min}$ is the first intersection of the curve with a-axis.*

constructed by considering that we have five regions based on $\theta(x)$, i.e.

$$u = \begin{cases} A_{1,2}\exp(\sqrt{1+\lambda^2}|x|), \ |x| > 3a, \\ B_{1,2}\cos(\sqrt{1-\lambda^2}(|x|-2a)) + C_{1,2}\sin(\sqrt{1-\lambda^2}(|x|-2a)), \ 3a > x > a, \\ D_1\cosh(\sqrt{1+\lambda^2}x) + D_2\sinh(\sqrt{1+\lambda^2}x), \ |x| < a. \end{cases} \tag{2.5.4}$$

Next, we have to determine all the coefficients using the continuity conditions: $u(c^-) = u(c^+)$ and $u_x(c^-) = u_x(c^+)$, $c = \pm a, \ \pm 3a$. In the matrix form, the eight linear homogeneous equations are written as

$$\Lambda\begin{pmatrix} A_1 & B_1 & C_1 & D_1 & D_2 & B_2 & C_2 & A_2 \end{pmatrix}^T = 0, \tag{2.5.5}$$

with Λ is the coefficient matrix. To calculate the minimum facet-length, we take $\lambda = 0$.

The above system has nontrivial solutions only if the determinant of the coefficient matrix vanishes. This leads to the equation

$$\begin{aligned} &\cosh^2(a)(16(\cos^4(a) - \cos^2(a)) + 2) + \\ &2\cosh(a)\sinh(a) + 8(-\cos^4(a) + \cos^2(a)) - 1 = 0. \end{aligned} \tag{2.5.6}$$

As shown in Fig. 2.10 numerically, this equation has several solutions. The minimum facet-length to obtain an antiferromagnetically ordered semifluxons is the smallest nonnegative root of Eq. (2.5.6). Then we conclude that $a^{(4)}_{min} \approx 0.65$ (normalized to λ_J). The next roots correspond to the minimum facet lengths of other solutions that bifurcate from zero solution to exist. But at those minimum facet lengths, the configurations of the semi- and antisemifluxons other than the antiferromagnetic one

are unstable. This is because the largest eigenvalue of the zero solution is already positive.

For a six corner junction, we find in this way that $a_{min}^{(6)} \approx 0.56$.

These are in accordance with the results of [23] that are obtained using direct numerical simulations.

So far we have calculated some minimum facet-lengths $a_{min}^{(N)}$ which show a dependence on the number of the π-discontinuity points N. The minimum facet-length itself approaches zero as the following arguments show.

In this limiting case, we consider the scattering problem with a periodic potential. Mathematically, we are looking for solution of the equation

$$\begin{aligned} &u_{xx} - \lambda^2 u = \cos[\theta(x)]u, \\ &\theta(x) = \theta(x + 4a). \end{aligned} \tag{2.5.7}$$

Let us assume that $\theta(x) = \pi$ for $0 < x < 2a$, and $\theta(x) = 0$ for $2a < x < 4a$.

According to Bloch-Floquet theorem, the general solution of Eq. (2.5.7) is of the form [25]

$$\begin{aligned} &u = e^{iKx}\varphi(x), \\ &\varphi(x) = \varphi(x + 4a), \end{aligned} \tag{2.5.8}$$

with K satisfying $K4a = 2n\pi$, $(n = 0, \ \pm 1, \ \pm 2, \ldots)$.

Substituting Eq. (2.5.8) to Eq. (2.5.7), we are left with an ordinary differential equation in φ. The solution is described by

$$\varphi = \begin{cases} Ae^{i(\kappa_+ - K)x} + Be^{-i(\kappa_+ + K)x}, & 0 < x < 2a, \\ Ce^{i(\kappa_- - K)x} + De^{-i(\kappa_- + K)x}, & 2a < x < 4a, \end{cases} \tag{2.5.9}$$

where $\kappa_\pm = \sqrt{\lambda^2 \pm 1}$. The coefficients A, B, C and D are obtained from continuity and periodicity conditions. With the same argument as before we get the condition

$$\cos a \cosh a = \cos K4a$$

which gives $a_{min}^{(\infty)} = 0$.

The calculation of $a_{min}^{(\infty)}$ also tells us that arrays of 0-π junctions forming a loop or annular junctions containing an even number of π-discontinuity points have zero minimum facet-length.

Zenchuk and Goldobin [26] also consider the same problem as well as the effect of boundary conditions on $a_{min}^{(N)}$ if one uses finitely long zigzag Josephson junction. Using the same method and a tricky formal expansion, one of the results they obtained is that $a_{min}^{(N)} \sim 1/\sqrt{N}$ for N even and $N \to \infty$.

2.6 Conclusions

We have discussed the existence of static semifluxons using phase plane analysis in one- and two-corner junctions. We have obtained the critical value of the applied bias current γ above which static semifluxons are not present. By phase-plane analysis we have also shown how to construct solutions with humps. We have not discussed the stability of these solutions[2].

For two-corner junctions, the exact relation between the magnetic flux of semifluxons and the facet length has been derived. There is a minimum facet-length for a semivortex-antisemivortex state at $\gamma = 0$.

For multi-corner junctions, the minimum facet-length of the antiferromagnetically ordered semifluxon state $a_{min}^{(N)}$ is determined by a stability analysis of the trivial state. For a junction with infinitely many discontinuity points, we have shown that $a_{min}^{(\infty)} \to 0$. A similar argumentation shows that an annular junction with discontinuity points also have zero minimum facet-length.

2 see Chapter 3 of this thesis.

Bibliography

[1] V.V. Ryazanov, V.A. Oboznov, A.Yu. Rusanov, A.V. Veretennikov, A.A. Golubov, and J. Aarts, *Coupling of two superconductors through a ferromagnet: Evidence for a π junction*, Phys. Rev Lett. **86**, 2427 (2001).

[2] J.J.A. Baselmans, A.F. Morpurgo, B.J. van Wees, and T.M. Klapwijk, *Reversing the direction of the supercurrent in a controllable Josephson junction*, Nature (London) **397**, 43 (1999).

[3] C.C. Tsuei and J.R. Kirtley, *Pairing symmetry in cuprate superconductors* Rev. Mod. Phys. **72**, 969 (2000).

[4] D.A. Wollman, D.J. Van Harlingen, W.C. Lee, D.M. Ginsberg, and A.J. Leggett, *Experimental determination of the superconducting pairing state in YBCO from the phase coherence of YBCO-Pb dc SQUIDs*, Phys. Rev. Lett. **71**, 2134 (1993).

[5] R.R. Schulz, B. Chesca, B. Goetz, C.W. Schneider, A. Schmehl, H. Bielefeldt, H. Hilgenkamp, and J. Mannhart, *Design and realization of an all d-wave dc π-superconducting quantum interference device* App. Phys. Lett. **76**, 912 (2000).

[6] D.A. Wollman, D.J. Van Harlingen, J. Giapintzakis, and D.M. Ginsberg, *Evidence for $d_{x^2-y^2}$ pairing from the magnetic field modulation of $YBa_2Cu_3O_7$-Pb Josephson junctions*, Phys. Rev. Lett. **74**, 797 (1995).

[7] H.J.H. Smilde, Ariando, D.H.A. Blank, G.J. Gerritsma, H. Hilgenkamp, H. Rogalla, *d-Wave-Induced Josephson current counterflow in $YBa_2Cu_3O_7$/Nb zigzag junctions*, Phys. Rev. Lett. **88**, 057004 (2002).

[8] H. Hilgenkamp, Ariando, H.J.H. Smilde, D.H.A. Blank, G. Rijnders, H. Rogalla, J.R. Kirtley and C.C. Tsuei, *Ordering and manipulation of the magnetic moments in large-scale superconducting π-loop arrays*, Nature (London) **422**, 50 (2003).

[9] J.R. Kirtley, C.C. Tsuei, Ariando, H.J.H. Smilde, and H. Hilgenkamp, *Antiferromagnetic ordering in arrays of superconducting π-rings*, Phys. Rev. B **72**, 214521 (2005).

[10] E. Goldobin, D. Koelle, and R. Kleiner, *Semifluxons in long Josephson 0-π-junctions* Phys. Rev. B **66**, 100508 (2002).

[11] L.N. Bulaevskii, V.V. Kuzii, and A. A. Sobyanin, *Superconducting system with weak coupling to the current in the ground state*, JETP Lett. **25**, 290 (1977).

[12] J.H. Xu, J.H. Miller, Jr., and C.S. Ting, *π-vortex state in a long 0-π Josephson junction*, Phys. Rev. B **51**, 11958 (1995).

[13] J.R. Kirtley, K.A. Moler, and D.J. Scalapino, *Spontaneous flux and magnetic-interference patterns in 0-π Josephson junctions*, Phys. Rev. B **56**, 886 (1997).

[14] T. Kato and M. Imada, *Vortices and quantum tunneling in current-biased 0-π-0 Josephson junctions of d-wave superconductors*, J. Phys. Soc. Jpn. **66**, 1445 (1997).

[15] M.B. Walker, *Mechanism for magnetic-flux generation in grain boundaries of* $YBa_2Cu_3O_{7-x}$, Phys. Rev. B **54**, 13269 (1996).

[16] V.N. Belykh, N.F. Pedersen, and O.H. Sorensen, *Shunted-Josephson-junction model. I. The autonomous case*, Phys. Rev. B **16**, 4853 (1977); *Shunted-Josephson-junction model. II. The nonautonomous case*, *ibid.* 4860 (1977).

[17] S. Pagano, B. Ruggiero, and E. Sarnelli, *Magnetic-field dependence of the critical current in long Josephson junctions*, Phys. Rev. B **43**, 5364 (1991); S. Pagano, B. Ruggiero, M. Russo, and E. Sarnelli, in *Nonlinear Superconductive Electronics and Josephson Devices*, edited by G. Costabile, S. Pagano, N. F. Pedersen, and M. Russo (Plenum Press, New York, 1991), pp. 369-380.

[18] D.K. Arrowsmith and C.M. Place, *Dynamical Systems: differential equations, maps and chaotic behavior*, Chapman & Hall, 1992.

[19] J. Guckenheimer and P. Holmes, *Nonlinear Oscillations, Dynamical Systems and Bifurcations of Vector Fields*, 2nd ed., Springer-Verlag NY, 1986.

[20] A.B. Kuklov, V.S. Boyko, and J. Malinsky, *Instability in the current-biased 0-π Josephson junction*, Phys. Rev. B **51**, 11965 (1995); **55**, 11878(E) (1997).

[21] P.F. Byrd and M.D. Friedman, *Handbook of Elliptic Integrals*, 2nd ed. revised, Berlin: Springer, 1971.

[22] E. Goldobin, K. Vogel, O. Crasser, R. Walser, W. P. Schleich, D. Koelle, and R. Kleiner, *Quantum tunneling of semifluxons in a 0-π-0 Josephson junction*, Phys. Rev. B **72**, 054527 (2005).

[23] E. Goldobin, D. Koelle, and R. Kleiner, *Ground states and bias-current-induced rearrangement of semifluxons in 0-π long Josephson junctions*, Phys. Rev. B **67**, 224515 (2003).

[24] P.G. Drazin and R.S. Johnson, *Solitons: an Introduction*, Cambridge: Cambridge University Press, 1989.

[25] The number of references on potential wells/barriers is enormous, e.g. K.T. Hecht, *Quantum Mechanics*, New York: Springer-Verlag, 2000; R.L. Liboff, *Introductory Quantum Mechanics*, 3rd ed., Reading: Addison-Wesley, 1997.

[26] A. Zenchuk and E. Goldobin, *Analysis of ground states of 0-π long Josephson junctions*, Phys. Rev. B **69**, 024515 (2004).

Stability analysis of solitary waves in a 0-π Josephson junction

Chapter 3

We consider a spatially non-autonomous discrete and continuous sine-Gordon equation describing a 0-π Josephson junction. The continuous equation is a special case of the discrete equation in the strong coupling limit. The non-autonomous character is due to the presence of a discontinuity point, namely a jump of π in the sine-Gordon phase. The system admits a solitary wave which is called π-kink and is attached to the discontinuity point. There are three types of π-kinks. We show numerically and analytically that one of the solitary waves is stable and the others are unstable. Even though the largest eigenvalue of a stable π-kink is on the imaginary axis, one can excite it through the origin using a constant force. There is a critical value of the constant force at which zero is the largest eigenvalue. This critical value coincides with the critical current for the existence of a static semifluxon. Applying a constant force above the critical value causes nucleation of 2π-kinks and -antikinks. Besides a π-kink, the system also admits a static 3π-kink when there is no applied bias current. This state is unstable. This 3π-kink state with a $-\pi$-kink forms one of the unstable π-kinks for a nonzero applied bias current. In addition it is shown that the unstable π-kinks cannot be stabilized by the discreteness, even though a 3π-kink is stable when the interaction is sufficiently weak.

3.1 Introduction

One important application of the sine-Gordon equation is to describe the propagation of magnetic flux (fluxons) in long Josephson junctions [1, 2]. The flux quanta or fluxons are described by the kinks of the sine-Gordon equation. When many small Josephson junctions are connected through the inductance of the superconductors, they form a discrete Josephson transmission line (see Fig. 3.1). The propagation of a fluxon is then described by the discrete sine-Gordon equation. For some materials, Josephson junctions are more easily fabricated in the form of a lattice than as a long continuous Josephson junction. In the strong coupling limit, a discrete Josephson junction lattice becomes a long Josephson junction.

It was proposed in the late 1970's that a phase-shift of π may occur inside a Josephson junction (in the sine-Gordon equation) due to magnetic impurities [3]. Recent technological advances can impose a π-phase-shift in a long Josephson junction using, e.g., superconductors with unconventional pairing symmetry [4], Superconductor-Ferromagnet-Superconductor (SFS) π-junctions [5], and Superconductor-Normal metal-Superconductor (SNS) junctions [6]. A junction containing a region with a phase jump of π is then called a 0-π Josephson junction and is described by a 0-π sine-Gordon

equation. The place where the 0-junction meets the π-junction is called a discontinuity point.

A 0-π Josephson junction admits a half magnetic flux (semifluxon), sometimes called *π-fluxon*, attached to the discontinuity point [7]. A semifluxon is represented by a π-kink of the 0-π sine-Gordon equation [8]. Later on, it was proposed [9] to have also a lattice π-kink by making a discrete version of Josephson junctions, i.e. a Josephson junction array. Such lattices can be made using the technology described in [7]. The presence of this π-kink opens a new field where many questions, that have been discussed in details for the sine-Gordon equation, can be addressed again to this kink. The fact that the kink does not move in space, even in the continuum case, will give a different qualitative behavior such as the disappearance of the zero eigenvalue (Goldstone mode) as will be shown later.

In this chapter we will study the continuous and discrete 0-π sine-Gordon equation, especially the stability of the solitary waves admitted by the equation. Knowing the eigenvalues of a kink is of interest for experimentalists, since the corresponding eigenfunctions (localized modes) can play an important role in the behavior of the kink [10].

The present chapter is organized as follows: in Sec. 3.2 we will describe the mathematical model of the problem and its interpretation as a Josephson junction system. We will describe the considered discrete system as well as several continuum approximations to the discreteness. In Sec. 3.3 we consider the continuous 0-π sine-Gordon equation that describes a long Josephson junction with one corner. We will derive analytically the expression for a π- and 3π-kink without external current and calculate the stability of a π-kink. It is shown that there is a critical value of the external force at which the largest eigenvalue of a π-kink is zero and above which there is no static π-kink. In Sec. 3.3 we also show that the time-independent 0-π sine-Gordon equation has other π-kink states. They are all unstable. One of the π-kinks can be interpreted as the continuation of a 3π-kink without external current. In Sec. 3.4 we study the existence and stability of the solitary waves that were discussed in the previous section in the presence of terms representing discreteness. The existence and stability of the solitary waves in the weakly coupled limit will be discussed in Sec. 3.5. Numerical calculations connecting the regions of weakly and strongly discrete system will be presented in Sec. 3.6. In this section we confirm our analytical results using the original discrete system. Conclusions and plans for future research are presented in Sec. 3.6.

3.2 Mathematical equation and its interpretation as junction model

3.2.1 Discrete 0-π sine-Gordon equation

The Lagrangian describing the phase of a 0-π array of Josephson junctions is given by

$$L = \int \sum_{n\in\mathbb{Z}} \left[\frac{1}{2}\left(\frac{d\phi_n}{dt}\right)^2 - \frac{1}{2}\left(\frac{\phi_{n+1}-\phi_n}{a}\right)^2 - 1 + \cos(\phi_n + \theta_n) + \gamma\phi_n \right] dt, \qquad (3.2.1)$$

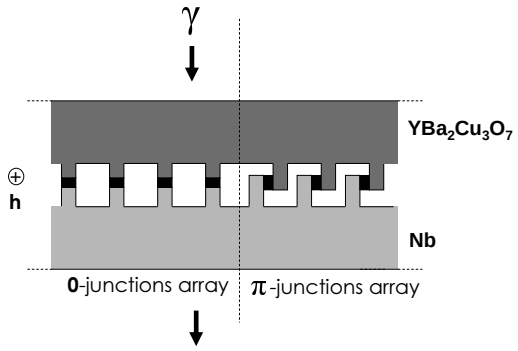

Figure 3.1: *A schematic drawing of a possibly fabricated 0-π Josephson junction array using ramp-type $YBa_2Cu_3O_7$/Au/Nb junctions.*

where ϕ_n is the Josephson phase of the nth junction. The phase jump of π in the Josephson phase is described by θ_n as follows:

$$\theta_n = \begin{cases} 0, & n \leq 0, \\ -\pi, & 0 < n. \end{cases} \tag{3.2.2}$$

Equation (3.2.1) is given in dimensionless form. The spatial coordinate x as well as the discreteness parameter a are normalized to the Josephson length λ_J, the time t is normalized to the inverse plasma frequency ω_0^{-1} and the applied bias current density $\gamma > 0$ is scaled to the critical current density J_c.

The equation of the phase motion generated by the Lagrangian (3.2.1) is then the following discrete 0-π sine-Gordon equation

$$\ddot{\phi}_n - \frac{\phi_{n-1} - 2\phi_n + \phi_{n+1}}{a^2} = -\sin(\phi_n + \theta_n) + \gamma. \tag{3.2.3}$$

For analytical calculations, we are interested in the case of $n \in \mathbb{Z}$, but the fabrication of the junction as well as the numerics is, of course, limited to a finite number of sites, say $2N$ sites. One then deals with boundary conditions. A reasonable choice is to take a boundary condition representing in which way the applied magnetic field $h = H/(\lambda_J J_c)$ enters the system:

$$\frac{\phi_{-N+1} - \phi_{-N}}{a} = \frac{\phi_N - \phi_{N-1}}{a} = h. \tag{3.2.4}$$

In the sequel we will always consider the absence of an applied magnetic field, i.e. we will take $h = 0$.

3.2.2 Various approximation to the discreteness in the continuum limit

There are various approximations of Eq. (3.2.3) in the continuum limit $a \ll 1$ that can be derived. For simplicity, first consider only the discrete sine-Gordon equation for $n \leq 0$

$$\ddot{\phi}_n - \frac{\phi_{n-1} - 2\phi_n + \phi_{n+1}}{a^2} = -\sin\phi_n + \gamma. \tag{3.2.5}$$

Writing $\phi_n = \phi(na)$ and expanding the difference terms using the Taylor expansion give

$$\frac{\phi_{n-1} - 2\phi_n + \phi_{n+1}}{a^2} = 2\sum_{k=0}^{\infty} \frac{a^{2k}}{(2k+2)!}\, \partial_{xx}^k \phi_{xx}(na) = L_a \phi_{xx}$$

and

$$\frac{\phi_{n+1} - \phi_n}{a} = \sum_{k=0}^{\infty} \frac{a^k}{(k+1)!}\, \partial_x^k \phi(na) = \widetilde{L}_a \phi_x.$$

Likewise, for $n \geq 1$, the continuum approximation for the equation is then given by

$$\phi_{tt} - L_a \phi_{xx} = -\sin(\phi + \theta) + \gamma, \tag{3.2.6}$$

and the continuum approximation for the Lagrangian is

$$L = \iint_{-\infty}^{\infty} \left[\frac{1}{2}(\phi_t)^2 - \frac{1}{2}\left(\widetilde{L}_a \phi_x\right)^2 - 1 + \cos(\phi + \theta) + \gamma\phi \right] dx\, dt\,,$$

where θ is defined similar to Eq. (3.2.2), i.e.,

$$\theta = \begin{cases} 0, & x < 0, \\ -\pi, & x > 0. \end{cases}$$

There are several ways to derive approximations (for $a \to 0$) for a continuum model (similar ideas can be found in Rosenau [11]). The first obvious approximation is

$$\phi_{tt} - \phi_{xx} - \frac{a^2}{12}\phi_{xxxx} = -\sin(\phi + \theta) + \gamma. \tag{3.2.7}$$

Another approximation can be found by using that L_a is invertible (in the right type of function space), hence $\phi_{xx} = L_a^{-1}(\phi_{tt} + \sin(\phi + \theta) - \gamma)$ and $L_a^{-1} = 1 - \frac{a^2}{12}\partial_{xx} + \ldots$, so we get

$$\phi_{xx} = \phi_{tt} + \sin(\phi + \theta) - \gamma - \frac{a^2}{12}\partial_{xx}(\phi_{tt} + \sin(\phi + \theta)), \quad x \neq 0. \tag{3.2.8}$$

Expanding this equation and using the expression for ϕ_{xx} again, we get

$$\begin{aligned} \phi_{xx} \;=\; & \phi_{tt} + \sin(\phi + \theta) - \gamma \\ & - \tfrac{a^2}{12}(\phi_{tttt} + [\sin(\phi + \theta)]_{tt} - \phi_x^2 \sin(\phi + \theta) \\ & + \cos(\phi + \theta)[\phi_{tt} + \sin(\phi + \theta) - \gamma]), \quad x \neq 0. \end{aligned} \tag{3.2.9}$$

The steady state equation for Eq. (3.2.7) is

$$\phi_{xx} + \frac{a^2}{12}\phi_{xxxx} = \sin(\phi+\theta) - \gamma, \quad x \neq 0,$$

while Eq. (3.2.8) yields the equation

$$\phi_{xx} = (1 - \frac{a^2}{12}\partial_{xx})\sin(\phi+\theta) - \gamma, \quad x \neq 0,$$

and Eq. (3.2.9) gives

$$\phi_{xx} = \sin(\phi+\theta) - \gamma - \frac{a^2}{12}\left\{-\phi_x^2\sin(\phi+\theta) + \cos(\phi+\theta)[\sin(\phi+\theta)-\gamma]\right\}, \quad x \neq 0.$$

Unfortunately the last two equations are not Hamiltonian, so we have lost the Hamiltonian properties, while the first equation is singularly perturbed.

Yet another approximation that has variational structure and is not singularly perturbed can be obtained by combining the two equations that have lost their variational character. Indeed, taking (3.2.8) twice and substracting (3.2.9) gives

$$\begin{aligned}\phi_{xx} \;=\; & \phi_{tt} + \sin(\phi+\theta) - \gamma \\ & - \tfrac{a^2}{12}\left(2\phi_{xxtt} + 2\phi_{xx}\cos(\phi+\theta) - \phi_x^2\sin(\phi+\theta) - \phi_{tttt} - \phi_{tt}\cos(\phi+\theta)\right. \\ & \left.+\phi_t^2\sin(\phi+\theta) - \cos(\phi+\theta)(\phi_{tt} + \sin(\phi+\theta) - \gamma)\right), \quad x \neq 0.\end{aligned} \tag{3.2.10}$$

The Lagrangian for this system is

$$\begin{aligned}L \;=\; & \iint \tfrac{1}{2}\phi_t^2 - \tfrac{1}{2}\phi_x^2 - 1 + \cos(\phi+\theta) + \gamma\phi \\ & + \tfrac{a^2}{2}\left[\phi_x\partial_x(\phi_{tt} + \sin(\phi+\theta)) + \tfrac{1}{2}(\phi_{tt} + \sin(\phi+\theta) - \gamma)^2\right] dx\,dt\,.\end{aligned}$$

The static equation for (3.2.10) is

$$\begin{aligned}&\phi_{xx} = \sin(\phi+\theta) - \gamma \\ &-\tfrac{a^2}{12}\left(2\phi_{xx}\cos(\phi+\theta) - \phi_x^2\sin(\phi+\theta) - \cos(\phi+\theta)(\sin(\phi+\theta)-\gamma)\right), \quad x \neq 0.\end{aligned}$$

This equation is a regularly perturbed Hamiltonian system with the Hamiltonian

$$H = \phi_x^2\left(\frac{1}{2} + \frac{a^2}{12}\cos(\phi+\theta)\right) + \gamma\phi + \cos(\phi+\theta) - \frac{a^2}{24}(\sin(\phi+\theta)-\gamma)^2\,.$$

The analysis of the kink solutions will be very similar to the one in the section with $a = 0$. All phase portrait constructions in the next section will carry through for small values of a.

After considering several possible approximations, we will refer Eq. (3.2.10) as *the* continuum approximation to the discrete 0-π sine-Gordon equation (3.2.3), with the boundary conditions at the discontinuity point $x = 0$ are given by [12, 13, 9]

$$\lim_{x\uparrow 0}\phi = \lim_{x\downarrow 0}\phi, \quad \lim_{x\uparrow 0}\phi_x = \lim_{x\downarrow 0}\phi_x. \tag{3.2.11}$$

3.3 π-kink and its spectra in the continuum limit

Throughout all the section here we take $a = 0$ in Eq. (3.2.10), corresponding to the differential equation for a perfect continuous long 0-π Josephson junction

$$\phi_{tt} - \phi_{xx} + \sin(\phi + \theta) = \gamma. \tag{3.3.1}$$

For a Josephson junction without an applied bias current and a phase jump, i.e. $\gamma = 0$ and $\theta(x) \equiv 0$, the basic (normalized) stationary, stable, monotonically increasing fluxon is given by

$$\phi_{\mathrm{fl}}(x) = 4 \arctan e^x, \quad \phi_{\mathrm{fl}}(0) = \pi \tag{3.3.2}$$

(see [14]).

In general when $\theta(x) \not\equiv 0$, the equation (3.3.1) will introduce a discontinuity at $x = 0$ for the second derivative ϕ_{xx}, hence a natural space for the solutions are the functions which are C^1 in x. The behaviour at infinity is regulated by requiring that the solution belongs to $H_2(\mathbb{R})$.

The π-kinks are static waves, connecting equilibrium states at $x = \pm\infty$ with a phase-difference of π. Therefore, we can drop the time dependency and consider only the following static wave equation

$$\phi_{xx} - \sin(\phi + \theta) = -\gamma. \tag{3.3.3}$$

For $|\gamma| < 1$, the fixed points of this model equation are $\phi_s^+ = \arcsin(\gamma)$ and $\phi_c^+ = \pi - \arcsin(\gamma)$ when $\theta = 0$ and $\phi_s^- = \pi + \arcsin(\gamma)$ and $\phi_c^- = 2\pi - \arcsin(\gamma)$ when $\theta = -\pi$. In the x-dynamics of (3.3.3), the points $\phi_s^\pm$ are saddle points and the points with $\phi_c^\pm$ are centre points.

By taking suitable combinations of the phase portraits for $\theta = 0$ and $\theta = -\pi$, the π-fluxons are constructed in [8]. The phase portraits for fixed $\theta = 0$ or $\theta = -\pi$ for $\gamma = 0$ are essentially different from the ones for $0 < \gamma < 1$ (the case $-1 < \gamma < 0$ follows from this one by taking $\phi \mapsto -\phi$ and $\gamma \mapsto -\gamma$). In case $\gamma > 0$, we have homoclinic connections at $k\pi + \arcsin(\gamma)$, $k \in \mathbb{Z}$, k even ($\theta = 0$) or k odd ($\theta = -\pi$). If $\gamma = 0$, then these homoclinic connections break to heteroclinic connections between $k\pi + \arcsin(\gamma)$ and $(k + 2)\pi + \arcsin(\gamma)$.

Following the notation in [8],[1] in case $\gamma = 0$, there are two types of heteroclinic connections (fluxons) in the corner junction. The first one, called *type 1* and denoted by $\phi_\pi^1(x; 0)$, connects 0 and π. The point in the phase plane where the discontinuity lies is denoted by $d_1(0)$. The second one, called *type 2* and denoted by $\phi_\pi^2(x; 0)$, connects 0 and 3π. Now the point in the phase plane where the discontinuity lies is denoted by $d_2(0)$. This solution is not a semifluxon, but it will be important in the analysis of semifluxons with a hump for $\gamma \neq 0$ as will be discussed below.

If $0 < \gamma \ll 1$, then there are three types of π-fluxons (heteroclinic connections) in the corner junction, all connecting 0 and π [8].[2] The first semifluxon, called *type 1* and

1 See Fig. 2.2 in Chapter 2 of this thesis.
2 See Fig. 2.3.

denoted by $\phi_\pi^1(x;\gamma)$, is a continuation of the connection at $\gamma = 0$. The point in the phase plane where the discontinuity lies is denoted by $d_1(\gamma)$. This is a monotonically increasing π-fluxon.

The second one is called *type 2* and is denoted by $\phi_\pi^2(x;\gamma)$. In the limit for $\gamma \to 0$, it breaks in the type 2 heteroclinic wave and the heteroclinic connection between 3π and π. The point in the phase plane where the discontinuity lies is denoted by $d_2(\gamma)$. This π-fluxon is not monotonically increasing, but has a hump.

The third one is called *type 3* and is denoted by $\phi_\pi^3(x;\gamma)$. In the limit for $\gamma \to 0$, it breaks in the heteroclinic connection between 0 and 2π and an anti-fluxon like the type 1 wave which connects 2π and π. The point in the phase plane where the discontinuity lies is denoted by $d_3(\gamma)$. This π-fluxon is also not monotonically increasing and it has a hump, but lower than the hump of the type 2 wave.

If γ increases, the points $d_2(\gamma)$ and $d_3(\gamma)$ approach each other, until they coincide at

$$\gamma = \gamma^* = \frac{2}{\sqrt{4+\pi^2}} \tag{3.3.4}$$

at the point $(\pi + \arcsin(\gamma^*), 0)$.[3] At this point, the type 2 wave $\phi_\pi^2(x;\gamma^*)$ ceases to exist (in the limit it breaks into half the homoclinic connection for $x < 0$ and the full homoclinic connection for $x > 0$). The type 3 wave $\phi_\pi^2(x;\gamma^*)$ consists of half the homoclinic connection for $x < 0$ and the fixed point for $x > 0$.

If γ increases further, the points $d_1(\gamma)$ and $d_3(\gamma)$ approach each other until they coincide[4] at

$$\gamma = \gamma_{\rm cr} = \frac{2}{\pi}. \tag{3.3.5}$$

For $\gamma > \gamma_{\rm cr}$, no static wave π-fluxons can exist.

Using the homoclinic (heteroclinic) connections in the systems with $\theta = 0, \pi$, we can describe the fluxon in more detail. Let $\phi_h(x;\gamma)$ denote the even homoclinic connection to $\arcsin(\gamma)$ for $\theta = 0$ and $\gamma > 0$. For $\gamma = 0$, let $\phi_h(x;0)$ denote the even heteroclinic connection between 0 and 2π. Finally, let $\phi_s(x;\gamma)$ denote the solution of the system with $\theta = 0$ and $\gamma \geq 0$, which decays to $\arcsin(\gamma)$ for $x \to +\infty$ (i.e., the stable part of the "tail of the fish" when $\gamma > 0$). Note that $\phi_s(x;0) = \phi_h(x;0) - 2\pi$.

Then we have for $0 < \gamma < \gamma^*$

$$\phi_\pi^1(x;\gamma) = \begin{cases} \phi_h(x + x_1^+(\gamma);\gamma), & \text{for} \quad x < 0 \\ \phi_s(x + x_1^-(\gamma);\gamma) + \pi, & \text{for} \quad x > 0 \end{cases}$$

$$\phi_\pi^i(x;\gamma) = \begin{cases} \phi_h(x + x_i^+(\gamma);\gamma), & \text{for} \quad x < 0 \\ \phi_h(x + x_i^-(\gamma);\gamma) + \pi, & \text{for} \quad x > 0 \end{cases}$$

with $i = 2, 3$. The coordinate shifts $x_i^\pm$, $i = 1, 2, 3$ are such that

$$d_i = (\phi_h(x_i^+), D_x\phi_h(x_i^+)) = (\phi_{s,h}(x_i^-) + \pi, D_x\phi_{s,h}(x_i^-)).$$

3 See Fig. 2.5.
4 See Fig. 2.6.

Hence $x_2^{\pm}(\gamma) = -x_3^{\pm}(\gamma)$. Note that both x_2^+ and x_3^+ converge to 0 for $\gamma \to \gamma^*$ and $x_2^- \to -\infty$ for $\gamma \to \gamma^*$ and $x_3^- \to +\infty$ for $\gamma \to \gamma^*$.

For $\gamma > \gamma^*$, we have

$$\phi_\pi^1(x;\gamma) = \begin{cases} \phi_h(x + x_1^+(\gamma);\gamma), & \text{for} \quad x < 0 \\ \phi_s(x + x_1^-(\gamma);\gamma) + \pi, & \text{for} \quad x > 0 \end{cases}$$
$$\phi_\pi^3(x;\gamma) = \begin{cases} \phi_h(x + x_3^+(\gamma);\gamma), & \text{for} \quad x < 0 \\ \phi_s(x + x_3^-(\gamma);\gamma) + \pi, & \text{for} \quad x > 0 \end{cases}$$

Hence the homoclinic orbit ϕ_h is replaced with the solution ϕ_s in the type 3 solution.

At $\gamma = 0$, we have an explicit expression for the π-fluxons (see (3.3.2) for the expression of ϕ_{fl}):

$$\begin{aligned} \phi_\pi^1(x;0) &= \begin{cases} \phi_{\text{fl}}(x - \ln(1+\sqrt{2})), & \text{for} \quad x < 0 \\ \pi - \phi_{\text{fl}}(-x - \ln(1+\sqrt{2})), & \text{for} \quad x > 0 \end{cases} \\ \phi_\pi^2(x;0) &= \begin{cases} \phi_{\text{fl}}(x + \ln(1+\sqrt{2})), & \text{for} \quad x < 0 \\ 3\pi - \phi_{\text{fl}}(-x + \ln(1+\sqrt{2})), & \text{for} \quad x > 0 \end{cases} \end{aligned} \tag{3.3.6}$$

Hence both functions are even and $\cos(\phi_\pi^i(x;0) + \theta)$ is continuous and even, since $\phi_\pi^i(0;0) = \frac{\pi}{2} \pmod{2\pi}$.

For small value of γ, we can approximate the homoclinic orbit $\phi_h(x;\gamma)$ up to order γ by using the 2π-fluxon ϕ_{fl} and its linearization.

Lemma 3.1. *For γ small, we have for the even homoclinic connection $\phi_h(x;\gamma)$*

$$\phi_h(x;\gamma) = \phi_{\text{fl}}(x + L_\pi(\gamma)) + \gamma\,\phi_1(x + L_\pi(\gamma)) + \gamma^2 R_2(x + L_\pi(\gamma);\gamma), \quad x < 0, \tag{3.3.7}$$

where $L_\pi(\gamma)$ is such that $\frac{d}{dx}\phi_h(L_\pi(\gamma);\gamma) = 0$. Then,

$$L_\pi(\gamma) = \frac{1}{2}|\ln\gamma| + \ln\frac{4}{\sqrt{\pi}} + O(\sqrt{\gamma}) \tag{3.3.8}$$

$$\phi_1(x) = \frac{1}{2}\left[-1 + \cosh x + \int_0^x \frac{\xi}{\cosh\xi}d\xi\right]\frac{1}{\cosh x} - \arctan e^x\left(\frac{x}{\cosh x} + \sinh x\right). \tag{3.3.9}$$

In here $\gamma^2 R_2(x + L_\pi(\gamma);\gamma) = O(\gamma)$, uniform for $x < 0$ and $\gamma\phi_1(L_\pi(\gamma)) = O(\sqrt{\gamma})$. Explicitly:

$$\phi_h(L_\pi) = 2\pi - 2\sqrt{\pi}\sqrt{\gamma} + O(\gamma). \tag{3.3.10}$$

Furthermore, $\phi_1(\tilde{x};\gamma) = O(1)$ and $R_2(\tilde{x};\gamma) = O(1)$, uniform for $\tilde{x} < 0$.

Proof. We introduce the expansion

$$\phi_h(x;\gamma) = \phi_{\rm fl}[x + L_\pi(\gamma)] + \gamma\phi_1[x + L_\pi(\gamma)] + \gamma^2 R_2[x + L_\pi(\gamma);\gamma].$$

Since it is more convenient in the following perturbation analysis to follow the normalization of $\phi_{\rm fl}(x)$ (see (3.3.2)), we set $\phi_h(0;\gamma) = \pi$ and thus shift the point $x = 0$ of $\phi_h(x;\gamma)$ to a yet undetermined position $L_\pi(\gamma)$. In the new coordinates, the position $L_\pi(\gamma) > 0$ is determined by the condition $\frac{d}{dx}\phi_h(L_\pi;\gamma) = 0$. By linearizing, it follows that the equation for ϕ_1 is,

$$\mathcal{L}(x)\,\phi_1 = -1, \quad \text{where} \quad \mathcal{L}(x) = \frac{d^2}{dx^2} - \cos(\phi_{\rm fl}(x)). \tag{3.3.11}$$

The operator $\mathcal{L}(x)$ is identical to the operator associated to the stability of $\phi_{\rm fl}(x)$. The homogeneous problem $\mathcal{L}\psi = 0$ has the following two independent solutions,

$$\psi_b(x) = \frac{1}{\cosh x}, \quad \psi_u(x) = \frac{x}{\cosh x} + \sinh x, \tag{3.3.12}$$

where $\psi_b(x) = \frac{1}{2}\frac{d}{dx}\phi_{\rm fl}(x)$ is bounded and $\psi_u(x)$ unbounded as $x \to \pm\infty$. By the variation-of-constants method, we find the general solution to (3.3.11),

$$\begin{aligned}\phi_1(x;A,B) &= \left[A + \frac{1}{2}\cosh x + \frac{1}{2}\int_0^x \frac{\xi}{\cosh\xi}d\xi\right]\frac{1}{\cosh x} \\ &\quad + [B - \arctan e^x]\left(\frac{x}{\cosh x} + \sinh x\right),\end{aligned}$$

with $A, B \in \mathbb{R}$. The solution $\phi_1(x)$ of (3.3.11) must be bounded as $x \to -\infty$ and is normalized by $\phi_1(0) = 0$ (since $\phi_h(0) = \phi_{\rm fl}(0) = \pi$). Thus, we find that $A = -\frac{1}{2}$ and $B = 0$. Note that $\lim_{x\to-\infty}\phi_1(x) = 1$, which agrees with the fact that $\lim_{x\to-\infty}\phi_h(x) = \arcsin\gamma = \gamma + O(\gamma^3)$. The solution $\phi_1(x)$ is clearly not bounded as $x \to \infty$, the unbounded parts of $\phi_1(x)$ and $\frac{d}{dx}\phi_1(x)$ are given by

$$\phi_1|_u(x) = -\arctan e^x \sinh x, \quad \frac{d}{dx}\phi_1|_u(x) = -\arctan e^x \cosh x. \tag{3.3.13}$$

It follows that $\phi_1(x) = O(\frac{1}{\gamma^\sigma})$ for some $\sigma > 0$ if $e^x = O(\frac{1}{\gamma^\sigma})$, i.e., if $x = \sigma|\log\gamma|$ at leading order. Using this, it is a straightforward procedure to show that the rest term $\gamma^2 R_2(x;\gamma)$ in (3.3.7) is of the order $\gamma^{2-2\sigma}$ for $x = \sigma|\log\gamma| + O(1)$ (and $\sigma > 0$). Hence, the approximation of $\phi_h(x)$ by expansion (3.3.7) breaks down as x is of the order $|\log\gamma|$. On the other hand, it also follows that $\phi^1_{\rm appr}(x) = \phi_{\rm fl}(x) + \gamma\phi_1(x)$ is a uniform $O(\gamma)$-accurate approximation of $\phi_h(x)$ on an interval $(-\infty, L]$ for $L = \frac{1}{2}|\log\gamma| + O(1)$. Since $\phi_{\rm fl}(L) + \gamma\phi_1(L) = O(\sqrt{\gamma})$ for such L, we can compute $L_\pi = \frac{1}{2}|\log\gamma| + O(1)$, the value of x at which

$$0 = \frac{d}{dx}\phi_h(x) = \frac{d}{dx}\phi^1_{\rm appr}(x) + O(\gamma) = \frac{d}{dx}\phi_{\rm fl}(x) + \gamma\frac{d}{dx}\phi_1|_u(x) + O(\gamma).$$

We introduce Y by $e^x = \frac{Y}{\sqrt{\gamma}}$, so that it follows by (3.3.2) and (3.3.13) that $Y = \frac{4}{\sqrt{\pi}} + O(\sqrt{\gamma})$, i.e.

$$L_\pi(\gamma) = \frac{1}{2}|\log\gamma| + \log\frac{4}{\sqrt{\pi}} + O(\sqrt{\gamma}).$$

A straightforward calculation shows that

$$\phi_h(L_\pi) = 2\pi - 2\sqrt{\pi}\sqrt{\gamma} + O(\gamma).$$

□

3.3.1 Stability of the type 1 solution

We will show analytically that the type 1 wave $\phi^1_\pi(x;\gamma)$ is linearly stable for $0 \le \gamma \le \gamma_{\rm cr}$. To linearize about a solution $\phi^i_\pi(x;\gamma)$, write $\phi(x,t) = \phi^i_\pi(x;\gamma) + v(x,t)$, substitute it in the model equation (3.3.1) and disregard all higher order terms:

$$[D_{xx} - \cos(\phi^i_\pi(x;\gamma) + \theta(x))]\, v = D_{tt}\, v. \tag{3.3.14}$$

Using the spectral Ansatz $v(x,t) = e^{\lambda t}\tilde{v}(x)$, where $v(x)$ is a continuously differentiable function and dropping the tildes, we get the eigenvalue problem

$$\mathcal{L}^i(x;\gamma)\, v = \lambda^2\, v, \tag{3.3.15}$$

where $\mathcal{L}^i$ is defined as

$$\mathcal{L}^i(x;\gamma) = D_{xx} - \cos(\phi^i_\pi(x;\gamma) + \theta(x)). \tag{3.3.16}$$

The natural domain for $\mathcal{L}^i$ is $C^1(\mathbb{R}) \cap H_2(\mathbb{R})$. We call Λ an eigenvalue of $\mathcal{L}^i$ if there is a function $v \in C^1(\mathbb{R}) \cap H_2(\mathbb{R})$, which satisfies $\mathcal{L}^i(x;\gamma)\, v = \Lambda v$. Since $\mathcal{L}^i$ depends smoothly on γ, the eigenvalues of $\mathcal{L}^i$ will depend smoothly on γ too.

The operator $\mathcal{L}^i$ is symmetric, hence all eigenvalues will be real. A straightforward calculation gives that the continuous spectrum of $\mathcal{L}^i$ is in $(-\infty, -\sqrt{1-\gamma^2})$

Since the eigenfunctions are continuously differentiable functions in $H_2(\mathbb{R})$, Sturm's Theorem [15] can be applied, leading to the fact that the eigenvalues are bounded from above. Furthermore, if v_1 is an eigenfunction of $\mathcal{L}^i$ with eigenvalue Λ_1 and v_2 is an eigenfunction of $\mathcal{L}^i$ with eigenvalue Λ_2 with $\Lambda_1 > \Lambda_2$, then there is at least one zero of v_2 between any pair of zeros of v_1 (including the zeros at $\pm\infty$). Hence if the eigenfunction v_1 has fixed sign, than Λ_1 is the largest eigenvalue of $\mathcal{L}^i$.

The following lemma gives a necessary and sufficient condition for $\mathcal{L}^i$ to have an eigenvalue $\Lambda = 0$.

Lemma 3.2. *The eigenvalue problem*

$$\mathcal{L}^i(x;\gamma)v = \Lambda v, \quad x \in \mathbb{R},$$

has an eigenvalue $\Lambda = 0$ *if and only if one of the following two conditions holds*

1. $\phi^i_\pi(0;\gamma) = k\pi$, *for some* $k \in \mathbb{Z}$;
2. $D_x\phi^i_\pi(0;\gamma) = 0$ *and there are some* $x_\pm$ *such that* $D_x\phi^i_\pi(x_\pm;\gamma) \neq 0$.

Proof. Since $\phi^i_\pi(x)$ converges to a saddle point $|x| \to \infty$, this implies that $D_x\phi_\pi(x)$ decays exponentially fast to 0 for $|x| \to \infty$. Since $\phi^i_\pi(x)$ solves (3.3.3), differentiating this ODE with respect to x, gives

$$\mathcal{L}^i(x)\, D_x\phi^i_\pi(x) = 0, \quad \text{for} \quad x \neq 0.$$

This implies that for any constant K, the function $w^i_K(x) = K\, D_x\phi^i_\pi(x)$ satisfies $\mathcal{L}^i(x)\, w^i_K(x) = 0$ for $x \neq 0$. Hence for any K_- and K_+, the solution

$$w^i(x) = \begin{cases} w^i_{K_-}(x), & x < 0; \\ w^i_{K_+}(x), & x > 0. \end{cases}$$

solves $\mathcal{L}^i(x)\, w^i(x) = 0$ for $x \neq 0$. The function $w^i(x)$ is continuously differentiable if and only if the following two conditions hold

1. $w^i_{K_-}(0-) = w^i_{K_+}(0+)$, in other words, $K_-\, D_x\phi^i_\pi(0) = K_+\, D_x\phi^i_\pi(0)$, since ϕ^i_π is continuously differentiable;
2. $D_x w^i_{K_-}(0-) = D_x w^i_{K_+}(0+)$, in other words, $K_-\, D_{xx}\phi^i_\pi(0-) = K_+\, D_{xx}\phi^i_\pi(0+)$.

The first condition is satisfied if $K_- = K_+$ or $D_x\phi^i_\pi(0) = 0$. If $D_x\phi^i_\pi(0) = 0$, we can choose $K_\pm$ such that the second condition is satisfied and we do not end up with the trivial solution.

If $D_x\phi^i_\pi(0) \neq 0$, we need $D_{xx}\phi^i_\pi$ to be continuous at $x = 0$ in order to satisfy the second condition. Since $D_{xx}\phi^i_\pi(x) = \sin(\phi^i_\pi(x) + \theta(x)) - \gamma$, $D_{xx}\phi^i_\pi$ is continuous at $x = 0$ if and only if $\sin(\phi^i_\pi(0)) = 0$. These arguments prove that if one of the two conditions are satisfied, then $\Lambda = 0$ is an eigenvalue of $\mathcal{L}^i$.

Next we assume that $\Lambda = 0$ is an eigenvalue of $\mathcal{L}^i$, hence there is some continuously differentiable function $v^i(x)$ such that $\mathcal{L}^i(x)v^i(x) = 0$ for $x \neq 0$ and $v^i(x) \to 0$ for $|x| \to \infty$. The only solutions decaying to zero at $+\infty$ are the solutions on the one dimensional stable manifold and similarly, the only solutions decaying to zero at $-\infty$ are the solutions on the one dimensional unstable manifold. The stable and unstable manifold are formed by multiples of $D_x\phi^i_\pi$. So we can conclude that there exist $K_\pm$ such that

$$v^i(x) = \begin{cases} K_- D_x\phi^i_\pi(x) & \text{for} \quad x < 0; \\ K_+ D_x\phi^i_\pi(x) & \text{for} \quad x > 0. \end{cases}$$

Now we are back in the same situation as above, so we can conclude that either one of the two conditions in the lemma must be satisfied. □

The second condition in the lemma does not occur. Indeed, the first part of the second condition, i.e., $D_x\phi^i_\pi(0;\gamma) = 0$ happens only if d_i has its second coordinate zero, hence only at $\gamma = \gamma^*$ for $d_2 = d_3$. The solution $\phi^2_\pi(x;\gamma^*)$ has ceased to exist and the solution $\phi^3_\pi(x;\gamma^*)$ consists of the fixed point for $x > 0$. Hence this solution does not satisfy the second part of the second condition.

The first condition of the lemma is satisfied at $\gamma = \gamma_{\rm cr}$ for $i = 1, 3$ (for this value of γ, the solutions ϕ_π^1 and ϕ_π^3 are equal). At $\gamma = \gamma_{\rm cr}$, the homoclinic orbit ϕ_h^+ and the orbit ϕ_s^- are tangential in the phase portrait, thus guaranteeing that the second derivative $D_{xx}\phi_\phi^i$ is continuous at $x = 0$. To see that this is the only value of γ for which the first condition is satisfied, we derive the relation between $\phi_\pi^i(0;\gamma)$ and γ. Multiplying the static equation (3.3.3) with $D_x\phi_\pi^i$ and rewriting it gives

$$D_x[(\phi_\pi^i(x;\gamma))^2] = 2D_x[-\gamma\phi_\pi^i(x;\gamma) - \theta(x)\cos(\phi_\pi^i(x;\gamma))].$$

Integration $\pm\infty$ to 0 and using that $D_x\phi_\pi^i(\pm\infty;\gamma) = 0$, shows

$$\begin{aligned}(\phi_\pi^i(0;\gamma))^2 &= 2[-\gamma(\phi_\pi^i(0;\gamma) - \phi_\pi^i(-\infty;\gamma) - \cos(\phi_\pi^i(0;\gamma)) + \cos(\phi_\pi^i(-\infty;\gamma))]\\ (\phi_\pi^i(0;\gamma))^2 &= 2[-\gamma(\phi_\pi^i(0;\gamma) - \phi_\pi^i(+\infty;\gamma) + \cos(\phi_\pi^i(0;\gamma)) - \cos(\phi_\pi^i(+\infty;\gamma))]\end{aligned}$$

Subtracting these two equations and using that $\phi_\pi^i(+\infty;\gamma) = \phi_\pi^i(-\infty;\gamma) + \pi$, we get that

$$0 = -\pi\gamma - 2\cos(\phi_\pi^i(0;\gamma)), \quad \text{hence} \quad \cos(\phi_\pi^i(0;\gamma)) = \frac{\pi\gamma}{2}. \tag{3.3.17}$$

If the first condition is satisfied, then $\cos(\phi_\pi^i(0;\gamma)) = 1$, hence $\gamma = \frac{2}{\pi} = \gamma_{\rm cr}$.

Next we will show that the spectrum of the operator $\mathcal{L}^1$ is stable for $0 \le \gamma < \gamma_{\rm cr}$.

Lemma 3.3. *For all $0 \le \gamma < \gamma_{\rm cr}$, all eigenvalues of $\mathcal{L}^1(x;\gamma)$ are strictly negative. For $\gamma = \gamma_{\rm cr}$, the operator $\mathcal{L}^1(x;\gamma_{\rm cr})$ has 0 as its largest eigenvalue. For $\gamma = 0$, the largest eigenvalue is $-\frac{1}{4}(\sqrt{5}+1)$.*

Proof. From Lemma 3.2, it follows that $\mathcal{L}^1$ has an eigenvalue $\Lambda = 0$ at $\gamma = \gamma_{\rm cr}$. The eigenfunction is $D_x\phi_\pi^1(x;\gamma_{\rm cr})$ and this function is always positive, since $\phi_\pi^1(x;\gamma_{\rm cr})$ is monotonically increasing. From Sturm's Theorem, it follows that $\Lambda = 0$ is the largest eigenvalue of $\mathcal{L}^1$ at $\gamma = \gamma_{\rm cr}$.

We can explicitly determine all eigenvalues of $\mathcal{L}^1(x;0)$. From the explicit expression for ϕ_π^1 it follows that $\mathcal{L}^1(x;0)$ is a continuous even operator. For fixed Λ, the operator $\mathcal{L}^1(x;0) - \Lambda$ has two linearly independent solutions. Since the fixed point is a saddle point, there is one solution that is exponentially decaying at $+\infty$ and there is one solution that is exponentially decaying at $-\infty$. If we denote the exponentially decaying function at $-\infty$ by $v_-(x;\Lambda)$, then the exponentially decaying function at $+\infty$ up to a constant is given by $v_+(x;\Lambda) = v_-(-x;\Lambda)$ (since $\mathcal{L}^1$ is symmetric). Obviously, $v_+(0;\Lambda) = v_-(0;\Lambda)$, hence Λ is an eigenvalue if $D_xv_+(0;\Lambda) = D_xv_-(0;\Lambda)$, i.e., when $D_xv_-(0;\Lambda) = 0$ or when $v_-(0;\Lambda) = 0$.

Using Mann [16], we can derive explicit expression for the solutions $v_-(0;\Lambda)$ (see also [14]). Using $x_1 = \ln(\sqrt{2}+1)$, we get

$$v_-(x;0) = \operatorname{sech}(x - x_1), \quad v_-(x;\Lambda) = e^{\mu(x-x_1)}[\tanh(x-x_1) - \mu], \quad \mu = \sqrt{\Lambda+1}.$$

A straightforward calculation shows that $v_-(0;\Lambda) \neq 0$. The condition $D_xv_-(0;\Lambda) = 0$ gives that

$$\mu^2 - \frac{1}{2}\sqrt{2}\mu - \frac{1}{2} = 0, \quad \text{hence} \quad \sqrt{\Lambda+1} = \frac{1}{4}\sqrt{2}(\sqrt{5}-1) : \Lambda = -\frac{1}{4}(\sqrt{5}+1).$$

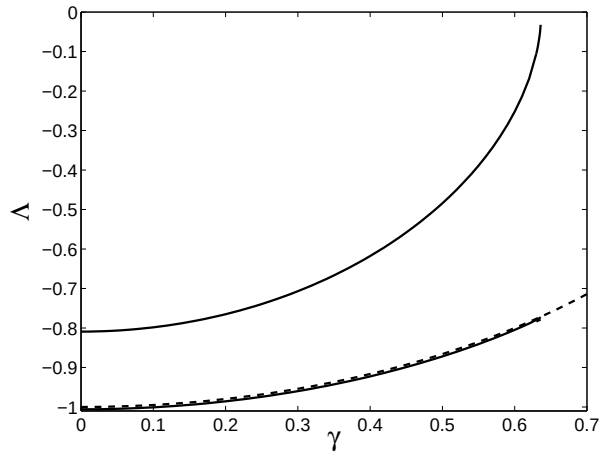

(a)

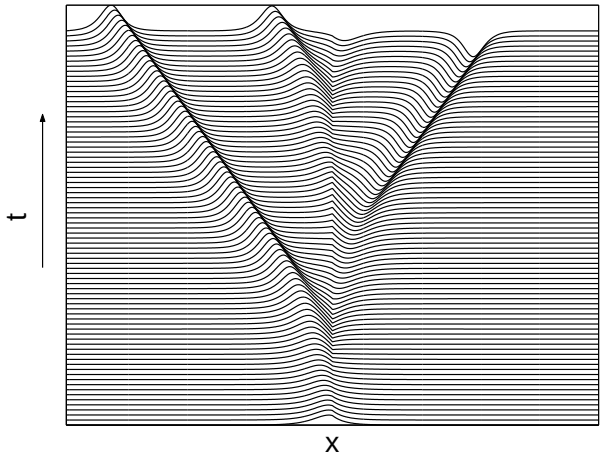

(b)

Figure 3.2: *(a) The eigenvalue of the stable semifluxon as a function of the bias current γ. The dashed line is the boundary of the continuous spectrum. (b) A sketch of the evolution of a π-kink in the continuum limit in the presence of a bias current above the critical value. The release of fluxons can be seen as well. The plot is presented in terms of the magnetic field ϕ_x.*

Now assume that the operator $\mathcal{L}^1(x;\gamma)$ has a positive eigenvalue $\Lambda^1(\gamma)$ for some $0 \leq \gamma < \gamma_{\text{cr}}$. Since Λ depends continuously on γ, there has to be some $0 < \widehat{\gamma} < \gamma_{\text{cr}}$ such that $\Lambda^1(\widehat{\gamma}) = 0$. However, from Lemma 3.2 it follows that this is not possible. □

The eigenvalues of the linearization are solution of the equation $\lambda^2 - \Lambda^1(\gamma) = 0$, hence $\lambda = \pm\sqrt{\Lambda^1(\gamma)}$. Since $\Lambda^1(\gamma) \leq 0$, this implies that $\Re(\lambda) \leq 0$, hence the waves of type 1 are stable.

We also have used numerics using standard procedures in MATLAB to compute the eigenvalues of this stable semifluxon as a function of the applied bias current. Further explanations of the computation procedure will be presented later in Sec. 3.6. In Fig. 3.2(a), we show the first two largest eigenvalues of the semifluxon obtained numerically.

One can see that the largest eigenvalue tends to zero when the bias current γ approaches the critical one $\gamma_{\rm cr}$ as is calculated analytically. The critical current $\gamma_{\rm cr}$ has been calculated before in [12, 13, 9, 8]. It was first proposed in [12, 13] that a constant driving force can excite the largest eigenvalue of a semifluxon towards zero. Later, it is shown in [8] that the critical current indeed corresponds to the disappearance of a static semifluxon.

When we apply a bias current above the critical value, the semifluxon reverses its polarity and releases a fluxon. As long as γ is larger than $\gamma_{\rm cr}$ the process repeats itself. The semifluxon changes its direction back and forth while releasing a fluxon or antifluxon alternately. A sketch of the release of fluxons from a semifluxon is presented in Fig. 3.2(b). In experiments, the polarity of a semifluxon can also be reversed by applying a magnetic field [7].

When $\gamma = \gamma_{\rm cr}$, there is at least one eigenvalue bifurcating from the edge of the continuous spectrum. This conjecture is obtained by considering also the stability of a type 3 semifluxon which is discussed later in Subsection 3.3.3. A similar picture as Fig. 3.2 for a type 3 semifluxon is presented in Fig. 3.4. From that figure, one can deduce that a type 3 semifluxon for $\gamma = \gamma_{\rm cr}$ has at least two eigenvalues, one of which is attached to the continuous spectrum. Because a type 1 semifluxon is the same as a type 3 semifluxon when $\gamma = \gamma_{\rm cr}$, we can conclude that at that value of bias current, a stable semifluxon has an additional eigenvalue.

Next we will prove that the type 2 and type 3 waves are linearly unstable for all values of γ for which they exist.

3.3.2 Instability of type 2 solutions

Lemma 3.4. *For all $0 < \gamma < \gamma^*$, the largest eigenvalue of $\mathcal{L}^2(x;\gamma)$ is strictly positive. In the limit $\gamma \to 0$, the largest eigenvalue of $\mathcal{L}^2(x;\gamma)$ converges to $\frac{1}{4}(\sqrt{5}-1)$.*

Proof. Using the approximation for the homoclinic orbit $\phi_h(x;\gamma)$ in Lemma 3.1, we see that, for γ small, an approximation for the π-fluxon of type 2 is given by (recall that $x_1 = \ln(1+\sqrt{2})$)

$$\phi_\pi^2(x;\gamma) = \begin{cases} \phi_{\rm fl}(x+x_1) + O(\gamma),\ x < 0 \\ \pi + \phi_{\rm fl}(x-x_1) + \gamma\phi_1(x-x_1) + \gamma^2 R_2(x-x_1;\gamma), \\ \qquad\qquad 0 < x < L_\pi(\gamma) + x_1 \\ \pi + \phi_{\rm fl}(-\widehat{x}) + \gamma\phi_1(-\widehat{x}) + \gamma^2 R_2(-\widehat{x};\gamma),\ x > L_\pi(\gamma) + x_1 \end{cases}$$

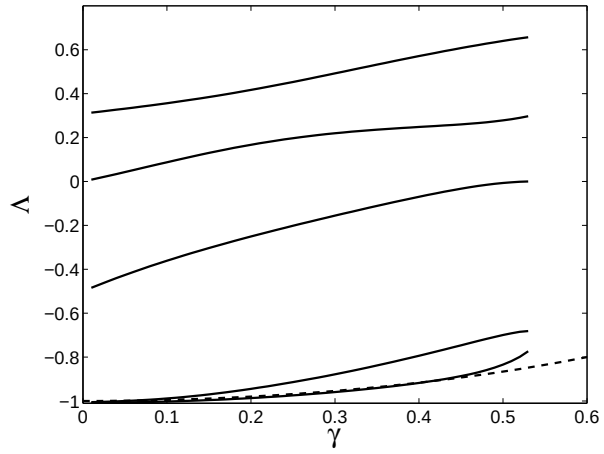

(a)

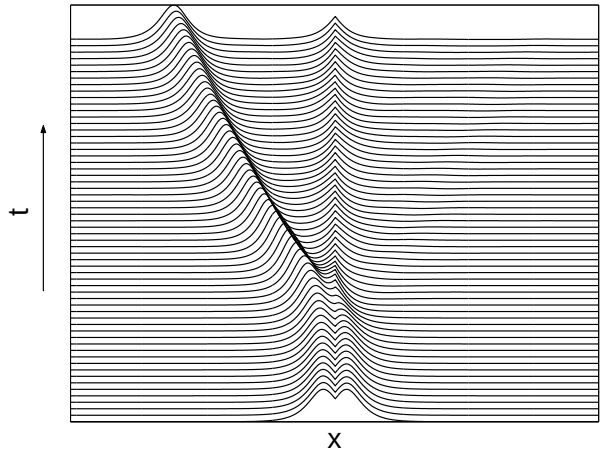

(b)

Figure 3.3: *(a) The eigenvalues of type 2 semifluxon as a function of the external force γ. The result that the largest eigenvalue is always positive shows the instability of type 2 semifluxon. When $\gamma \to 0$, $\Lambda \to \frac{1}{4}(\sqrt{5}-1)$ which is the largest eigenvalue of a 3π-kink. There are two eigenvalues bifurcating from the edge of the continuous spectrum (dashed line). (b) A sketch of the evolution of a 3π-kink (3.3.6) in the continuum limit. The separation of a fluxon from the semifluxon can be seen as well. The plot is presented in terms of the magnetic field ϕ_x.*

with $\widehat{x} = x - 2L_\pi(\gamma) - x_1$, since $x_2^+(\gamma) = x_1 - L_\pi(\gamma) + O(\gamma)$ and $x_2^-(\gamma) = -x_1 - L_\pi(\gamma) + O(\gamma)$.

There is no limit for $\gamma \to 0$, since the fluxon breaks in two parts, one of them being the 3π-fluxon denoted by $\phi_\pi^2(x;0)$. In a similar way as we found the largest eigenvalue for the linearization operator $\mathcal{L}^1(x;0)$ about the π-fluxon $\phi_\pi^1(x;0)$, we can find the largest eigenvalue for the linearization operator $\mathcal{L}^2(x;0)$ about the 3π-fluxon $\phi_\pi^2(x;0)$. The

largest eigenvalue is $\Lambda^2(0) = \frac{1}{4}(\sqrt{5}-1)$ and the eigenfunction is

$$\psi^2(x;0) = \begin{cases} e^{\mu(x+x_1)}(\mu - \tanh(x+x_1)), & x < 0 \\ e^{\mu(-x+x_1)}(\mu - \tanh(-x+x_1)), & x > 0 \end{cases},$$

where $\mu = \sqrt{\Lambda+1} = \frac{1}{4}\sqrt{2}(1+\sqrt{5})$.

For γ small, we approximate the eigenfunction on the whole interval $x \in \mathbb{R}$ by

$$\psi^2(x;\gamma) = \begin{cases} e^{\mu(x+x_1)}(\mu - \tanh(x+x_1)) + O(\sqrt{\gamma}), \ x < 0, \\ k_2\, e^{\mu(-x+x_1)}(\mu - \tanh(-x+x_1)) + \\ \quad k_3\, e^{\mu(x-x_1)}(\mu - \tanh(x-x_1)) + O(\sqrt{\gamma}), \ 0 < x < L_\pi(\gamma) + x_1 \\ k_4\, e^{\mu(-\widehat{x})}(\mu + \tanh(\widehat{x})) + O(\sqrt{\gamma}), \ x > L_\pi(\gamma) + x_1. \end{cases}$$

In this approximation, we include the secular term which is growing at infinity with the multiplication factor k_3. When $\gamma = 0$ and $k_3 = 0$, the first two lines in the definition of ψ^2 describe an eigenfunction of the linearized problem about the heteroclinic connection between 0 and 3π. The corresponding eigenvalue is $\frac{1}{4}(\sqrt{5}-1)$.

When we construct an eigenfunction of the form $\psi^2(x,\gamma)$ given above for $\gamma > 0$, we need to determine the constants k_2, k_3 and k_4 such that the function is continuously differentiability at $x = 0$ and $x = L_\pi(\gamma) + x_1$. From the continuity conditions at $x = 0$, we obtain:

$$k_2 = \frac{\sqrt{2}}{4\mu(\mu-1)(\mu+1)}, \tag{3.3.18}$$

$$k_3 = \frac{(3+2\sqrt{2})^\mu(2\mu^2 - \mu\sqrt{2} - 1)(2\mu - \sqrt{2})}{4\mu(\mu^2-1)}. \tag{3.3.19}$$

From one of the continuity conditions at $x = L_\pi(\gamma) + x_1$, we determine k_4 as a function of k_2 and k_3. Now we are left with one more matching condition. Values of μ for which this condition is satisfied correspond to the eigenvalues of the operator $\mathcal{L}^2(x;\gamma)$ for γ small. More explicitly, the spectral parameter μ has to satisfy the equation

$$\mathcal{F}(\mu) = 16^\mu k_3(\mu-1)^2(\gamma\pi)^{-\mu}((3\mu+4)\pi\gamma + 16\mu) + O(\gamma^{-\mu+2}) = 0. \tag{3.3.20}$$

When $\gamma = 0$, it is as expected that there are four positive roots giving four squared eigenvalues, namely $\Lambda(0) = \frac{1}{4}(\sqrt{5}-1), -\frac{1}{2}$, and the double eigenvalue $\Lambda(0) = 0$. The first two come from the zeros of k_3 and the last ones are the eigenvalues of the fluxon. One can also notice that there is no term with a multiplication factor k_2 to this leading order. This term appears at most of order $O(\gamma^{\mu+2})$.

The proof that the largest eigenvalue is near $\frac{1}{4}(\sqrt{5}-1)$ for γ small will be complete if we can show that $\mathcal{F}_\mu\left(\sqrt{2}/4(1+\sqrt{5})\right) \neq 0$, i.e. the non-degeneracy condition that says that the eigenvalue can be continued continuously for γ small.

Simple algebraic calculations give that

$$\mathcal{F}_\mu\left(\frac{\sqrt{2}}{4}(1+\sqrt{5})\right) = c_1\gamma^{-\frac{\sqrt{2}}{4}(1+\sqrt{5})} + \mathcal{O}(\gamma^{1-\frac{\sqrt{2}}{4}(1+\sqrt{5})}) \tag{3.3.21}$$

with c_1 a positive constant. Hence, $\mathcal{F}_\mu(\frac{\sqrt{2}}{4}(1+\sqrt{5})) > 0$.

This finally shows that the largest eigenvalue is near $\frac{1}{4}(\sqrt{5}-1)$ for γ small but positive. Since the largest eigenvalue depends continuously on γ, it can only disappear at a bifurcation point. There are no bifurcation points and it is not possible that the eigenvalue becomes 0 (see Lemma 3.2), hence the largest eigenvalue will be positive as long as fluxon $\phi_\pi^2(x;\gamma)$ exists, i.e., for $0 < \gamma < \gamma^*$. □

Remark 3.1. We cannot use a comparison theorem, because $\phi_\pi^2 < \phi_\pi^3$ for $x < 0$ and $\phi_\pi^2 > \phi_\pi^3$ for $x > 0$.

The eigenvalues for the linearizations are solution of the equation $\lambda^2 - \Lambda^2(\gamma) = 0$, hence $\lambda = \pm\sqrt{\Lambda^2(\gamma)}$. Since $\Lambda^2(\gamma) > 0$, this implies that one of the two eigenvalues has $\Re(\lambda) > 0$, hence the fluxons of type 2 are unstable. The numerically obtained eigenvalues of semifluxons of this type as a function of γ are shown in Fig. 3.3(a). In Fig. 3.3(b), we present the evolution of a 3π-kink (3.3.6) which is the limit of a type 2 semifluxon when $\gamma \to 0$. The separation of a fluxon from the semifluxon is clearly seen and indicates the instability of the state.

Remark 3.2. A type 2 semifluxon can be seen as a concatenation of a 3π- and a -2π-kink which is clear in the limit $\gamma \to 0$. Therefore, in that limit the other eigenvalues of $\mathcal{L}^2(x;\gamma)$ converge to 0, -0.5, and -1. The eigenvalues 0 and -1 are contributions of the antikink. The eigenvalue $\Lambda^2(0) = -0.5$ corresponds to the first excited state of a 3π-kink with eigenfunction

$$\psi^2(x;0) = \begin{cases} e^{\mu(x+x_1)}(\mu - \tanh(x+x_1)), & x < 0 \\ e^{\mu(-x+x_1)}(\tanh(-x+x_1) - \mu), & x > 0 \end{cases},$$

where $\mu = \sqrt{\Lambda+1} = \frac{1}{\sqrt{2}}$.

3.3.3 Instability of type 3 solutions

Lemma 3.5. *For all $0 < \gamma < \gamma_{\rm cr}$, the largest eigenvalue of $\mathcal{L}^3(x;\gamma)$ is strictly positive. For $\gamma = \gamma_{\rm cr}$, the operator $\mathcal{L}^3(x;\gamma_{\rm cr})$ has 0 as its largest eigenvalue.*

Proof. The solution $\phi_\pi^3(x,\gamma_{\rm cr}) = \phi_\pi^1(x,\gamma_{\rm cr})$, hence from Lemma 3.3 it follows that the largest eigenvalue is $\Lambda^3 = 0$.

For γ near zero, we will use the approximation in Lemma 3.1 for the homoclinic orbit $\phi_h(x;\gamma)$ to get an approximation for the type 3 fluxon

$$\phi_\pi^3(x;\gamma) = \begin{cases} \phi_{\rm fl}(\widehat{x}) + \gamma\phi_1(\widehat{x}) + \gamma^2 R_2(\widehat{x};\gamma),\ x < -L_\pi(\gamma) + x_1 \\ \phi_{\rm fl}(-x + x_1) + \gamma\phi_1(-x + x_1) + \gamma^2 R_2(-x + x_1;\gamma), \\ \qquad\qquad -L_\pi(\gamma) + x_1 < x < 0 \\ \pi + \phi_{\rm fl}(-x - x_1) + O(\gamma),\ x > 0 \end{cases}$$

where $\widehat{x} = x - x_1 + 2L_\pi(\gamma)$.

For the largest eigenvalue, we set

$$\Lambda^3(\gamma) = \gamma\Lambda_1(\gamma).$$

To construct the first part of the approximation of the eigenfunction, we consider $x < -L_\pi(\gamma) + x_1$, i.e., $\widehat{x} < L_\pi(\gamma)$. In this part of the arguments, we will drop the hat in $\widehat{x}$. On $(-\infty, L_\pi)$, we expand $\psi^1_{\rm approx} = \psi_0 + \gamma\psi_1$, this yields the following equations for $\psi_{0,1}(x)$,

$$\mathcal{L}\psi_0 = 0,\quad \mathcal{L}\psi_1 = [\Lambda_1(0) - \phi_1(x)\sin\phi_{\rm fl}(x)]\psi_0. \tag{3.3.22}$$

We select $\psi_0(x)$ uniquely by assuming that $\psi(x) \to 0$ as $x \to -\infty$ and that $\psi(0) = 1$,

$$\psi_0(x) = \frac{1}{\cosh x} \tag{3.3.23}$$

(see 3.3.12). To solve the ψ_1-equation, we note that $\frac{d}{dx}\phi_1(x)$ is a solution of (see (3.3.11) and (3.3.2))

$$\mathcal{L}\psi = -\phi_1\sin\phi_{\rm fl}\frac{d}{dx}\phi_{\rm fl} = -2\phi_1\sin\phi_{\rm fl}\psi_0,$$

so that we find as general solution,

$$\begin{aligned} \psi_1(x) &= [A - \frac{1}{2}\Lambda_1(\log(\cosh x) + \int_0^x \frac{\xi}{\cosh^2\xi}d\xi)]\frac{1}{\cosh x} + \\ &\quad [B + \frac{1}{2}\Lambda_1\tanh x](\frac{x}{\cosh x} + \sinh x) + \frac{1}{2}\frac{d}{dx}\phi_1. \end{aligned}$$

By imposing $\lim_{x\to-\infty}\psi_1(x) = 0$ and $\psi_1(0) = 0$ we find that $A = \frac{\pi}{4}$, $B = \frac{1}{2}\Lambda_1(0)$. As in the case of $\phi_1(x)$, we are especially interested in the unbounded parts of $\psi_1(x)$ and $\frac{d}{dx}\psi_1(x)$,

$$\begin{aligned} \psi_1|_u(x) &= \tfrac{1}{2}\Lambda_1(1 + \tanh x)\sinh x - \tfrac{1}{2}\arctan e^x\cosh x, \\ \tfrac{d}{dx}\psi_1|_u(x) &= \tfrac{1}{2}\Lambda_1(1 + \tanh x)\cosh x - \tfrac{1}{2}\arctan e^x\sinh x. \end{aligned} \tag{3.3.24}$$

We note that the error term $|\psi(x) - \psi^1_{\rm appr}(x)| = \gamma^2|S_2(x;\gamma)|$ is at most $O(\gamma)$ on $(-\infty, L_\pi)$ (the analysis is similar to that for $\gamma^2|R_2(x;\gamma)|$).

Next consider the second part of the approximation, i.e., x between $-L_\pi(\gamma) + x_1$ and 0. Here we define the translated coordinate $x - x_1$, which is on the interval $(-L_\pi, -x_1)$. Since we have to match $\psi^1_{\text{appr}}(x)$ to the approximation $\psi^2_{\text{appr}}(x)$ of $\psi(x)$, along $\phi^2_{\text{appr}}(x)$ and is thus defined on the interval $(-L_\pi, -x_1)$, we need to compute $\psi^1_{\text{appr}}(L_\pi)$ and $\frac{d}{dx}\psi^1_{\text{appr}}(L_\pi)$ which to the leading order are calculated from (3.3.24), i.e.

$$\psi^1_{\text{appr}}(L_\pi) = \frac{2\Lambda_1(0)}{\sqrt{\pi}}\sqrt{\gamma} + O(\gamma), \quad \frac{d}{dx}\psi^1_{\text{appr}}(L_\pi) = \frac{2\Lambda_1(0) - \pi}{\sqrt{\pi}}\sqrt{\gamma} + O(\gamma). \tag{3.3.25}$$

Thus, both $\psi^1_{\text{appr}}(L_\pi)$ and $\frac{d}{dx}\psi^1_{\text{appr}}(L_\pi)$ are $O(\sqrt{\gamma})$. Now, we choose a special form for the continuation of $\psi(x)$, i.e. the part linearized along $\phi^2_{\text{appr}}(x)$. It is our aim to determine the value of Λ_1, for which there exists a positive integrable C^1 solution ψ of $\mathcal{L}^3(x;\gamma)\psi = \gamma\Lambda_1(0)\psi$. By general Sturm-Liouville theory [15] we know that this value of Λ_1 must be the critical (i.e. largest) eigenvalue. Our strategy is to try to continue $\psi(x)$ beyond $(-\infty, L_\pi)$ by a function that remains at most $O(\sqrt{\gamma})$, i.e. we do not follow the approach of the existence analysis and thus do not reflect and translate $\psi^1_{\text{appr}}(x)$ to construct $\psi^2_{\text{appr}}(x)$ (since this solution becomes (in general) $O(1)$ for $x = O(1)$). Instead, we scale $\psi(x)$ as $\gamma\tilde{\psi}(x)$. The linearization $\tilde{\psi}(x)$ along $\phi^2_{\text{appr}}(x)$ on the interval $(-L_\pi, x_1)$ must solve $\mathcal{L}\tilde{\psi} = O(\gamma)$, thus, at leading order

$$\tilde{\psi}(x) = \frac{\tilde{A}}{\cosh x} + \tilde{B}\left(\frac{x}{\cosh x} + \sinh x\right). \tag{3.3.26}$$

The approximation $\psi^2_{\text{appr}}(x) = \gamma\tilde{\psi}(x)$ must be matched to $\psi^1_{\text{appr}}(L_\pi)$ and $\frac{d}{dx}\psi^1_{\text{appr}}(L_\pi)$ at $x = -L_\pi$, i.e.

$$\frac{2\Lambda_1(0)}{\sqrt{\pi}} = -\frac{2\tilde{B}}{\sqrt{\pi}} + O(\sqrt{\gamma}), \quad \frac{2\Lambda_1(0) - \pi}{\sqrt{\pi}} = \frac{2\tilde{B}}{\sqrt{\pi}} + O(\sqrt{\gamma}).$$

Note that $\tilde{A}$ does not appear in these equations; as a consequence, $\psi^1_{\text{appr}}(x)$ and $\psi^2_{\text{appr}}(x)$ can only be matched for a special value of Λ_1, $\Lambda_1(0) = \frac{1}{4}\pi$, with $\tilde{B} = -\Lambda_1(0) < 0$. Thus, we have found for this special value of Λ_1 and for $\tilde{A} > 0$ a positive C^1-continuation of the solution $\psi(x)$ of the eigenvalue problem for $\mathcal{L}^3(x;\gamma)$ – recall that $x < 0$ in the domain of $\tilde{\psi}(x)$. At the point of discontinuity ($-x_1$ for $\tilde{\psi}(x)$, or at $x = 0$ in the original coordinates of (3.3.1)), we have

$$\begin{aligned}
\psi^2_{\text{appr}}(-x_1) = \gamma\tilde{\psi}(-x_1) &= \gamma[\tfrac{1}{2}\sqrt{2}\tilde{A} - \tfrac{\pi}{8}\sqrt{2}(\log(\sqrt{2}-1) - \sqrt{2})] + O(\gamma^2),\\
\tfrac{d}{dx}\psi^2_{\text{appr}}(-x_1) = \gamma\tfrac{d}{dx}\tilde{\psi}(-x_1) &= \gamma[\tfrac{1}{2}\tilde{A} - \tfrac{\pi}{8}(\log(\sqrt{2}-1) + 3\sqrt{2})] + O(\gamma^2).
\end{aligned} \tag{3.3.27}$$

Hence, we have constructed for a special choice of Λ, $\Lambda = \Lambda_* = \frac{\pi}{4}\gamma + O(\sqrt{\gamma}) > 0$, an approximation of a family of positive solutions of the eigenvalue problem for $\mathcal{L}^3(x;\gamma)$ on $x < 0$ – in the coordinates of (3.3.1) – that attain the values given by (3.3.27) at $x = 0$, and that decay to 0 as $x \to -\infty$. The question is now whether we can 'glue' an element of this family in a C^1-fashion to a solution of the eigenvalue problem for $\mathcal{L}^3(x;\gamma)$ on $x > 0$ – with $\Lambda = \Lambda_*$ – that decays (exponentially) as $x \to \infty$. If that is possible, we have constructed a positive integrable solution to the eigenvalue problem

for $\mathcal{L}^3(x;\gamma)$, which implies that $\Lambda_* > 0$ is the critical eigenvalue and that $\phi_\pi^3(x)$ is unstable.

An approximation of $\psi(x)$ on $x > 0$, $\psi^3_{\text{appr}}(x)$, is obtained by linearizing along $\phi^3_{\text{appr}}(x)$ and by translating x so that $x \in (x_1, \infty)$. Since $\psi^3_{\text{appr}}(x)$ has to match to expressions of $O(\gamma)$ (3.3.27) at x_1, we also scale $\psi^3_{\text{appr}}(x)$, $\psi^3_{\text{appr}}(x) = \gamma\hat{\psi}(x)$. We find that $\mathcal{L}\hat{\psi} = O(\gamma)$ so that $\hat{\psi}(x)$ again has to be (at leading order) a linear combination of $\psi_b(x)$ and $\psi_u(x)$ (3.3.12). However, $\hat{\psi}$ must be bounded as $x \to \infty$, which yields that $\hat{\psi}(x) = \hat{A}/\cosh x + O(\gamma)$ for some $\hat{A} \in \mathbb{R}$. At the point of discontinuity we thus have

$$\begin{array}{rcccl} \psi^3_{\text{appr}}(x_1) & = & \gamma\hat{\psi}(x_1) & = & \frac{1}{2}\sqrt{2}\hat{A}\gamma + O(\gamma^2), \\ \frac{d}{dx}\psi^3_{\text{appr}}(x_1) & = & \gamma\frac{d}{dx}\tilde{\psi}(x_1) & = & -\frac{1}{2}\hat{A}\gamma + O(\gamma^2). \end{array} \tag{3.3.28}$$

A positive C^1-solution of the eigenvalue problem for $\mathcal{L}^3(x;\gamma)$ exists (for $\Lambda = \Lambda_*$) if there exist $\tilde{A}, \hat{A} > 0$ such that (see Eqs. (3.3.27) and (3.3.28))

$$\begin{array}{rcccl} \frac{1}{2}\sqrt{2}\tilde{A} & - & \frac{\pi}{8}\sqrt{2}(\log(\sqrt{2}-1) - \sqrt{2}) & = & \frac{1}{2}\sqrt{2}\hat{A} \\ \frac{1}{2}\tilde{A} & - & \frac{\pi}{8}(\log(\sqrt{2}-1) + 3\sqrt{2}) & = & -\frac{1}{2}\hat{A} \end{array} \tag{3.3.29}$$

Since the solution of this system is given by $\tilde{A} = \frac{1}{4}\pi[\sqrt{2} + \log(\sqrt{2}-1)] > 0$ and $\hat{A} = \frac{1}{2}\pi\sqrt{2} > 0$, we conclude that the eigenvalue problem for the π-fluxon $\phi_\pi^3(x;\gamma)$ has a positive largest eigenvalue

$$\Lambda_* = \frac{\pi}{4}\gamma + O(\sqrt{\gamma}). \tag{3.3.30}$$

Hence the eigenvalue for γ small is positive. From Lemma 3.2 it follows that there are no zero eigenvalues between 0 and γ_{cr}, hence the largest eigenvalue of $\mathcal{L}^3(\gamma)$ is positive for all values of γ. □

Remark 3.3. For any $\lambda = O(\sqrt{\gamma})$, or equivalently any $\Lambda_1 = O(1)$, there exists a (normalized) solution to the eigenvalue problem for $\mathcal{L}^3(x;\gamma)$ on $x < 0$ that decays as $x \to -\infty$, and that is approximated by $\psi^1_{\text{appr}}(x)$ and $\psi^2_{\text{appr}}(x)$ (matched in a C^1-fashion at $\pm L_\pi$). If Λ_1 is not $O(\sqrt{\gamma})$ close to $\frac{1}{4}\pi$, however, $\psi^2_{\text{appr}}(x)$ cannot be scaled as $\gamma\tilde{\psi}(x)$ and the solution is not $O(\gamma)$ at the point of discontinuity – in general it is $O(1)$. Moreover, for any $\Lambda_1 = O(1)$, there also exists on $x > 0$ a 1-parameter family of (non-normalized) eigenfunctions for the eigenvalue problem for $\mathcal{L}^3(x;\gamma)$ that decay as $x \to \infty$. In this family there is one unique solution that connects continuously to the (normalized) solution at $x < 0$. In fact, one could define the jump in the derivative at $x = 0$, $\mathcal{J}(\lambda;\gamma)$, as an Evans function expression (note that $\mathcal{J}(\lambda;\gamma)$ can be computed explicitly). By definition, λ is an eigenfunction of $\mathcal{L}^3(x;\gamma)$ if and only if $\mathcal{J}(\lambda;\gamma) = 0$. In the above analysis we have shown that $\mathcal{J}(\lambda_*;\gamma) = 0$.

Remark 3.4. The classical, driven, sine-Gordon equation, i.e. $\theta \equiv 0$ in (3.3.1), has a standing pulse solution, that can be seen, especially for $0 < \gamma = \gamma \ll 1$, as a

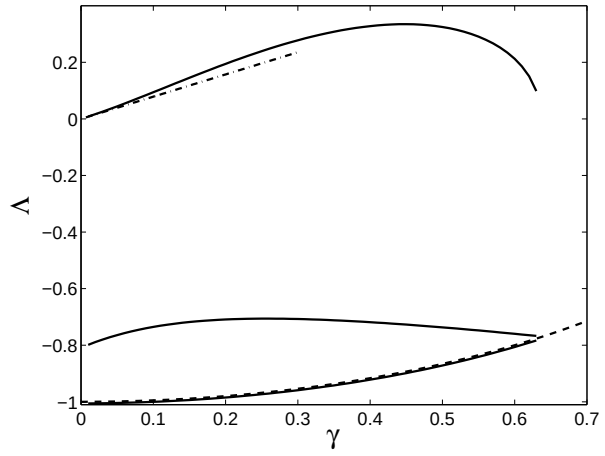

Figure 3.4: *The eigenvalues of type 3 semifluxon as a function of the external force γ. The result that the largest eigenvalue is always positive shows the instability of type 3 semifluxon. When $\gamma \ll 1$, according to Eq. (3.3.30) the largest eigenvalue is approximated by $\Lambda = \frac{\pi}{4}\gamma$ shown in dash-dotted line. The dashed line is the boundary of the continuous spectrum.*

fluxon/anti-fluxon pair. This solution is approximated for $\frac{d}{dx}\phi > 0$ (the fluxon) by $\phi^1_{\text{appr}}(x)$ and for $\frac{d}{dx}\phi < 0$ (the anti-fluxon) by $\phi^1_{\text{appr}}(-x)$. It is (of course) unstable, the (approximation of the) critical unstable eigenvalue can be obtained from (3.3.25). The corresponding eigenfunction is approximated by $\psi^1_{\text{appr}}(x)$ on $(-\infty, L_\pi)$, and we conclude from (3.3.25) that $\frac{d}{dx}\psi^1_{\text{appr}}(L_\pi) = 0$ for $\lambda^2 = \gamma\Lambda_1 = \gamma\frac{\pi}{2} + O(\gamma\sqrt{\gamma})$ (while $\psi^1_{\text{appr}}(L_\pi) > 0$). Hence, for this value of Λ_1, we can match $\psi^1_{\text{appr}}(x)$ to $\psi^2_{\text{appr}}(x) = \psi^1_{\text{appr}}(-x)$ in a C^1-fashion, it gives a uniform $O(\gamma)$-approximation of the critical, positive (even, 'two-hump') eigenfunction of the fluxon/anti-fluxon pair at the eigenvalue $\lambda_+ = \frac{1}{2}\sqrt{2\pi}\sqrt{\gamma} + O(\gamma) > 0$.

The eigenvalues for the linearizations are solution of the equation $\lambda^2 - \Lambda^3(\gamma) = 0$, hence $\lambda = \pm\sqrt{\Lambda^3(\gamma)}$. Since $\Lambda^3(\gamma) > 0$, this implies that one of the two eigenvalues has $\Re(\lambda) > 0$, hence the fluxons of type 3 are unstable. In Fig. 3.4, we present numerical calculations of the eigenvalues of type 3 semifluxon as a function of the bias current γ.

Remark 3.5. A type 3 semifluxon can be seen as a concatenation of a 2π- and a $-\pi$-kink. This can be seen clearly in the limit $\gamma \to 0$. Therefore, in that limit the other eigenvalues of $\mathcal{L}^3(x;\gamma)$ converge to $-\frac{1}{4}(\sqrt{5}+1)$ and -1 which are contributions of the $-\pi$- and 2π-kink, respectively.

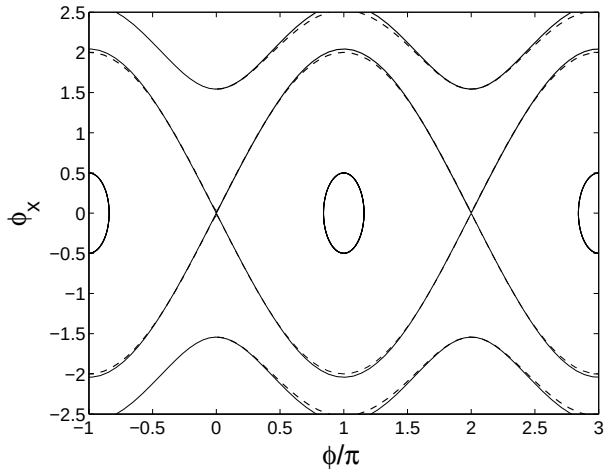

Figure 3.5: *The phase portrait of the system* (3.2.10) *with* $a = 0.5$ *for* $\gamma = 0$*. The effect of the perturbative term is shown by comparing it with the phase portrait of the unperturbed system* $a = 0$ *shown in dashed-lines.*

3.4 Lattice π-kinks and their spectra in the discrete case: continuum approximation

Now we consider the continuous 0-π sine-Gordon equation with the continuum approximation to the discreteness Eq. (3.2.10). Using the fact that the semifluxons of all types are constructed by heteroclinic connections with transversal intersection at $x = 0$ in the two-dimensional phase space, we can directly guarantee that all the semifluxons still exist in the perturbed system Eq. (3.2.10) [17]. In Fig. 3.5, we present the phase portraits of the perturbed and the unperturbed system.

For small value of a, we can approximate the heteroclinic orbit connecting 0 and 2π (mod 2π) up to order a^2 by using the 2π-fluxon $\phi_{\rm fl}$ and its linearization.

Lemma 3.6. *Let* $\phi^a_{\rm fl}(x)$ *denote the heteroclinic orbit of the sine-Gordon equation with the perturbation term representing the continuum approximation to the discreteness (Eq.* (3.2.10) *with* $\theta \equiv 0$*) with* $\gamma = 0$*. For a small, we have for the heteroclinic connection* $\phi^a_{\rm fl}(x)$

$$\phi^a_{\rm fl}(x) = \phi_{\rm fl}(x) + a^2\phi_a(x) + O(a^4), \tag{3.4.1}$$

where

$$\phi_a(x) = -\frac{1}{12}\frac{-3\sinh x + x\cosh x}{\cosh^2 x}. \tag{3.4.2}$$

Furthermore, $\phi_a(x) = O(1)$*, uniformly for* $x \in \mathbb{R}$*.*

Proof. The spatially localized correction to the kink shape $\phi_{\text{fl}}(x)$ due to the perturbation term representing discreteness is sought in the form of the perturbation series:

$$\phi^a_{\text{fl}}(x) = \phi_{\text{fl}}(x) + a^2\phi_a(x) + O(a^4).$$

It is a direct consequence that $\phi_a(x)$ must satisfy the equation:

$$\begin{aligned}\mathcal{L}^1(x;0)\phi_a(x) = f(x) = -\tfrac{1}{12}\big(&2\partial_{xx}\phi^1_\pi(x;0)\cos(\phi^1_\pi(x;0)+\theta) - \\ &(\partial_x\phi^1_\pi(x;0))^2\sin(\phi^1_\pi(x;0)+\theta) - \cos\phi^1_\pi(x;0)\sin\phi^1_\pi(x;0)\big),\end{aligned} \tag{3.4.3}$$

where $\mathcal{L}^1(x;0)$ is the operator given in (3.3.16).

Using the variation of constants method, we obtain the general solution of (3.4.3), i.e.

$$\begin{aligned}\phi_a(x) &= A\ \text{sech}\ x + B(x\ \text{sech}\ x + \sinh x), \qquad (3.4.4)\\ A &= A_0 + \frac{1}{24}\left[2\ln\left(\frac{\cosh x - 1 - \sinh x}{\cosh x - 1 + \sinh x}\right) + \frac{6\sinh x}{\cosh x} - \frac{4\sinh x}{\cosh^3 x} + \int_0^x \frac{\xi f(\xi)}{\cosh\xi}d\xi\right],\\ B &= B_0 - \frac{1}{24}\left[2 + \frac{1}{\cosh^2 x} - \frac{3}{\cosh^4 x}\right].\end{aligned}$$

The integration constants A_0 and B_0 are determined by the conditions for $\phi_a(x)$. Applying $\lim_{x\to-\infty}\phi_a(x) = 0$ and $\phi_a(x) = 0$ yields $A_0 = 0$, $B_0 = \frac{1}{12}$. The continuity of $D_x\phi_a(x)$ is automatically satisfied by its symmetry with respect to $x = 0$. □

Using the same procedure, the localized correction to the π- and 3π-kink due to the discreteness term up to order $O(a^2)$ can be presented as follows.

Lemma 3.7. *For a small and $\gamma = 0$, we have an explicit expression for the π- and 3π-fluxon up to order $O(a^2)$, respectively:*

$$\begin{aligned}\phi^1_\pi(x;a;0) &= \phi^1_\pi(x;0) + \begin{cases} -u^1_\pi(x - \ln(1+\sqrt{2})), & \text{for} \quad x<0\\ +u^1_\pi(-x - \ln(1+\sqrt{2})), & \text{for} \quad x>0\end{cases}\\ \phi^2_\pi(x;a;0) &= \phi^2_\pi(x;0) + \begin{cases} -u^1_{3\pi}(x + \ln(1+\sqrt{2})), & \text{for} \quad x<0\\ +u^1_{3\pi}(-x + \ln(1+\sqrt{2})), & \text{for} \quad x>0\end{cases}\end{aligned} \tag{3.4.5}$$

with $\phi^1_\pi(x;0)$ and $\phi^2_\pi(x;0)$ are given in (3.3.6) and

$$\begin{aligned}u^1_\pi(x) &= \frac{1}{12\cosh x}(-3 + 6\cos^2(\frac{\pi}{8}) + \ln\sin(\frac{\pi}{8}) - \ln\cos(\frac{\pi}{8}) + 3\tanh x - x)\\ u^1_{3\pi}(x) &= \frac{1}{12\cosh x}(3 - 6\cos^2(\frac{\pi}{8}) - \ln\sin(\frac{\pi}{8}) + \ln\cos(\frac{\pi}{8}) + 3\tanh x - x).\end{aligned}$$

Due to the discreteness term, there is also correction to γ^* and $\gamma_{\rm cr}$ [9], i.e.

$$\gamma^*(a) = \frac{2}{\sqrt{4+\pi^2}} + \underbrace{\frac{2}{3}\frac{\pi}{\pi^4+8\pi^2+16}}_{\approx 0.0109} a^2 + O(a^4), \tag{3.4.6}$$

$$\gamma_{\rm cr}(a) = \frac{2}{\pi} + \underbrace{\frac{\sqrt{1-\frac{4}{\pi^2}}\pi - \pi + 2\arcsin(\frac{2}{\pi})}{3\pi^2}}_{\approx 0.0223} a^2 + O(a^4). \tag{3.4.7}$$

For $\gamma > \gamma_{\rm cr}(a)$, there is no static semifluxon.

3.4.1 Stability of type 1 semifluxon

We will show that the type 1 wave $\phi_\pi^1(x;a;\gamma)$ is linearly stable for nonzero a and $0 \le \gamma \le \gamma_{\rm cr}$.

The eigenvalue problem of a solution $\phi_\pi^i(x;a;\gamma)$ is

$$\mathcal{L}^i(x;\gamma)\, v = \lambda^2 v, \tag{3.4.8}$$

where $\mathcal{L}^i(x;\gamma)$ is now defined as

$$\mathcal{L}^i(x;\gamma) = D_{xx} - \cos(\phi_\pi^i(x;a;\gamma) + \theta(x)). \tag{3.4.9}$$

The following lemma gives a necessary and sufficient condition for $\mathcal{L}^i(x;\gamma)$ to have an eigenvalue $\Lambda = 0$ for a nonzero a.

Lemma 3.8. *The eigenvalue problem*

$$\mathcal{L}^i(x;\gamma)v = \Lambda v, \quad x \in \mathbb{R},$$

has an eigenvalue $\Lambda = 0$ if and only if one of the following two conditions holds

1. $\phi_\pi^i(0;a;\gamma) = k\pi - a^2\frac{1}{6\pi} + O(a^4)$, *for some $k \in \mathbb{Z}$;*
2. $D_x\phi_\pi^i(0;a;\gamma) = 0$ *and there are some $x_\pm$ such that $D_x\phi_\pi^i(x_\pm;a;\gamma) \neq 0$.*

Proof. This lemma modifies Lemma 3.2 for the case of nonzero a. The proof is *mutatis mutandis the same as the one of Lemma 3.2, but we have*

$$\begin{aligned} D_{xx}\phi_\pi^i(x;a) &= \sin(\phi_\pi^i(x;a)+\theta(x)) - \gamma + \\ &\tfrac{1}{12}(\sin(\phi_\pi^i(x;a)+\theta(x))(-2\gamma\arcsin\gamma - 2\sqrt{1-\gamma^2} + \gamma\phi_\pi^i(x;a) + \\ &\cos(\phi_\pi^i(x;a)+\theta(x))) + \cos(\phi_\pi^i(x;a)+\theta(x))\gamma)a^2 + O(a^4). \end{aligned}$$

□

The first condition of the lemma is satisfied at $\gamma = \gamma_{\rm cr}(a)$ for $i = 1, 3$.

Next we will show that the spectrum of the operator $\mathcal{L}^1(x;\gamma)$ is stable for $0 \le \gamma \le \gamma_{\rm cr}(a)$.

Lemma 3.9. *For the discreteness parameter a sufficiently small and $0 \le \gamma < \gamma_{\rm cr}(a)$, the largest eigenvalue of $\mathcal{L}^1(x;\gamma)$ is strictly negative. For $\gamma = \gamma_{\rm cr}(a)$, the operator $\mathcal{L}^1(x;\gamma_{\rm cr}(a))$ has 0 as its largest eigenvalue. For $\gamma = 0$, the largest eigenvalue decreases as a increases and is proportional to $-\frac{1}{4}(\sqrt{5}+1) - 0.0652a^2 + O(a^4)$.*

Proof. Writing $v(x) = v^0(x) + a^2 v^1(x) + O(a^4)$ and $\Lambda = \Lambda_0 + a^2\Lambda_1 + O(a^4)$ and expanding the eigenvalue problem for the stability of $\phi^1_\pi(x;a;0)$ in a Taylor series result in the following equations

$$\begin{aligned} &\left(\mathcal{L}^1(x;0) - \Lambda_0\right) v^0(x) = 0, \\ &\left(\mathcal{L}^1(x;0) - \Lambda_0\right) v^1(x) = \left(\Lambda_1 - u^1_\pi(x)\,\sin(\phi^1_\pi(x;0)+\theta)\right) v^0(x) - g(x), \end{aligned} \tag{3.4.10}$$

with (see Lemma 3.3)

$$\begin{aligned} v^0(x) &= \begin{cases} e^{\mu(x-\ln(1+\sqrt{2}))}\,[\tanh(x - \ln(1+\sqrt{2})) - \mu], & \text{for} \quad x < 0 \\ e^{\mu(-x-\ln(1+\sqrt{2}))}\,[\tanh(-x - \ln(1+\sqrt{2})) - \mu], & \text{for} \quad x > 0 \end{cases}, \\ \mu &= \sqrt{\Lambda_0 + 1}, \quad \Lambda_0 = -\tfrac{1}{4}(\sqrt{5}+1), \\ g(x) &= \tfrac{1}{12}\Big[2v^0_{xx}\Lambda_0 + v^0 + 2v^0_{xx}\cos(\phi^1_\pi(x;0)+\theta) - 2\cos^2(\phi^1_\pi(x;0)+\theta)v^0 \\ &\quad -2\partial_{xx}(\phi^1_\pi(x;0))\sin(\phi^1_\pi(x;0)+\theta)v^0 - 2\partial_x\phi^1_\pi(x;0)\sin(\phi^1_\pi(x;0)+\theta)v^0_x \\ &\quad -(\partial_x\phi^1_\pi(x;0))^2\cos(\phi^1_\pi(x;0)+\theta)v^0 - v^0\Lambda_0^2 - 2v^0\Lambda_0\cos(\phi^1_\pi(x;0)+\theta)\Big]. \end{aligned}$$

The parameter value of Λ_1 is calculated by solving (3.4.10) for a bounded and decaying solution $v^1(x)$. The general solution can be derived by using the variation of constant method because we have the homogeneous solutions of the equation. One can also use the Fredholm's theorem (see, e.g., [18]), i.e. the sufficient and necessary condition for (3.4.10) to have $v^1 \in H_2(\mathbb{R})$ is provided that the inhomogeneity is perpendicular to the null space of the self-adjoint operator of $\mathcal{L}^1(x;0)$. In our case, we need to look for the solvability condition on half of the real line only because solution on the other semi-infinite domain will exist automatically and satisfies $v^1(x) = Kv^1(-x)$, with K is a suitably chosen constant. If $<,>$ denotes an inner product in $H_2(\mathbb{R})$ over $\mathbb{R}^+$ or $\mathbb{R}^-$, then we obtain

$$\begin{aligned} & < (\mathcal{L}^1(x;0) - \Lambda_0)v^1, v^0 > = < v^1, (\mathcal{L}^1(x;0) - \Lambda_0)v^0 >, \\ \Leftarrow: \quad & < \Lambda_1 v^0 - u^1_\pi v^0 \sin(\phi^1_\pi(x;0)+\theta) - g, v^0 > = 0, \\ \Leftarrow: \quad & \Lambda_1 = \frac{3584(70\sqrt{2}(1+\sqrt{5}) - 99(1+\sqrt{5}))}{24576(-70\sqrt{10} - 350\sqrt{2} + 495 + 99\sqrt{5})} \\ & \quad \approx -0.0652. \end{aligned} \tag{3.4.11}$$

Now assume that the operator $\mathcal{L}^1(x;\gamma)$ has a positive eigenvalue $\Lambda^1(\gamma)$ for some $0 \leq \gamma < \gamma_{\text{cr}}(a)$. Since Λ depends continuously on γ, there has to be some $0 < \widehat{\gamma} < \gamma_{\text{cr}}(a)$ such that $\Lambda^1(\widehat{\gamma}) = 0$. However, from Lemma 3.8 it follows that this is not possible.

□

3.4.2 Instability of type 2 semifluxon

We are not going to proceed discussing the stability issue of semifluxons of this type since the largest eigenvalue of the semifluxon is quite unstable for $a \to 0$. Introducing discreteness will not immediately stabilize the semifluxon. Here, we will consider only the special case when $\gamma = 0$.

Note that this semikink can be seen as a concatenation of a 3π-kink and a -2π-kink which is clearly seen in the case of $\gamma = 0$. For this value of γ, the largest eigenvalue of semifluxon of this type is equal to the largest eigenvalue of a 3π-kink.

Because a 2π-fluxon in the 'ordinary' sine-Gordon equation can be pinned by the discreteness, one might expect to have a stable 3π-kink in the discrete 0-π sine-Gordon equation. A stable state might exist when the repelling force between the semifluxon and the fluxon is smaller than the energy to move a fluxon along lattices (the Peierls-Nabarro barrier, see Remark 5.6). But for this kind of 3π-kink solution as is expressed analytically in Eq. (3.3.6), we will show using the perturbation method that the discreteness cannot stabilize this kink for $a \ll 1$. The largest eigenvalue grows even as the discreteness parameter a increases. Later on in Section 3.6, we will show numerically that there is no minimum coupling a for this semifluxon to be stable. A semifluxon of this type will always be unstable in its existence region.

Lemma 3.10. *For the discreteness parameter a sufficiently small, the largest eigenvalue of $\mathcal{L}^2(x;0)$ is strictly positive. Moreover, it increases as a increases and is proportional to $\frac{1}{4}(\sqrt{5}-1) + 0.0652a^2 + O(a^4)$.*

Proof. Notice that the analytic expression of a π- and a 3π-kink differs only in the sign of the 'kink-shift' (see Eq. (3.4.5)). Because of this, we can directly follow the proof of Lemma 3.9. Writing the largest eigenvalue of a 3π-kink as $\Lambda = \Lambda_0 + a^2\Lambda_1 + O(a^4)$, with $\Lambda_0 = (\sqrt{5}-1)/4$ as has been calculated in Lemma 3.4, then we compute Λ_1 to be:

$$\begin{aligned}\Lambda_1 &= \frac{3584(665857(\sqrt{5}-1) - 470832\sqrt{2}(\sqrt{5}+1))}{24576(3329285 - 2354160\sqrt{2} - 665857\sqrt{5} + 470832\sqrt{10})} \\ &\approx 0.0652. \end{aligned} \tag{3.4.12}$$

□

This result says that up to order $O(a^4)$ introducing the discreteness even destabilizes a 3π-kink compared to the corresponding solution of the continuous equation.

3.4.3 Instability of type 3 semifluxon

Semifluxons of type 3 have been shown in Lemma 3.5 to be weakly unstable. Then it is natural to expect that the perturbation term representing discreteness might stabilize the semifluxon. This is however not the case.

Lemma 3.11. *For all $0 < \gamma < \gamma_{\rm cr}(a)$ and a small, the largest eigenvalue of $\mathcal{L}^3(x;\gamma)$ is strictly positive. For $\gamma = \gamma_{\rm cr}(a)$, the operator $\mathcal{L}^3(x;\gamma_{\rm cr})$ has 0 as its largest eigenvalue.*

Proof. Let $\phi_\pi^3(x;a;\gamma)$ represent the type 3 semifluxon for a small non-negative value of a. The solution $\phi_\pi^3(x;a;\gamma_{\rm cr}(a)) = \phi_\pi^1(x;a;\gamma_{\rm cr}(a))$, hence from Lemma 3.9 it follows that the largest eigenvalue is $\Lambda^3 = 0$.

We are going to follow the proof of Lemma 3.5. For this, it is necessary to scale the parameter a in Eq. (3.2.10) to $\sqrt{\gamma}a$, i.e. $a^2 \to \gamma a^2$. For γ and a near zero, an approximation for the type 3 fluxon now can be written as

$$\phi_\pi^3(x;\gamma) = \begin{cases} \phi_{\rm fl}(\widehat{x}) + \gamma\phi_1(\widehat{x}) + \gamma a^2\phi_a(\widehat{x}) + \gamma^2 R_2(\widehat{x};\gamma), & x < -L_\pi(\gamma) + x_1 \\ \phi_{\rm fl}(-x+x_1) + \gamma\phi_1(-x+x_1) + \gamma^2 R_2(-x+x_1;\gamma) + O(\gamma a^2), & \\ \qquad -L_\pi(\gamma) + x_1 < x < 0 & \\ \pi + \phi_{\rm fl}(-x-x_1) + O(\gamma,\gamma a^2), & x > 0 \end{cases}$$

where $\widehat{x} = x - x_1 + 2L_\pi(\gamma)$.

For the largest eigenvalue, again we set $\Lambda^3(\gamma) = \gamma\Lambda_1(0)$.

Next, we can recalculate the results of the proof of Lemma 3.5, only now with some additional new terms.

First, we consider the first part of the approximation of the eigenfunction, i.e. the approximation on $x < -L_\pi(\gamma) + x_1$ or $\widehat{x} < L_\pi(\gamma)$. In this part of the arguments, again we drop the hat in $\widehat{x}$. On $(-\infty, L_\pi)$, the general solution of the eigenvalue problem of the order $O(\gamma)$ after expanding $\psi^1_{\rm approx} = \psi_0 + \gamma\psi_1$ is

$$\begin{aligned} \psi_1(x) \;=\; & [\frac{\pi}{4} - \frac{1}{2}\Lambda_1(\log(\cosh x) + \int_0^x \frac{\xi}{\cosh^2\xi}d\xi)]\frac{1}{\cosh x} \\ & +[\frac{1}{2}\Lambda_1(0) + \frac{1}{2}\Lambda_1\tanh x](\frac{x}{\cosh x} + \sinh x) + \frac{1}{2}\left(\frac{d}{dx}\phi_1 + \frac{d}{dx}\phi_a\right) \\ & -\frac{e^x}{360(e^{2x}+1)^3}\Big[16\ln 2 + e^{2x}(32\ln 2 - 295 + 60x) + 30x - \\ & 16\ln(e^{2x}+1)(e^{2x}+1)^2 + 137 + e^{4x}(151 + 30x + 16\ln 2) + 7e^{6x}\Big]. \end{aligned} \tag{3.4.13}$$

We note that the error term $|\psi(x) - \psi^1_{\rm appr}(x)| = \gamma^2|S_2(x;\gamma)|$ is still at most $O(\gamma)$ on $(-\infty, L_\pi)$.

Next consider the second part of the approximation, i.e., x between $-L_\pi(\gamma) + x_1$ and 0. Here, as before, we define the translated coordinate $x - x_1$, which is on the interval $(-L_\pi, -x_1)$, and scale $\psi(x)$ as $\gamma\tilde{\psi}(x)$. The linearization $\tilde{\psi}(x)$ along $\phi^2_{\text{appr}}(x)$ on the interval $(-L_\pi, -x_1)$ must solve $\mathcal{L}\tilde{\psi} = O(\gamma)$. Thus, at leading order

$$\tilde{\psi}(x) = \frac{\tilde{A}}{\cosh x} + \tilde{B}\left(\frac{x}{\cosh x} + \sinh x\right). \tag{3.4.14}$$

The last part of the approximation of $\psi(x)$ on $x > 0$, $\psi^3_{\text{appr}}(x)$, is obtained by linearizing along $\phi^3_{\text{appr}}(x)$ and by translating x so that $x \in (x_1, \infty)$. We also scale $\psi^3_{\text{appr}}(x)$, $\phi^3_{\text{appr}}(x) = \gamma\hat{\psi}(x)$. However, $\hat{\psi}$ must be bounded as $x \to \infty$, which yields that $\hat{\psi}(x) = \hat{A}/\cosh x + O(\gamma)$ for some $\hat{A} \in \mathbb{R}$.

After defining all parts of the approximate eigenfunction on all the real line, now we have to connect them in a C^1-fashion. This can be done for a specific combination of $\Lambda_1(0)$, $\tilde{A}$, $\tilde{B}$, and $\hat{A}$, i.e.

$$\Lambda_1(0) = \tfrac{1}{4}\pi + \tfrac{7}{180}a^2, \quad \tilde{B} = -\Lambda_1(0) < 0,$$
$$\tilde{A} = \tfrac{1}{4}\pi[\sqrt{2} + \log(\sqrt{2} - 1)] > 0, \quad \hat{A} = \tfrac{1}{2}\pi\sqrt{2} > 0.$$

Now, we can conclude that the eigenvalue problem for the π-fluxon $\phi^3_\pi(x; a; \gamma)$ has a positive largest eigenvalue

$$\Lambda_* = \left(\frac{\pi}{4} + \frac{7}{180}a^2\right)\gamma + O(\sqrt{\gamma}). \tag{3.4.15}$$

Hence the eigenvalue for γ small is positive. From Lemma 3.8, it follows that there are no zero eigenvalues between 0 and γ_{cr}, hence the largest eigenvalue of $\mathcal{L}^3(\gamma)$ is positive for all values of γ. □

3.5 Semikinks in the weak-coupling limit

Now we consider the discrete 0-π sine-Gordon equation (3.2.3). The time independent equation of (3.2.3) corresponds to the so-called Standard or Taylor-Greene-Chirikov map when $\gamma = 0$ [19] and Josephson map when $\gamma \neq 0$ [20].

In this discrete system, one would expect that the three types of semikinks discussed in the previous sections should be present. Yet, not all of the types of the semifluxon can be studied analytically. This is because it is not clear which semifluxons in the discrete case that can be continued from and to the continuum limit. Most of configurations in the discrete case will end in a saddle node bifurcation. Only the configuration that corresponds to the type 1 semifluxon is known which in the uncoupled limit $a \to \infty$, is given by

$$\phi^1_\pi(n; \infty; \gamma) = \begin{cases} \arcsin\gamma, & n = 0, -1, -2, \ldots \\ \pi + \arcsin\gamma, & n = 1, 2, 3, \ldots. \end{cases} \tag{3.5.1}$$

Therefore, in this section we will only discuss the type 1 semifluxon. Nonetheless, let us denote the lattice semifluxon of type i with lattice spacing a that corresponds to $\phi^i_\pi(x;\gamma)$ as $\phi^i_\pi(n;a;\gamma)$, $n \in \mathbb{Z}$.

The existence of the continuation of (3.5.1) for sufficiently large a is guaranteed by the following lemma.

Lemma 3.12. *Let us denote $\epsilon = 1/a^2$. The steady state solution representing the semifluxon of type 1 in the uncoupled limit $\epsilon = 0$, $\phi^1_\pi(n;\infty;\gamma)$, can be continued for a small enough. For γ small $\gamma = \epsilon\widetilde{\gamma}$, the solution up to $O(\epsilon^2)$ is given by*

$$\phi^1_\pi(n;a;\gamma) = \begin{cases} \epsilon\widetilde{\gamma} + O(\epsilon^3), & n = -1,-2,-3,\ldots \\ \epsilon(\pi + \widetilde{\gamma}) + O(\epsilon^2), & n = 0, \\ \pi + \epsilon(\widetilde{\gamma} - \pi) + O(\epsilon^2), & n = 1, \\ \pi + \epsilon\widetilde{\gamma} + O(\epsilon^3), & n = 2,3,4\ldots. \end{cases} \tag{3.5.2}$$

For γ close to one $\gamma = 1 - \epsilon\widetilde{\gamma}$, the solution up to $O(\epsilon^1)$ is given by

$$\phi^1_\pi(n;a;\gamma) = \begin{cases} \pi/2 - \sqrt{\epsilon}\sqrt{2\widetilde{\gamma}} + O(\epsilon^{3/2}), & n = -1,-2,-3,\ldots \\ \pi/2 - \sqrt{\epsilon}\sqrt{2(\widetilde{\gamma} - \pi)} + O(\epsilon), & n = 0, \\ 3\pi/2 - \sqrt{\epsilon}\sqrt{2(\widetilde{\gamma} + \pi)} + O(\epsilon), & n = 1, \\ 3\pi/2 - \sqrt{\epsilon}\sqrt{2\widetilde{\gamma}} + O(\epsilon^{3/2}), & n = 2,3,4\ldots. \end{cases} \tag{3.5.3}$$

From (3.5.3), we obtain the critical bias current for the existence of static semifluxon, i.e.

$$\gamma_{\mathrm{cr}} = 1 - \epsilon\pi + O(\epsilon^2). \tag{3.5.4}$$

Proof. The existence proof follows from the implicit function theorem as given in [21] Theorem 2.1 or [22] Lemma 2.2.

To determine the critical bias current for the existence of a static lattice semifluxon, note that $\phi^1_\pi(n;a;1-\epsilon\widetilde{\gamma})$ must be real. Up to $O(\epsilon)$, from (3.5.3) there is a restriction for the value of $\widetilde{\gamma}$ for $\phi^1_\pi(n;a;1-\epsilon\widetilde{\gamma})$ to be real, i.e. for the site $n = 0$ where $\widetilde{\gamma} \leq \pi$. Because the other sites have no such a restriction, it can be concluded that $\gamma_{\mathrm{cr}} = 1 - \epsilon\pi + O(\epsilon^2)$. □

From the uncoupled solution (3.5.1), we can see that there is no solution for (3.2.3) that represents a semifluxon sitting on a site, different from the case of kinks in the ordinary sine-Gordon equation [23]. A 2π-kink sitting between two consecutive lattices means that in the uncoupled system, the sites where $\phi = 0$ and those where $\phi = 2\pi$ are separated by a site where $\phi = \pi$. For a semifluxon, there is no such a configuration as there is no value of ϕ between 0 and π that satisfies the uncoupled discrete sine-Gordon equation.

Remark 5.6. In the ordinary discrete sine-Gordon equation, there is a barrier for a kink to move in space, the so-called Peierls-Nabarro barrier [2]. The barrier is defined as the energy difference between a kink sitting on a site and a kink sitting between two consecutive sites. This barrier exists because 2π-kinks have space translational invariance, while there is no such property for a semifluxon. Therefore for a lattice semifluxon the barrier with the above definition *unlikely* exists, contrary to what was suggested earlier in [9].

The spectral stability of $\phi_\pi^i(n;a;\gamma)$ is obtained by substituting $\phi_n = \phi_\pi^i(n;a;\gamma) + v_n e^{\lambda t}$ to the model equation (3.2.3). Disregarding the higher order terms gives the following eigenvalue problem

$$L^i(a;\gamma)v = \Lambda v, \tag{3.5.5}$$

where $v = (\dots, v_{-1}, v_0, v_1, \dots)^T$ and $L^i(a;\gamma)$ is a linear discrete operator

$$L^i(a;\gamma) = \frac{1}{a^2}\begin{pmatrix} \ddots & \ddots & \ddots & & & & 0 \\ & 1 & J^i_{-1} & 1 & & & \\ & & 1 & J^i_0 & 1 & & \\ & & & 1 & J^i_1 & 1 & \\ 0 & & & & \ddots & \ddots & \ddots \end{pmatrix}$$

$$J^i_n = -2 - a^2\cos\left(\phi^i_\pi(n;a;\gamma) + \theta_n\right), \quad n \in \mathbb{Z},$$

that corresponds to the continuous operator $\mathcal{L}^i(x;\gamma)$. This is an infinite dimensional matrix problem which is real and symmetric. Thus, the eigenvalues must be real.

In the discrete case, the continuous spectrum of semikinks is finite. The spectrum is obtained by substituting $v_n = e^{-i\kappa an}$ to Eq. (3.5.5) with $J^i_n = -2 - a^2\sqrt{1-\gamma^2}$ from which one obtains the following dispersion relation for such linear waves

$$\Lambda = -\left(\sqrt{1-\gamma^2} + \frac{4}{a^2}\sin^2(\frac{\kappa a}{2})\right). \tag{3.5.6}$$

Hence, we get that the continuous spectrum λ ranges in the interval $\pm i[\sqrt[4]{1-\gamma^2}, \sqrt{\sqrt{1-\gamma^2} + 4/a^2}]$.

Lemma 3.13. *Let $\epsilon = 1/a^2$. Given $\gamma = \epsilon\tilde{\gamma}$, for ϵ small enough, the largest eigenvalue of the operator $L^1(a;\gamma)$ is strictly negative up to $O(\epsilon^2)$.*

Proof. The eigenvalue problem to calculate the stability of the monotonically increasing series representing a π-kink $\phi^1_\pi(n;\infty;\gamma)$, $n \in \mathbb{Z}$ is given by (see (3.5.5)):

$$L^1(a;\gamma)v = \Lambda v, \tag{3.5.7}$$

with $v = (\dots, v_{-1}, v_0, v_1, \dots)$.

The spatially decaying solution that corresponds to the largest eigenvalue of the above eigenvalue problem, following Baesens, Kim, and MacKay [24] can be approximated by

$$v_n = \begin{cases} c\ell^{-n}, & n \leq 0, \\ c\ell^{n-1}, & n \geq 1, \end{cases} \tag{3.5.8}$$

for some c and $|\ell| < 1$. Considering the type 1 semifluxon that is given by (3.5.1), this Ansatz is a solution of the eigenvalue problem (3.5.7) up to and including $O(\epsilon)$.

For small nonzero ϵ, if we can match exponentially decaying solutions (3.5.8) on both sides from either end of the lattice to a central site, then we obtain a candidate for an eigenfunction. For $|n| \to \infty$, Eq. (3.5.7) will determine the decay exponent ℓ, i.e.

$$\Lambda = -\sqrt{1 - \epsilon^2\tilde{\gamma}^2} + \epsilon(\ell - 2 + 1/\ell). \tag{3.5.9}$$

The matching condition at the central sites $n = 0, 1$ is given by the relation:

$$\Lambda = -\cos(\epsilon(\pi + \tilde{\gamma})) + \epsilon(-1 + \ell). \tag{3.5.10}$$

Combining (3.5.9) and (3.5.10) leads to the eigenvalue Λ and the decay exponent ℓ as a function of ϵ and $\tilde{\gamma}$, i.e.

$$\ell = 1 + \frac{1}{2}(\tilde{\gamma}^2 - (\pi + \tilde{\gamma})^2)\epsilon + O(\epsilon^2), \tag{3.5.11}$$

$$\Lambda = -1 + \frac{1}{2}\tilde{\gamma}^2\epsilon^2 + O(\epsilon^3). \tag{3.5.12}$$

□

Remark 5.7. One can show that a semikink of type 1 in the weak-coupling case has only one eigenvalue by proving that there is no antisymmetric solution to the eigenvalue problem. This is according to Atkinson's theorem [25] which is the discrete version of the Sturm-Liouville theorem. According to [24], an approximation to the eigenfunction that corresponds to the next largest eigenvalue can be given by

$$v_n = \begin{cases} c\ell^{-n}, & n \leq 0, \\ -c\ell^{n-1}, & n \geq 1. \end{cases}$$

When the applied bias current γ is close to $\gamma_{\rm cr}(a)$, we have the following stability result of a type 1 lattice semifluxon.

Lemma 3.14. *Let $\epsilon = 1/a^2$. Given $\gamma = 1 - \epsilon\tilde{\gamma}$, for $0 < \widetilde{\gamma} - \pi \ll 1$, the largest eigenvalue of the operator $L^1(a;\gamma)$ is strictly negative up to $O(\epsilon)$. For $\widetilde{\gamma} = \pi$, the operator $L^1(a; 1 - \epsilon\widetilde{\gamma})$ has $0 + O(\epsilon)$ as its largest eigenvalue.*

Proof. In the proof of Lemma 3.13, we take a symmetric approximation to the spatially decaying solution of the eigenvalue problem (3.5.7). The fact that the ansatz is symmetric is because the type 1 lattice solution $\phi_\pi^1(n;\infty;\gamma)$ is symmetric up to $O(\epsilon^2)$ for small γ.

Since for large γ, $\phi_\pi^1(n;\infty;\gamma)$ is asymmetric up to $O(\epsilon)$ (see (3.5.3)), it is natural to expect that our approximate function to the solution of (3.5.7) should also be asymmetric. Therefore, as an Ansatz, we take

$$v_n = \begin{cases} c_1\ell^{-n}, & n \le 0, \\ c_2\ell^{n-1}, & n \ge 1, \end{cases} \tag{3.5.13}$$

for some c_1 and c_2 and $|\ell| < 1$. This is a solution of the eigenvalue problem (3.5.7) up to and including $O(\sqrt{\epsilon})$.

Doing the same steps as in the proof of Lemma 3.13, the eigenvalue problem (3.5.7) gives the following equations

$$\epsilon(1/\ell - 2 + \ell) - \Lambda - \sin(\sqrt{\epsilon 2\widetilde{\gamma}}) = 0, \tag{3.5.14}$$

$$\epsilon(c_l\ell - 2c_1 + c_2) - \Lambda c_1 - \sin(\sqrt{2\epsilon(\widetilde{\gamma} - \pi)})c_1 = 0, \tag{3.5.15}$$

$$\epsilon(c_1 - 2c_2 + c_2\ell) - \Lambda c_2 - \sin(\sqrt{2\epsilon(\widetilde{\gamma} + \pi)})c_2 = 0. \tag{3.5.16}$$

Equation (3.5.15) gives

$$c_1 = \frac{\epsilon c_2}{\Lambda + \sqrt{2\epsilon}\sqrt{\gamma - \pi} - \epsilon(\ell - 2)}.$$

Subsequently, from (3.5.14) and (3.5.16) we obtain

$$\ell = K_1(\widetilde{\gamma})\sqrt{\epsilon} + O(\epsilon) \approx \left(\frac{(\sqrt{\pi} + \sqrt{\widetilde{\gamma} - \pi})(3\sqrt{2} - 4)}{2(-1 + \sqrt{2})^2\pi} + O(\widetilde{\gamma} - \pi)\right)\sqrt{\epsilon}, \tag{3.5.17}$$

$$\Lambda = K_2(\widetilde{\gamma})\sqrt{\epsilon} + O(\epsilon) \approx \left(\underbrace{-\frac{(4\sqrt{2} - 6)\sqrt{\widetilde{\gamma} - \pi}}{4 - 3\sqrt{2}}}_{1.4142\sqrt{\widetilde{\gamma} - \pi}} + O(\widetilde{\gamma} - \pi)\right)\sqrt{\epsilon}, \tag{3.5.18}$$

with $K_2(\pi) \equiv 0$.

□

3.6 Numerical computations of the discrete system

To accompany our analytical results, we have used numerical calculations. For that purpose, we have made a continuation program based on Newton iteration technique to obtain the stationary kink equilibria of Eqs. (3.2.3) and (3.2.4) and an eigenvalue problem solver in MATLAB. To start the iteration, one can choose either the

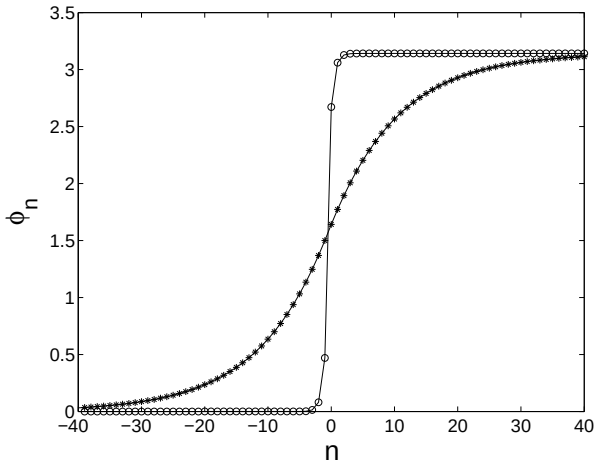

Figure 3.6: *Two lattice semifluxons of type 1 are plotted as a function of the lattice index, namely the kink for a very weakly discrete array $a = 0.1$ $(-*-)$, i.e. close to Eq. (3.3.6) and the kink for a very strongly discrete array $a = 2$ $(-o-)$.*

continuum solutions discussed in the previous section or trace the equilibria from the uncoupled limit $a \to \infty$. We use the number of computational sites $2N = 800$ for parameter values of $a = 0.05$ or larger.

3.6.1 Stability of type 1 lattice soliton

The type 1 lattice semifluxon $\phi_\pi^1(n; a; \gamma)$, $n \in \mathbb{Z}$ admitted by the system for two different values of discreteness parameter a is presented in Fig. 3.6. For a given value of a, one can use as the initial guess either a solution from the continuous limit (3.3.6) or from the uncoupled limit that has been discussed in the preceeding sections.

In Fig. 3.7 we present the numerically calculated spectra of type 1 semifluxon as a function of the discreteness parameter. The approximate function (3.4.11) for a small and the one for a large derived in Lemma 3.13 are in a good agreement with the numerically obtained largest eigenvalue. Any eigenvalue below $\Lambda = -1$ belongs to the continuous spectrum. For a close to zero we do not see dense spectra because of the number of sites we used. By increasing the sites-number we will obtain a denser spectrum.

There is only one eigenvalue outside the phonon bands which is in agreement with our theoretical prediction given in Remark 5.7. This is in contrast to the case of an ordinary lattice 2π-kink [26, 27] where there is an internal mode bifurcating from the essential spectrum when the parameter a increases.

When a bias current is applied, it has been shown that there is a critical bias current for the existence of a static type 1 lattice semifluxon. The numerically calculated $\gamma_{\rm cr}$

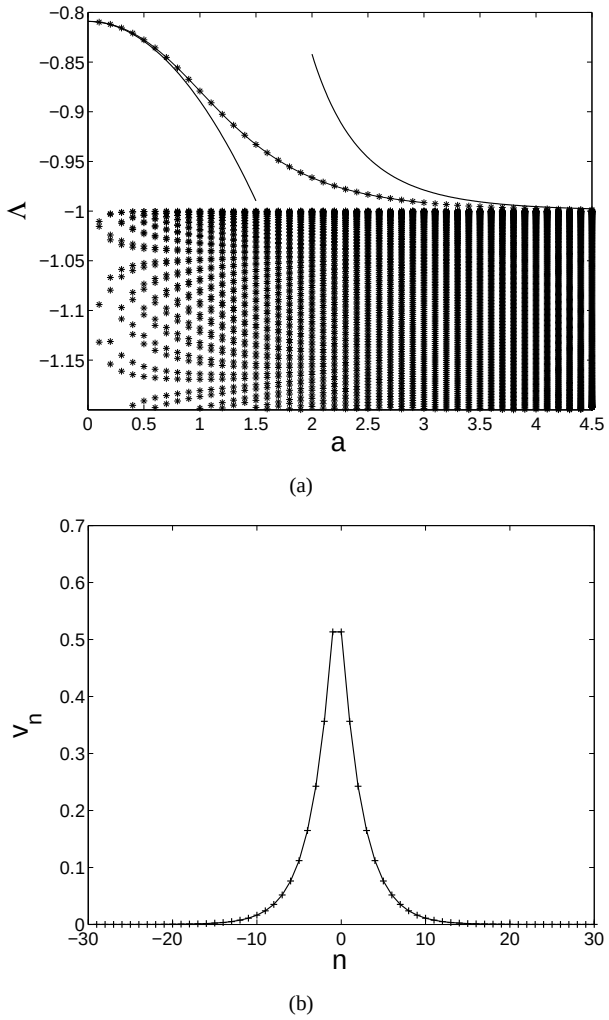

Figure 3.7: *(upper) Numerically computed point spectrum of a lattice semifluxon againsts the discreteness parameter with $\gamma = 0$. We used the number of sites $2N = 300$. We zoom in the plot of spectra around -1 for clarity. The bold-solid-line is the calculated approximate function for the point spectrum using perturbation theory. (lower) The eigenfunction (localized mode) of the point spectrum for $a = 1.5$.*

of the real discrete system (3.2.3) as a function of a is presented in Fig. 3.8. The approximate functions for small a (3.4.7) and large a (3.5.4) calculated in the previous sections are presented as dashed lines.

Our numerical computation shows that the value of γ above which static lattice semi-fluxons disappear is also the value of γ at which the largest eigenvalue is zero.

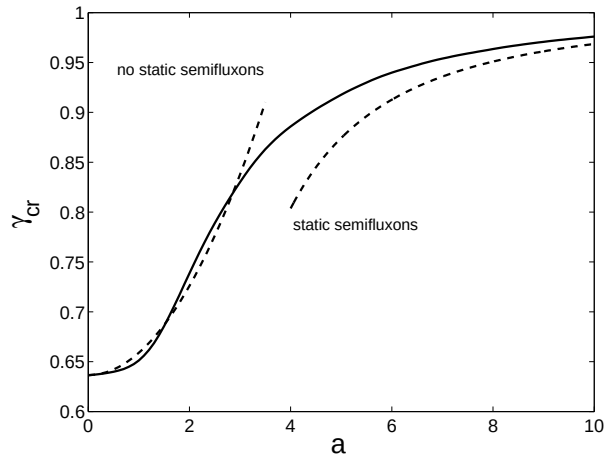

Figure 3.8: *The critical bias current of a stable π-kink as a function of the discreteness parameter a. For γ above the critical current there is no static π-kink solution. The solid line is numerically obtained curve. Dashed lines are calculated from the case of $a \ll 1$ and from the weak-coupling case $a \gg 1$. For a clear explanation on the derivation of the curves see the text.*

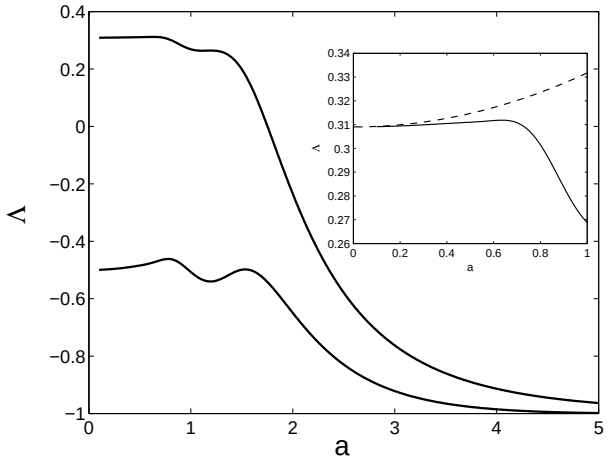

Figure 3.9: *Plot of the eigenvalues of a 3π-kink as a function of the discreteness parameter a. We zoom in the almost continuous region $a \ll 1$ where it shows that discreteness even destabilizes the kink. The dashed line depicts our analytically computed approximation to the largest eigenvalue of the kink* (3.4.12).

3.6.2 Instability of type 2 lattice soliton

First, the stability of a 3π-kink which is the limiting solution of lattice type 2 semifluxons when $\gamma \to 0$, i.e. $\phi_\pi^2(n;\infty;0)$, will be studied numerically.

In the previous section on weak coupling limit, type 2 lattice semifluxons were not considered because $\phi_\pi^2(n;\infty;\gamma)$ was not known in that limit. Using our continuation program, we have followed a 3π-kink solution from the continuous limit $0 < a \ll 1$ up to the uncoupled situation $a = \infty$. We obtain that $\phi_\pi^2(n;\infty;0)$ is given by

$$\phi_\pi^2(n;\infty;0) = \begin{cases} 0, & n = -1, -2, \ldots \\ 2\pi, & n = 0, \\ \pi, & n = 1, \\ 3\pi, & n = 2, 3, \ldots. \end{cases} \tag{3.6.1}$$

Note that this stable configuration is not monotonically increasing.

In Fig. 3.9, we present the numerically obtained eigenvalues of a 3π-kink as a function of the discreteness. For small a, the largest eigenvalue is indeed increasing as is predicted by the perturbation theory (3.4.12). As soon as the discreteness is of order one, the largest eigenvalue decreases and becomes zero at approximately $a = 1.7521$.

Interestingly, when $\gamma \neq 0$ discreteness cannot stabilize a type 2 semikink, contrary to the case of $\gamma = 0$. In Fig. 3.10, we show plot of type 2 semikinks as well as their largest eigenvalue as a function of $\epsilon = 1/a^2$ for two particular values of γ, namely $\gamma = 0.01$ and $\gamma = 0.1$. The scaling in the horizontal axis is made in that way because an eigenvalue can have a peculiar behavior when the system is weakly coupled.

It is important to notice from Fig. 3.10 that the solutions are unstable even in the weak-coupling limit. It is interesting because this always unstable type 2 semikink is a concatenation of a 3π-kink and a -2π-kink, while a 3π-kink has been shown to be stable in the uncoupled limit. A -2π-kink itself can also be stable in that limit.

This instability issue can be explained by looking at the final expression of a type 2 semikink when it is uncoupled. For the two particular choices of γ above, it is given by

$$\phi_\pi^2(n;\infty;0.01) = \begin{cases} 0, & n = -1, -2, \ldots \\ \pi, & n = 0, 1, \\ 3\pi, & n = 2, \ldots, 8, \\ 2\pi, & n = 9, \\ \pi, & n = 10, 11, \ldots, \end{cases} \tag{3.6.2}$$

and

$$\phi_\pi^2(n;\infty;0.1) = \begin{cases} 0, & n = -1, -2, \ldots \\ \pi, & n = 0, 1, \\ 3\pi, & n = 2, \ldots, 6, \\ 2\pi, & n = 7, \\ \pi, & n = 8, 9, \ldots. \end{cases} \tag{3.6.3}$$

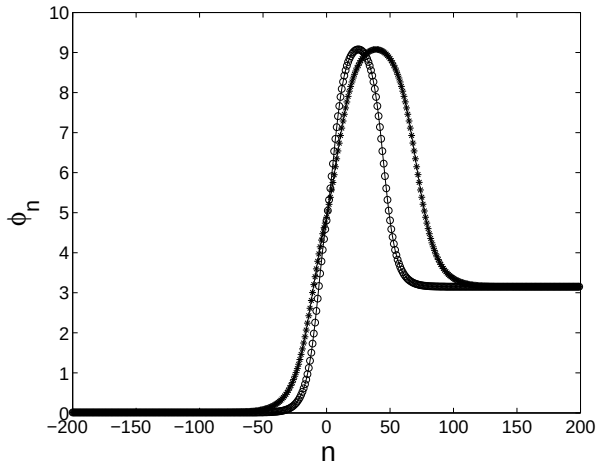

(a)

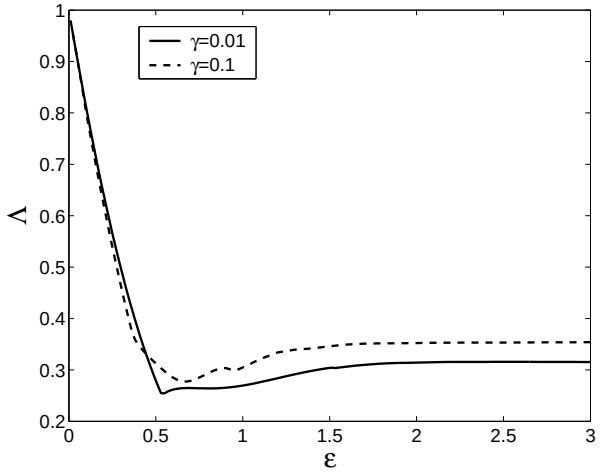

(b)

Figure 3.10: *((a) Plot of a type 2 semikink with* $\gamma = 0.01$ *for two different values of* ϵ*, i.e.* $\epsilon = 100$ *(*$-*$*$-$*) and* $\epsilon = 40$ *(*$-o-$*). (b) Plot of the largest eigenvalue of a lattice type 2 semikink as a function of discreteness parameter* ϵ*. When* $\epsilon = 0$*, the eigenvalue is* $\Lambda = \sqrt{1-\gamma^2}$*.*

We see that there are two sites, i.e. $n = 0$ and $n = 9$ for $\gamma = 0.01$ and $n = 0$ and $n = 7$ for $\gamma = 0.1$, where ϕ takes the 'wrong' value, that is of an unstable fixed point of the mapping $\phi \to -\sin\phi$. Looking only at sites numbered $n = 2$ to $n \to \infty$, $\phi_\pi^2(n;\infty;\gamma)$ can be viewed as a -2π lattice kink sitting on a site which is known to be unstable. If we look only at sites numbered $n = 1$ to $n \to -\infty$, $\phi_\pi^2(n;\infty;\gamma)$ can be seen as a deformed 3π lattice kink. Hence, it can be concluded that coupling between the two kinks due to the presence of a nonzero γ is responsible for the instability.

Concerning the applied bias current, it has been discussed in the previous sections that there is a critical current γ^* for the existence of a type 2 lattice semikink. Nevertheless, we did not calculate $\gamma^*(a)$ of the real discrete system (3.2.3) because it has less physical interest as $\phi_\pi^2(n;\infty;\gamma)$ is always unstable.

3.6.3 Instability of type 3 lattice solution

In this subsection, we will consider lattice semikinks of type 3, $\phi_\pi^3(n;a;\gamma)$, that has been shown in Lemma 3.5 to be unstable in the continuous version.

The largest eigenvalue of a lattice type 3 semifluxon for three particular values of γ, i.e. $\gamma = 0.01, 0.1, 0.55$, is presented in Fig. 3.11. Even though a semifluxon of this type is a concatenation of a 2π-kink and a $-\pi$-kink that can be stable in the discrete case, it is unstable as a whole from the continuous limit all the way to the very discrete case. The explanation is similar to the case of a lattice type 2 semikink discussed above.

For the three particular choices of γ above, $\phi_\pi^3(n;\infty;\gamma)$ is given by

$$\phi_\pi^3(n;\infty;0.01) = \begin{cases} 0, & n = -1,-2,\dots \\ \pi, & n = -6, \\ 2\pi, & n = -5,\dots,0, \\ \pi, & n = 1,2,\dots, \end{cases} \tag{3.6.4}$$

$$\phi_\pi^3(n;\infty;0.1) = \begin{cases} 0, & n = -1,-2,\dots \\ \pi, & n = -2, \\ 2\pi, & n = -1,0, \\ \pi, & n = 1,2,\dots, \end{cases} \tag{3.6.5}$$

and

$$\phi_\pi^3(n;\infty;0.55) = \begin{cases} 0, & n = -1,-2,\dots \\ \pi, & n = 0,1,2,\dots. \end{cases} \tag{3.6.6}$$

One interesting point to note for a type 3 lattice semikink is that the number of sites with value 2π is decreasing as γ increases. Starting from the continuous version of a type 3 lattice semikink as the initial guess for the continuation program, it disappears for $\gamma \geq \gamma^*(a)$ (see (3.4.6)). Its final configuration is similar to the stable π-kink (3.5.1), but translated by one site.

3.7 Conclusions

To conclude, we have done stability analysis for three types of lattice π-kink of the discrete 0-π sine-Gordon equation numerically and analytically. Analytical calcu-

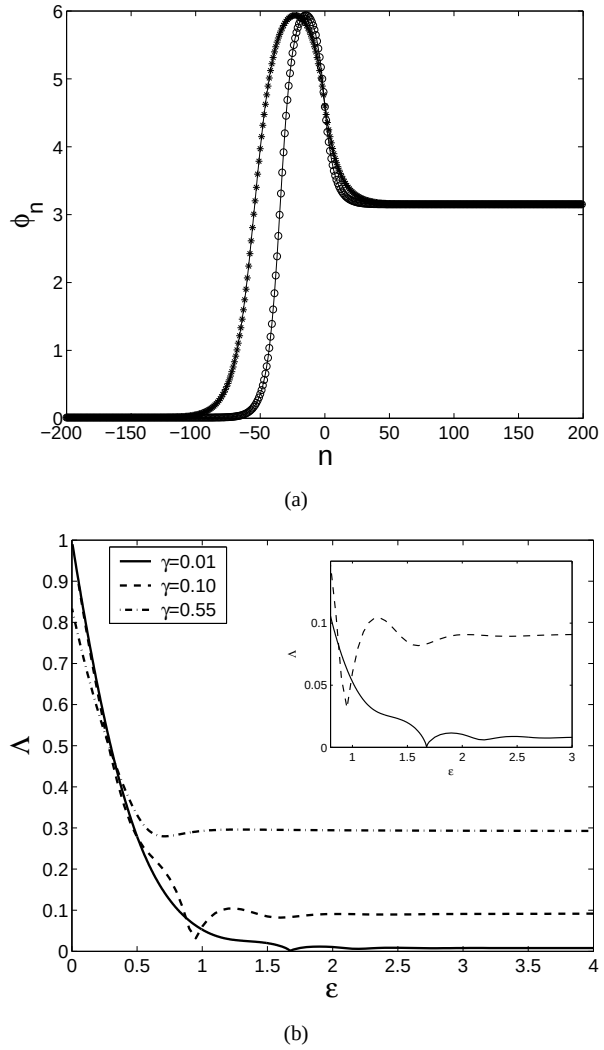

Figure 3.11: *The same as Fig. 3.11 but for type 3 semikink. We zoom in the region where the largest eigenvalues oscillate.*

lations have been done in the continuum limit, i.e. the 0-π sine-Gordon equation, and the weak-coupling case. It has been shown that in the continuous 0-π sine-Gordon equation, π-kinks of type 1 are stable and the other types are unstable. In the discrete case, we have computed the spectrum of the π-kinks and obtained the curve of the eigenvalues as a function of the discreteness parameter. An approximate function to the curves has been derived. For a 3π-kink, we have shown that relatively small discreteness even destabilizes a 3π-kink.

For future research, it is of interest to see what happens to the isolated eigenvalues of a lattice π- and 3π-kink if we, e.g., replace the potential with the Peyrard-Remoissenet (PR) potential [29]. Using PR potential, one might expect to have many isolated eigenvalues and the bifurcation of high-frequency internal modes from the continuous spectrum [30]. The nucleation of kinks and antikinks when we apply a constant force above the critical value is also interesting for further studies. One question that can be addressed is the frequency of the nucleation as a function of the applied constant force in the presence of a damping coefficient (the α-term). Note also that even though type 3 semifluxons are unstable, but the largest eigenvalue is close to zero. In fact, a type 3 semifluxon consists of a fluxon and a semifluxon with the opposite polarity. In experiments, the presence of a fluxon near by a semifluxon can influence a junction measurement [31]. Because a fluxon can be pinned by a defect [1], one can expect to have a stable type 3 semifluxon when there is a defect present in the system.

Bibliography

[1] Yu. S. Kivshar and B. A. Malomed, *Dynamics of solitons in nearly integrable systems*, Rev. Mod. Phys. **61**, 763 (1989); *ibid.* **63**, 211(A) (1991).

[2] O. M. Braun and Yu. S. Kivshar, *Nonlinear dynamics of the Frenkel-Kontorova model*, Phys. Rep. **306**, 1 (1998).

[3] L.N. Bulaevskii, V.V. Kuzii, and A. A. Sobyanin, *Superconducting system with weak coupling to the current in the ground state*, JETP Lett. **25**, 290 (1977); L.N. Bulaevskii, V.V. Kuzii, A. A. Sobyanin, and P.N. Lebedev, *On possibility of the spontaneous magnetic flux in a Josephson junction containing magnetic impurities*, Solid State Comm. **25**, 1053 (1978).

[4] C.C. Tsuei and J.R. Kirtley, *Pairing symmetry in cuprate superconductors*, Rev. Mod. Phys. **72**, 969 (2000).

[5] V.V. Ryazanov, V.A. Oboznov, A.Yu. Rusanov, A.V. Veretennikov, A.A. Golubov, and J. Aarts, *Coupling of Two Superconductors through a Ferromagnet: Evidence for a π Junction*, Phys. Rev Lett. **86**, 2427 (2001).

[6] J.J.A. Baselmans, A.F. Morpurgo, B.J. van Wees, and T.M. Klapwijk, *Reversing the direction of the supercurrent in a controllable Josephson junction*, Nature (London) **397**, 43 (1999).

[7] H. Hilgenkamp, Ariando, H. J. H. Smilde, D.H.A. Blank, G. Rijnders, H. Rogalla, J.R. Kirtley, and C.C. Tsuei, *Ordering and manipulation of the magnetic moments in large-scale superconducting π-loop arrays*, Nature (London) **422**, 50 (2003).

[8] H. Susanto, S. A. van Gils, T. P. P. Visser, Ariando, H. J. H. Smilde, and H. Hilgenkamp, *Static semifluxons in a long Josephson junction with π-discontinuity points*, Phys. Rev. B. **68**, 104501 (2003).

[9] H. Susanto and S. A. van Gils, *Instability of a lattice semifluxon in a current-biased 0-π array of Josephson junctions* Phys. Rev. B **69**, 092507 (2004).

[10] N. R. Quintero, A. Sánchez, and F. G. Mertens, *Anomalous Resonance Phenomena of Solitary Waves with Internal Modes*, Phys. Rev. Lett. **84**, 871 (2000).

[11] P. Rosenau, *Hamiltonian dynamics of dense chains and lattices: or how to correct the continuum*, Phys. Lett. A **311**, 39 (2003).

[12] T. Kato and M. Imada, *Vortices and Quantum tunneling in Current-Biased 0-π-0 Josephson Junctions of d-wave Superconductors*, J. Phys. Soc. Jpn. **66**, 1445 (1997).

[13] A. B. Kuklov, V.S. Boyko, and J. Malinsky, *Instability in the current-biased 0-π Josephson junction*, Phys. Rev. B **51**, 11965 (1995); *ibid.* **55**, 11878(E) (1997).

[14] G. Derks, A. Doelman, S. A. van Gils and T. P. P. Visser, *Traveling waves in a singularly perturbed sine-Gordon equation*, Physica D **180**, 40 (2003).

[15] E.C. Titchmarsh, *Eigenfunction expansions associated with second-order differential equations* (2nd edition), Oxford University Press, 1962.

[16] E. Mann, *Systematic perturbation theory for sine-Gordon solitons without use of inverse scattering methods*, J. Phys. A: Math. Gen. **30**, 1227 (1997).

[17] J. Guckenheimer and P. Holmes, *Nonlinear Oscillations, Dynamical Systems and Bifurcation of Vector Fields*, 2nd ed. (Springer-Verlag, New York, 1986).

[18] A. Scott, *Nonlinear science: emergence and dynamics of coherent structures*, Oxford University Press, 1999.

[19] B. V. Chirikov, *A Universal Instability of Many-Dimensional Oscillator Systems*, Phys. Rep. **52**, 264 (1979).

[20] Y. Nomura, Y. H. Ichikawa, and A. T. Filippov, *Stochasticity in the Josephson Map*, J. Plasma Phys. **56**, 493 (1996).

[21] R. S. MacKay and J. A. Sepulchre, *Multistability in networks of weakly coupled bistable units*, Physica D **82**, 243 (1995).

[22] D. E. Pelinovsky, P. G. Kevrekidis, and D. J. Frantzeskakis, *Stability of discrete solitons in nonlinear Schrödinger lattices* , Physica D **212**, 1 (2005).

[23] N. J. Balmforth, R. V. Craster, and P. G. Kevrekidis, *Being stable and discrete*, Physica D **135**, 212 (2000).

[24] C. Baesens, S. Kim, and R. S. MacKay, *Localised modes on localised equilibria*, Physica D **113**, 242 (1998).

[25] F. V. Atkinson, *Discrete and Continuous Boundary Problems*, vol. 8 of Mathematics in Science and Engineering, (Academic Press, New York, 1964).

[26] P. G. Kevrekidis and C. K. R. T. Jones, *Bifurcation of internal solitary wave modes from the essential spectrum*, Phys. Rev. E **61**, 3114 (2000).

[27] Yu. S. Kivshar, D. E. Pelinovsky, T. Cretegny, and M. Peyrard, *Internal Modes of Solitary Waves*, Phys. Rev. Lett. **80**, 5032 (1998).

[28] M. Peyrard and M. D. Kruskal, *Kink dynamics in the highly discrete sine-Gordon system*, Physica D **14**, 88 (1984).

[29] M. Peyrard and M. Remoissenet, *Solitonlike excitations in a one-dimensional atomic chain with a nonlinear deformable substrate potential*, Phys. Rev. B **26**, 2886 (1982).

[30] O. M. Braun, Yu. S. Kivshar, and M. Peyrard, *Kink's internal modes in the Frenkel-Kontorova model*, Phys. Rev. E **56**, 6050 (1997).

[31] D. J. van Harlingen, *Phase-sensitive tests of the symmetry of the pairing state in the high-temperature superconductors–Evidence for* $d_{x^2-y^2}$ *symmetry*, Rev. Mod. Phys. **67**, 515 (1995).

Stability analysis of solitary waves in a tricrystal junction

Chapter 4

We consider a tricrystal junction, i.e. a system of three long Josephson junctions coupled at a common end point. The system admits solitary waves sitting at or near the common point. Especially when one of the junctions is a π-junction, there is a solitary wave created at the common point. The stability and the dynamics of all existing solitary waves of the time-independent system are studied analytically and numerically. The present study is of interest also for experimentalists since the system is a base for a network of transmission lines.

4.1 Introduction

An attractive application of Josephson junctions is their applicability for logic devices based on the Josephson effect for high-performance computers [1, 2]. Employing flux quanta as information bits, the method is based on manipulating the properties, e.g. the stability, of fluxons. Nakajima, Onodera and Ogawa [3] proposed a network of Josephson junctions that is made by several junctions connected at a point. Following Nakajima et al., we also call this common point *the turning point*, which is denoted by the point 0 in Fig. 4.1. The circuits allow one to control the behavior of Josephson vortices to achieve a complete logic capability [2, 3, 4]. One of the circuits is named STP (selective turning point) where a moving integer fluxon can be trapped at the turning point.

Later, it is discussed in [6, 7] that the STP equation can be used to describe an edge dislocation formed by an incomplete copper-oxide layer. The situation can be realized during the preparation of a stacked system. The authors show that a trapped vortex at the turning point executes harmonic oscillations around the equilibrium position.

Recently, Kogan, Clem and Kirtley [5] considered Josephson vortices at tricrystal boundaries. This tricrystal problem is also described by the same equations as the above mentioned STP circuit. In [5], the presence of a half-flux-quantum $\Phi_0/2$ vortex is discussed when one of the three Josephson junctions is a π-junction. They also consider the existence of vortices with multiple half-flux-quantum $3\Phi_0/2$ and $5\Phi_0/2$.

Here, we will calculate analytically the stability of solitary waves admitted by a tricrystal junction. Knowing the eigenvalues of a state can be of importance from an application point of view. In the time-independent case, a static solitary wave of a tricrystal junction can be sitting at or near the turning point depending on the combination of the Josephson lengths. We will consider a general case when the Josephson lengths of the junctions λ_J's are not the same.

The present chapter is organized in the following way. In Section 4.2 we will recall the governing equations as derived in [3, 4, 5]. In Section 4.3 we discuss the stability of integer fluxons sitting at or near the common point. This section consists of two parts, respectively discussing one and two vortices sitting at or near the common point. The case when one junction is a π-junction is discussed in Section 4.4. We give the conclusion in Section 4.5.

4.2 Mathematical Model

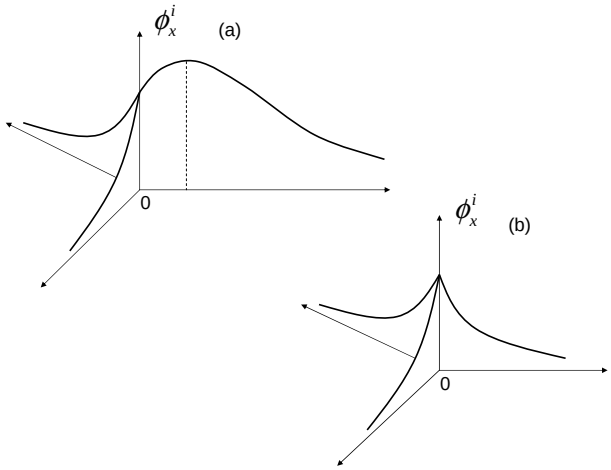

Figure 4.1: *A sketch of two possible field distributions ϕ_x^i of a static solitary wave in the tricrystal junction. If the maximum field is not at the intersection point, then we say that the solitary wave is sitting outside the intersection (a). In (b), the maximum of ϕ_x^i is achieved at the common point.*

The phase difference along the junctions is described by the following perturbed sine-Gordon equation [3, 4]

$$\lambda_i^2 \phi_{xx}^i - \phi_{tt}^i = \sin[\phi^i(x) + \theta^i], \tag{4.2.1}$$

with $i = 1, 2, 3,\ x > 0,\ t > 0$. The position of the common end point is then at $x = 0$. The parameter λ_i denotes the Josephson length of the ith junction. The subscript J of the Josephson length is omitted for brevity. The index i numbers the junction. The constant parameter θ^i represents the type of the ith junction, i.e. θ^i equals 0 or π. The boundary conditions at the intersection $x = 0$ are

$$\begin{aligned} &\phi^1 + \phi^2 + \phi^3 = 0, \\ &\phi_x^1 = \phi_x^2 = \phi_x^3. \end{aligned} \tag{4.2.2}$$

The first equation is given by the condition that the magnetic flux through an infinitesimally small contour is zero. The second equations describe the continuity of the

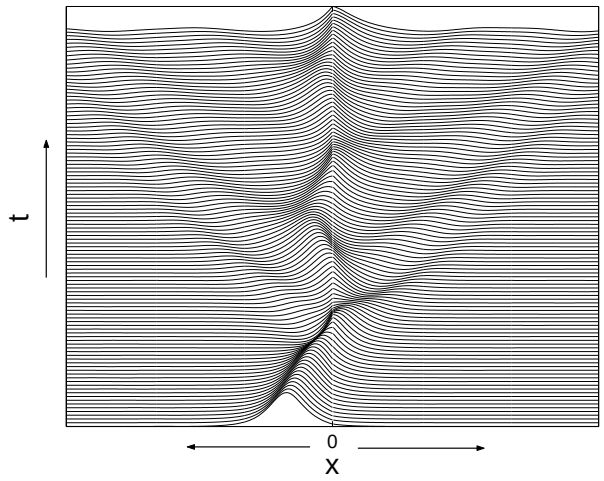

Figure 4.2: *The evolution of a fluxon moving with velocity 0.5 toward $x = 0$ that is trapped at the turning point. The plot is made in terms of the magnetic field ϕ^i_x. In the figure, to the left and to the right of $x = 0$ is junction 1 and 2, respectively. When $\lambda_2 = \lambda_3$, $\phi^2 = \phi^3$. The parameter values we take are $\lambda_1 = \lambda_2 = \lambda_3$. The scattered-waves can be seen as well.*

magnetic fields. One reaches the same value of the field at the origin no matter along which of the junctions the origin is approached.

The total energy that corresponds to Eq. (4.2.1) is given by [5]

$$H = \sum_i \int_0^\infty \frac{1}{2}\left(\lambda_i \phi^i_x\right)^2 + \cos(\theta^i)\left(1 - \cos\phi^i\right) dx. \tag{4.2.3}$$

We consider the time-independent solution of Eq. (4.2.1). The equation can admit static localized solutions, two of which are sketched in Fig. 4.1. The magnetic field configuration of each state is determined by the Josephson lengths of the junctions. Here, we will calculate analytically the linear stability of those static solutions.

4.3 Conventional tricrystal junctions

The first case that we will consider is a conventional tricrystal junction which is represented by $\theta^i = 0$ for all i in (4.2.1). A fluxon moving in a conventional tricrystal junction toward the common point can be either trapped, reflected or pass through the point. This is the basic operation of a tricrystal junction as a logic gate proposed in [2]. In Fig. 4.2, we show the evolution of a fluxon that is trapped by the common point. In this case, the common point acts as a potential well. One can see that the trapped fluxon oscillates about the common point. The oscillation frequency for the case of $\lambda_1 = \lambda_2 = \lambda_3$ has been calculated in [7].

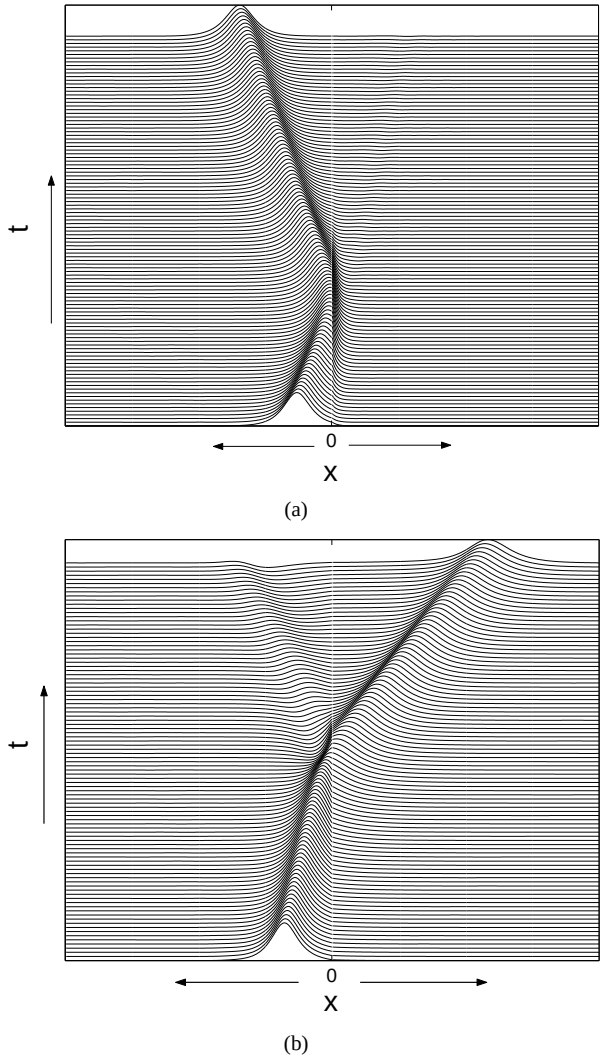

Figure 4.3: *The same as Fig. 4.2, but in the reflection (a) and the transmission (b) case. The parameter values we take are (a)* $\lambda_1 = 1$ *and* $\lambda_2 = \lambda_3 = 0.4$*; and (b)* $\lambda_2 = 1$, $\lambda_2 = 2$ *and* $\lambda_3 = 0.5$*. The reflection and the transmission of a* 2π*-kink can be caused by either the instability of a time-independent* 2π *kink solution admitted by (4.2.1) at the same parameter values or by the non-existence of such static solitary waves.*

When the Josephson penetration depth λ_i of the junctions differs from each other, an incoming fluxon can either pass or be reflected by the common point. Examples of such evolutions are shown in Fig. 4.3. It is then of interest to know which combinations of Josephson lengths correspond to transmission, reflection, and trapping of an incident fluxon.

To proceed, we will assume that the incoming fluxon moves with an infinitesimal velocity. In this case we only need to consider the existence and the linear stability of a time-independent solitary wave admitted by equation (4.2.1). If a static solitary wave is stable, then it is an indication that an incident fluxon will be trapped by the common point.

A static solution of Eq. (4.2.1) representing a 2π-fluxon sitting at or near the common point is given by [5]

$$\begin{aligned} \phi_0^1 &= 4\tan^{-1} e^{(x-x_1)/\lambda_1}, \\ \phi_0^2 &= 4\tan^{-1} e^{(x-x_2)/\lambda_2} - 2\pi, \\ \phi_0^3 &= 4\tan^{-1} e^{(x-x_3)/\lambda_3} - 2\pi, \end{aligned} \tag{4.3.1}$$

where the x_i are determined by (4.2.2). For simplicity we scale the Josephson lengths to $\sum \lambda_i = 1$, so that we have only two free parameters, e.g., λ_2 and λ_3, and $\lambda_1 = 1 - \lambda_2 - \lambda_3$. The domain of the Josephson parameter is then bounded by the lines $\lambda_2 = 0$, $\lambda_3 = 0$, and $\lambda_2 + \lambda_3 = 1$.

Expression (4.3.1) does indeed represent a 2π-kink because the total Josephson phase is 2π when one circles the common point at large distances, i.e. $\sum_i \phi_0^i(\infty) = 2\pi$.

First we will derive how x_i, $i = 1, 2, 3$, from Eq. (4.2.1) depend on λ_2 and λ_3. The procedure we will present below is a summary of the steps given in [5].

Substituting (4.3.1) into the boundary conditions (4.2.2) gives the following equations

$$\begin{aligned} &\gamma_2\eta = \sin 2\alpha_2,\ \gamma_3\eta = \sin 2\alpha_3, \\ &\alpha_3 = \pi - \alpha_1 - \alpha_2, \end{aligned} \tag{4.3.2}$$

where

$$\begin{aligned} \gamma_i &= \lambda_i/\lambda_1, \\ \eta &= \sin 2\alpha_1, \\ \alpha_i &= \tan^{-1} e^{-x_i/\lambda_i}. \end{aligned} \tag{4.3.3}$$

After some algebraic calculations, the last equation of (4.3.2) gives the following equation for η

$$\gamma_3\eta = \eta\sqrt{1-(\gamma_2\eta)^2} + \gamma_2\eta\sqrt{1-\eta^2}. \tag{4.3.4}$$

This equation has a positive root $0 < \eta < 1$ that is given by

$$\eta = \frac{\sqrt{-1 + 2(\gamma_2^2 + \gamma_3^2 + \gamma_2^2\gamma_3^2) - \gamma_2^4 - \gamma_3^4}}{2\gamma_2\gamma_3}. \tag{4.3.5}$$

The above η is real provided positive expression in the square root. When η is not a real number, the same is true for x_i's. Hence, there is no static solution representing a fluxon sitting at or near the common point. In this case, an incident fluxon can be either transmitted or reflected as shown in Fig. 4.3.

Once we know the value of η for given values of λ_2 and λ_3, we can calculate x_i from $\gamma_i\eta = \sin 2\alpha_i = 1/\cosh(x_i/\lambda_i)$, i.e.

$$e^{x_i/\lambda_i} = \frac{1 \pm \sqrt{1-\gamma_i^2\eta^2}}{\gamma_i\eta}. \tag{4.3.6}$$

The '±' sign corresponds to $x_i < 0$ and $x_i > 0$, respectively. Solutions that satisfy the governing equations have certain combinations of the signs of x_i. If one of the x_i's is positive, then the configuration of the magnetic field will be as Fig. 4.1(a), i.e. the fluxon is sitting outside the common point.

After obtaining the value of x_i's for given λ_i's, we can proceed with the stability analysis of the static solitary wave. First, we linearize about the solution ϕ_0^i. We write $\phi^i(x,t) = \phi_0^i + u^i(x,t)$ and substitute the spectral ansatz $u^i = e^{\omega t}v^i(x)$. Retaining the terms linear in u^i gives the following eigenvalue problem

$$\lambda_i^2 v_{xx}^i - (\omega^2 + \cos(\phi_0^i + \theta^i))v^i = 0, \tag{4.3.7}$$

with boundary conditions at $x = 0$ given by

$$\begin{aligned} &v^1 + v^2 + v^3 = 0, \\ &v_x^1 = v_x^2 = v_x^3. \end{aligned} \tag{4.3.8}$$

The spectrum ω consists of the continuous spectrum and the point spectrum (isolated eigenvalues). The continuous spectrum is given by those ω for which there exist a solution to

$$\lambda_i^2 v_{xx}^i - \left\{\omega^2 + \lim_{x\to\infty}\cos[\phi_0^i(x) + \theta^i]\right\} v^i = 0,$$

i.e.

$$\lambda_i^2 v_{xx}^i - (\omega^2 + 1)v^i = 0 \tag{4.3.9}$$

of the form $v^i = e^{i\kappa x/\lambda_i}$, with κ real.

It follows that

$$\omega = \pm\sqrt{-(1+\kappa^2)}. \tag{4.3.10}$$

This relation is the usual dispersion relation of a linear wave in a sine-Gordon equation. This relation yields a semi-infinite continuous spectrum on the imaginary axis.

The above stability analysis shows that solution (4.3.1) can be stable. We cannot conclude whether the solution is linearly stable or not before analyzing the point spectrum.

Our next task is to find the point spectrum ω and the corresponding eigenfunction v^i. The point spectrum consists of those value of ω for which there exist solutions v^i to (4.3.7) and (4.3.8) that converge to 0 at $x = \infty$.

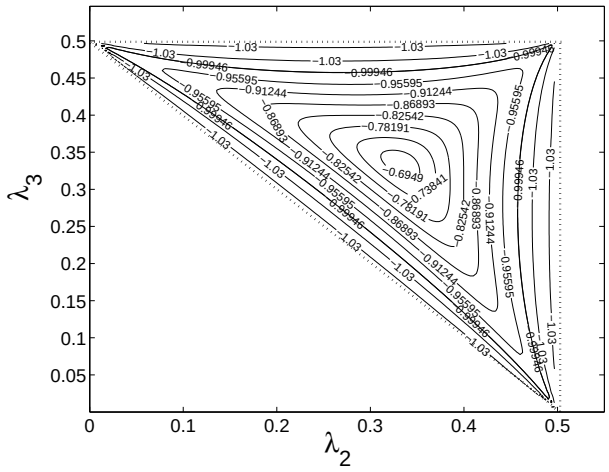

Figure 4.4: *The smallest spectral parameter μ for a standing 2π-fluxon. There is an empty region with no contour lines below the parameter domain boundary $\lambda_2 + \lambda_3 = 1/2$. In this region there is no standing fluxon. In the existence region, there is also an instability region indicated by the value $\mu < -1$.*

The eigenfunction v^i that corresponds to the eigenvalue ω is of the form [8, 9]

$$v^i(x) = c_i e^{\mu \frac{x-x_i}{\lambda_i}} \left(\tanh \frac{x - x_i}{\lambda_i} - \mu \right), \; \mu^2 = \omega^2 + 1, \tag{4.3.11}$$

where $\mathrm{Re}(\mu) \leq 0$ and c_i needs to be determined from (4.3.8).

To obtain an expression for the eigenvalues of the fluxon state for the general case, we have to find the zero's of a fifth order polynomial with coefficients depending on λ_i, $i = 1, 2, 3$. We derive the form of this polynomial in the Appendix.

When all the Josephson lengths are the same, then $x_i = -\lambda_i \ln \sqrt{3}$, $i = 1, 2, 3$. In this special case, the roots of the polynomial are

$$\mu = \frac{1}{2}, \frac{1 \pm \sqrt{13}}{4}.$$

The last two roots have multiplicity two. The eigenvalue is then obtained by recalling that $\mathrm{Re}(\mu) \leq 0$ and $\mu^2 = \omega^2 + 1$ from which we obtain

$$\omega = \pm i \sqrt{\frac{1 + \sqrt{13}}{8}}, \tag{4.3.12}$$

which is in agreement with [6].

The spectral parameter μ for the general case of λ_2 and λ_3 is shown in Fig. 4.4.

It is interesting to note that our parameter domain is bounded by the line $\lambda_2 + \lambda_3 = 1$. Yet, there is a region in that parameter domain where the expression within the square

root of (4.3.5) has negative values, which means that there is no static solitary wave satisfying Eq. (4.2.1) and (4.2.2). In Fig. 4.4, this region is shown as an empty space. This existence region is bounded by lines $\lambda_2 = 1/2$, $\lambda_3 = 1/2$, and $\lambda_2 + \lambda_3 = 1/2$. There is also an instability region in the existence domain that corresponds to $\mu < -1$. In the region, the magnetic field configuration is as Fig. 4.1(a).

Whether there is a static standing fluxon, but unstable, or there is no static fluxon for a given combination of parameter values, a fluxon moving toward the common point in a tricrystal junction with those parameter values will not be trapped.

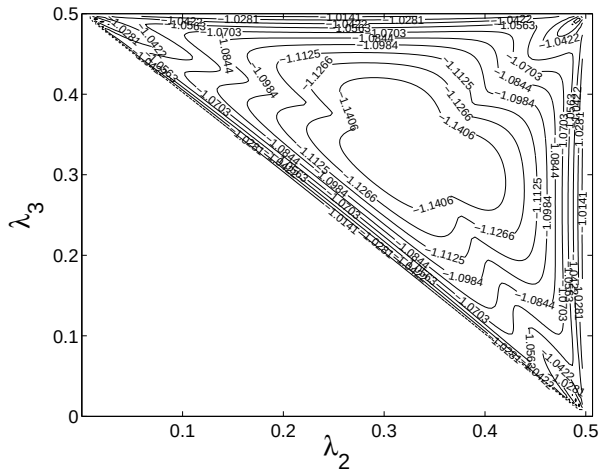

Figure 4.5: *The smallest spectral parameter μ for a standing 4π-fluxon. It is clear that in all the existence region the state is unstable. It means that there is no possibility to trap two fluxons at the common point.*

Next we will consider the linear stability of two fluxons sitting at or near the common point. If we can find a combination of Josephson lengths that gives a stable 4π-kink, then two incident fluxons in a tricrystal junction can be trapped by the common point. The stability calculation can be done as before. A solution that corresponds to a static 4π-kink state is given by

$$\begin{aligned} \phi_0^1 &= 4\tan^{-1} e^{(x-x_1)/\lambda_1}, \\ \phi_0^2 &= 4\tan^{-1} e^{(x-x_2)/\lambda_2}, \\ \phi_0^3 &= 4\tan^{-1} e^{(x-x_3)/\lambda_3} - 2\pi. \end{aligned} \tag{4.3.13}$$

The spectrum parameter μ of a 4π-state in the (λ_2, λ_3)-plane is shown in Fig 4.5. This state has the same existence domain as a 2π-state. Since the largest eigenvalue is always positive in the existence region, then two fluxons can never be trapped at the same time by the common point.

For three standing fluxons, we find that there is no static solution representing such a state.

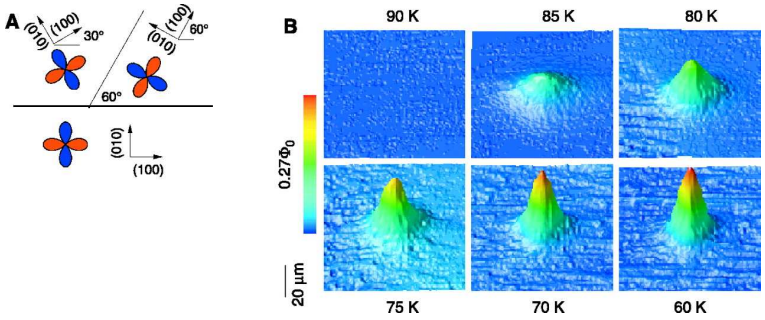

Figure 4.6: *(A) Tricrystal experimental geometry of a YBCO film grown on a tricrystal $SrTiO_3$ substrate used in [10]. The crystalline orientations of the tricrystal were chosen such that the system is frustated. (B) Scanning SQUID microscope images of the π-fluxon in the film for various ambient temperature (Josephson length λ_J). This picture is courtesy of J. R. Kirtley.*

4.4 Tricrystal junctions with a π-junction

In the next problem we address, one of the junctions is a π-junction. This problem appears in superconducting tricrystals with d-wave symmetry [11]. Josephson boundaries between anisotropic superconductors with the d-wave symmetry is sensitive to crystalline misorientation. In a particular case, the phase difference can have a phase addition of π.

In the presence of a phase-jump of π in the phase difference of one junction, the spontaneously generated π-kink is the ground state of the system [5]. Therefore, the presence of a π-kink is used to probe the unconventional symmetry of the order parameter in novel superconductors [12, 13]. Only recently it is proposed to use half-flux quanta, but in a different system, in superconducting memory devices [14]. We show in Fig. 4.6 a scanning SQUID microscope image of a π-fluxon in a tricrystal junction.

The problem is described by taking $\theta^1 = \pi$ and $\theta^{2,3} = 0$ in Eq. (4.2.1). A static solution representing a π-kink, which is the ground state of the system, is given as

$$\begin{aligned} \phi_0^1 &= 4\tan^{-1} e^{(x-x_1)/\lambda_1} - \pi, \\ \phi_0^2 &= 4\tan^{-1} e^{(x-x_2)/\lambda_2} - 2\pi, \\ \phi_0^3 &= 4\tan^{-1} e^{(x-x_3)/\lambda_3} - 2\pi. \end{aligned} \tag{4.4.1}$$

Like before, we need to determine x_i, $i = 1, 2, 3$ by requiring (4.4.1) to satisfy the boundary conditions (4.2.2). Defining η as in (4.3.2) and (4.3.3), we arrive at the following equation [5]

$$\sqrt{(1-\eta^2)(1-\lambda_2^2\eta^2)} - \lambda_2\eta^2 = \lambda_3\eta. \tag{4.4.2}$$

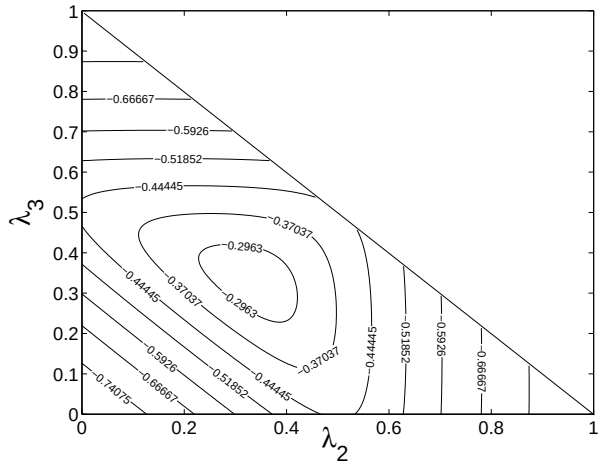

Figure 4.7: *The smallest spectral parameter μ for a π-fluxon. It is clear that in all regions the state is stable. The region above the line $\lambda_2 + \lambda_3 = 1$ is not a physical region since in this region $\lambda_1 < 0$ due to our scaling $\sum \lambda_i = 1$.*

In a special case when all $\lambda_i = 1/3$, we obtain $x_i = \lambda_i \ln(2 - \sqrt{3}) < 0$. In this case the parameter μ [see (4.3.11)] is given by

$$\mu = \frac{\sqrt{3} - \sqrt{7}}{4}$$

from which we obtain the following eigenvalues

$$\omega = \pm i \frac{3 + \sqrt{21}}{8} \approx \pm 0.9478i. \tag{4.4.3}$$

These eigenvalues have double multiplicity. For the general case, the parameter μ in the (λ_2, λ_3)-plane is shown in Fig. 4.7. It is not surprising that the existence and the stability region of a π-fluxon are the same as the parameter domain. It is because a π-fluxon is the ground state of the system.

Kogan, Clem and Kirtley [5] also consider the presence of $(2n + 1)\pi$-fluxon in system (4.2.1) with $n = 1, 2$. This state is rather interesting since for some combinations of the Josephson lengths, a 3π-fluxon has a lower energy than a combination of a π-fluxon at the common point and a 2π-fluxon at infinity [5]. From this energetical reasoning, it was stated that there might be a stable 3π-fluxon in a tricrystal junction. Yet, we found that a 3π-fluxon is unstable. Only with some combinations that are unphysical we can have a 3π-state with the largest eigenvalue zero.

It has been shown by Kogan et al. [5] that there are two possible configurations representing a 3π-fluxon, i.e. configuration with one '+' and two '+'s in the sign-set (sign(x_1),sign(x_2),sign(x_3)). For given values of λ_i, a solution with two +'s has a higher energy than its corresponding solution with one +. In Fig. 4.8(a), we show

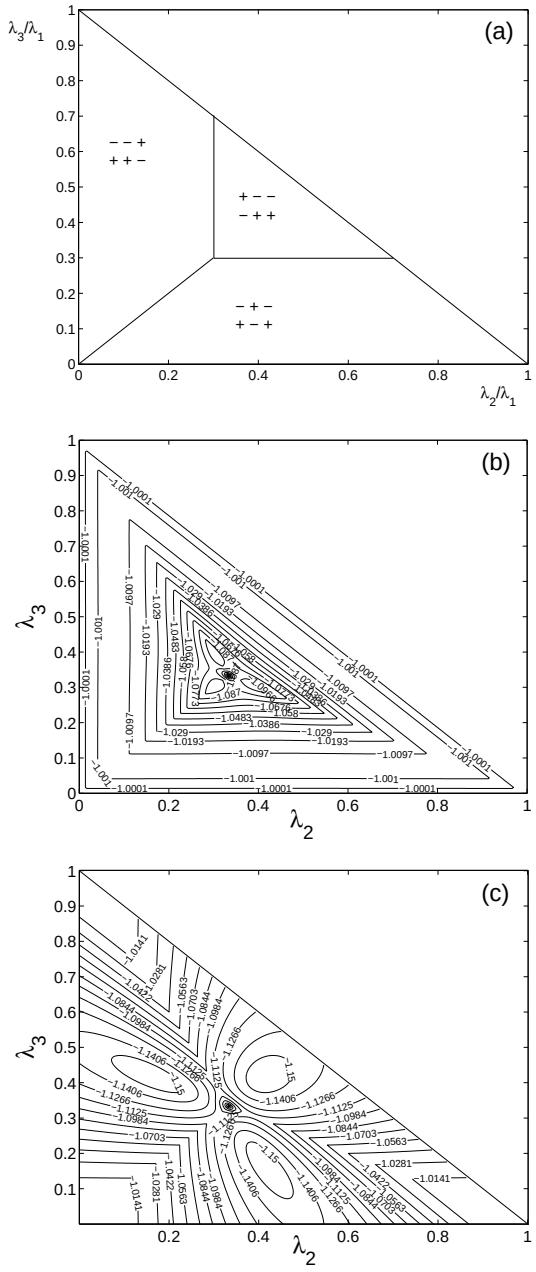

Figure 4.8: *(a) The sign-set diagram* $(sign(x_1), sign(x_2), sign(x_3))$ *for a* 3π*-fluxon. This picture corresponds to Fig. 4 in [5]. (b-c) Similar pictures as Fig. 4.7 for a* 3π*-fluxon with (b) one positive* x_i *and (c) two positive* x_i*'s. From the picture we know that zero can be the largest eigenvalue of a* 3π*-kink, i.e.* $\mu = -1$*, but only at unphysical combinations of Josephson lengths, e.g. when* λ_i *is exactly* $1/3$*.*

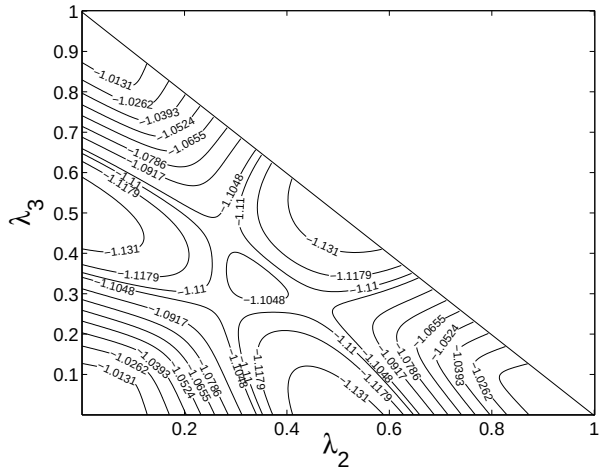

Figure 4.9: *The same picture as Fig. 4.7 but for a* 5π*-fluxon. Because the smallest* μ *is always less than -1 for any combinations of Josephson lengths, then there is no stable* 5π*-kink.*

the sign-set diagram showing combinations of signs of x_i that are needed for a solution to satisfy the governing equations.The parameter μ for this state is shown in Fig. 4.8(b,c). In the evolution of this state in time, a 3π-fluxon will dissolve into a π- and a 2π-fluxon.

We have also considered the existence and the stability of a static 5π-fluxon which is represented by

$$\begin{aligned}\phi_0^1 &= 4\tan^{-1}(e^{(x-x_1)/\lambda_1}) - \pi,\\ \phi_0^2 &= 4\tan^{-1}(e^{(x-x_2)/\lambda_2}),\\ \phi_0^3 &= 4\tan^{-1}(e^{(x-x_3)/\lambda_3}).\end{aligned} \tag{4.4.4}$$

We find that it is even more unstable than a 3π-fluxon. The parameter μ is shown in Fig. 4.9.

A static 7π-fluxon does not exist in a tricrystal junction with a single π-arm.

Using the same analysis, one can show that the 3π state can be stable in a tetracrystal junction with one π-arm. Experimental reports of these tetracrystals can be read in [11]. An experimental scanning SQUID microscope image of a π-fluxon in a tetracrystal junction is shown in Fig. 4.10. One can also calculate that the 5π state will be linearly stable in pentacrystals with one π-arm. Therefrom we conjecture that a stable $(2n+1)\pi$ state exists in $2(n+1)$ or more junctions connected to a joint with one of the arms is a π-junction. All the stable states require the maximum field to be at the joint (see Fig. 4.1(b)).

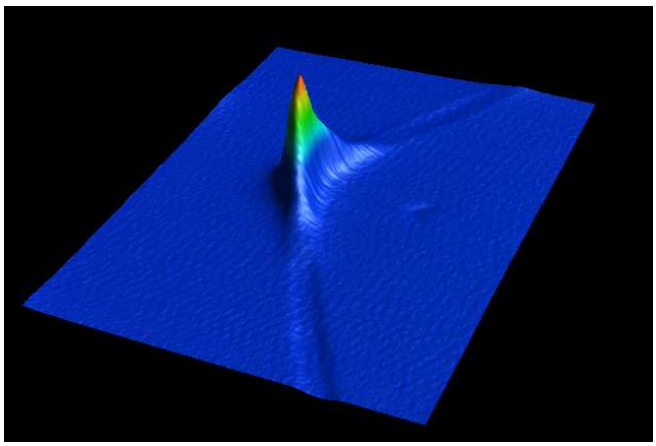

Figure 4.10: *A scanning SQUID microscope image of a π-fluxon in a $Tl_2Ba_2CuO_{6+\delta}$ film grown on a tetracrystal $SrTiO_3$ substrate. This picture is courtesy of J. R. Kirtley.*

4.5 Conclusions

To summarize, we have discussed the existence and the (in)stability of all possible states in a tricrystal junction. The stability analysis presented here should be applicable to other Josephson junction systems. We also have predicted that a multicrystal junction with $2(n+1)$ or more arms with one of the arms is a π-junction can have a stable $(2n+1)\Phi_0/2$ vortex. This stability analysis is important for experimental investigations of the order parameter symmetry in novel superconductors. Such systems can also be used in high-performance computers.

Appendix: Polynomial equation of the spectral parameter μ

The parameter μ that gives eigenvalues of a static kink is obtained by requiring (4.3.11) to solve (4.3.8). The unknown constant c_i cannot be zero for all i as $v^i \neq 0$. To get rid of the trivial solution, we set, for instance, $c_1 = 1$.

From equations $(v_i + v_2 + v_3)|_{x=0} = 0$ and $(v_1 - v_2)|_{x=0} = 0$ (see (4.3.8)), we obtain that

$$
\begin{aligned}
c_2 &= \frac{e^{-\frac{x_1}{\lambda_1}\mu}(-\mu\tanh(\frac{x_1}{\lambda_1}) - \mu^2 + \mathrm{sech}^2(\frac{x_1}{\lambda_1}))}{e^{-\frac{x_2}{\lambda_2}\mu}(-\mu\tanh(\frac{x_2}{\lambda_2}) - \mu^2 + \mathrm{sech}^2(\frac{x_2}{\lambda_2}))}, \\
c_3 &= -\frac{e^{-\frac{x_1}{\lambda_1}\mu}\left(\tanh(\frac{x_1}{\lambda_1}) + \mu\right) + c_2 e^{-\frac{x_2}{\lambda_2}\mu}\left(\tanh(\frac{x_2}{\lambda_2}) + \mu\right)}{e^{-\frac{x_3}{\lambda_3}\mu}(+\tanh(\frac{x_3}{\lambda_3}) + \mu)}.
\end{aligned}
$$

The last equation of (4.3.8) $(v_2 - v_3)|_{x=0} = 0$ will then give the following fifth order

polynomial equation of the parameter μ, i.e.

$$\sum_{i=0}^{5} A_i \mu^i = 0,$$

with

$$\begin{aligned}
A_5 &= 3\cosh(\tfrac{x_1}{\lambda_1})^2 \cosh(\tfrac{x_2}{\lambda_2})^2 \cosh(\tfrac{x_3}{\lambda_3})^2,\\
A_4 &= 3\cosh(\tfrac{x_1}{\lambda_1}) \cosh(\tfrac{x_2}{\lambda_2}) \cosh(\tfrac{x_3}{\lambda_3}) \Big(\cosh(\tfrac{x_1}{\lambda_1}) \sinh(\tfrac{x_3}{\lambda_3}) \cosh(\tfrac{x_2}{\lambda_2}) +\\
&\quad \cosh(\tfrac{x_1}{\lambda_1}) \sinh(\tfrac{x_2}{\lambda_2}) \cosh(\tfrac{x_3}{\lambda_3}) + \sinh(\tfrac{x_1}{\lambda_1}) \cosh(\tfrac{x_3}{\lambda_3}) \cosh(\tfrac{x_2}{\lambda_2})\Big),\\
A_3 &= -2\cosh(\tfrac{x_1}{\lambda_1})^2 \cosh(\tfrac{x_3}{\lambda_3})^2 +\\
&\quad 3\sinh(\tfrac{x_2}{\lambda_2}) \sinh(\tfrac{x_3}{\lambda_3}) \cosh(\tfrac{x_1}{\lambda_1})^2 \cosh(\tfrac{x_2}{\lambda_2}) \cosh(\tfrac{x_3}{\lambda_3} +\\
&\quad 3\sinh(\tfrac{x_2}{\lambda_2}) \sinh(\tfrac{x_1}{\lambda_1}) \cosh(\tfrac{x_1}{\lambda_1}) \cosh(\tfrac{x_2}{\lambda_2}) \cosh(\tfrac{x_3}{\lambda_3})^2 +\\
&\quad 3\sinh(\tfrac{x_3}{\lambda_3}) \sinh(\tfrac{x_1}{\lambda_1}) \cosh(\tfrac{x_1}{\lambda_1}) \cosh(\tfrac{x_2}{\lambda_2})^2 \cosh(\tfrac{x_3}{\lambda_3}) -\\
&\quad 2\cosh(\tfrac{x_2}{\lambda_2})^2 \cosh(\tfrac{x_3}{\lambda_3})^2 - 2\cosh(\tfrac{x_1}{\lambda_1})^2 \cosh(\tfrac{x_2}{\lambda_2})^2,\\
A_2 &= 3\sinh(\tfrac{x_2}{\lambda_2}) \sinh(\tfrac{x_3}{\lambda_3}) \sinh(\tfrac{x_1}{\lambda_1}) \cosh(\tfrac{x_1}{\lambda_1}) \cosh(\tfrac{x_2}{\lambda_2}) \cosh(\tfrac{x_3}{\lambda_3}) -\\
&\quad 2\sinh(\tfrac{x_3}{\lambda_3}) \cosh(\tfrac{x_2}{\lambda_2})^2 \cosh(\tfrac{x_3}{\lambda_3}) - 2\sinh(\tfrac{x_1}{\lambda_1}) \cosh(\tfrac{x_1}{\lambda_1}) \cosh(\tfrac{x_2}{\lambda_2})^2 -\\
&\quad 2\sinh(\tfrac{x_3}{\lambda_3}) \cosh(\tfrac{x_1}{\lambda_1})^2 \cosh(\tfrac{x_3}{\lambda_3}) - 2\sinh(\tfrac{x_2}{\lambda_2}) \cosh(\tfrac{x_2}{\lambda_2}) \cosh(\tfrac{x_3}{\lambda_3})^2 -\\
&\quad 2\sinh(\tfrac{x_1}{\lambda_1}) \cosh(\tfrac{x_1}{\lambda_1}) \cosh(\tfrac{x_3}{\lambda_3})^2 - 2\sinh(\tfrac{x_2}{\lambda_2}) \cosh(\tfrac{x_1}{\lambda_1})^2 \cosh(\tfrac{x_2}{\lambda_2}),\\
A_1 &= \cosh(\tfrac{x_1}{\lambda_1})^2 + \cosh(\tfrac{x_2}{\lambda_2})^2 + \cosh(\tfrac{x_3}{\lambda_3})^2 -\\
&\quad 2\sinh(\tfrac{x_2}{\lambda_2}) \sinh(\tfrac{x_3}{\lambda_3}) \cosh(\tfrac{x_2}{\lambda_2}) \cosh(\tfrac{x_3}{\lambda_3}) -\\
&\quad 2\sinh(\tfrac{x_3}{\lambda_3}) \sinh(\tfrac{x_1}{\lambda_1}) \cosh(\tfrac{x_1}{\lambda_1}) \cosh(\tfrac{x_3}{\lambda_3}) -\\
&\quad 2\sinh(\tfrac{x_2}{\lambda_2}) \sinh(\tfrac{x_1}{\lambda_1}) \cosh(\tfrac{x_1}{\lambda_1}) \cosh(\tfrac{x_2}{\lambda_2}),\\
A_0 &= \sinh(\tfrac{x_2}{\lambda_2}) \cosh(\tfrac{x_2}{\lambda_2}) + \sinh(\tfrac{x_1}{\lambda_1}) \cosh(\tfrac{x_1}{\lambda_1}) + \sinh(\tfrac{x_3}{\lambda_3}) \cosh(\tfrac{x_3}{\lambda_3}).
\end{aligned}$$

Only roots of the polynomial with negative real part correspond to an eigenvalue of the considered state.

Bibliography

[1] P.D. Shaju and V.C. Kuriakose, *Logic gates using stacked Josephson junctions*, Physica C **322**, 163 (1999).

[2] K. Nakajima, H. Mizusawa, H. Sugahara, and Y. Sawada, *Phase mode Josephson computer system*, IEEE Trans. Appl. Supercond. **1**, 29 (1991) and references therein.

[3] K. Nakajima, Y. Onodera and Y. Ogawa, *Logic design of Josephson network*, J. Appl. Phys. **47**, 1620 (1976).

[4] K. Nakajima and Y. Onodera, *Logic design of Josephson network. II*, J. Appl. Phys. **49**, 2958 (1978).

[5] V.G. Kogan, J. R. Clem and J. R. Kirtley, *Josephson vortices at tricrystal boundaries*, Phys. Rev. B **61**, 9122 (2000).

[6] A. Grunnet-Jepsen, F.N. Fahrendorf, S.A. Hattel, N. Grønbech-Jensen and M.R. Samuelsen, *Fluxons in three long coupled Josephson junctions*, Phys. Lett. A **175**, 116 (1993).

[7] S.A. Hattel, A. Grunnet-Jepsen and M.R. Samuelsen, *Dynamics of three coupled long Josephson junctions*, Phys. Lett. A **221**, 115 (1996).

[8] E. Mann, *Systematic perturbation theory for sine-Gordon solitons without use of inverse scattering methods*, J. Phys. A: Math. Gen. **30**, 1227 (1997).

[9] G. Derks, A. Doelman, S.A. van Gils and T.P.P. Visser, *Travelling waves in a singularly perturbed sine-Gordon equation*, Physica D **180**, 40 (2003).

[10] J. R. Kirtley, C. C. Tsuei, and K. A. Moler, *Temperature Dependence of the Half-Integer Magnetic Flux Quantum*, Science **285**, 1373 (1999).

[11] C.C. Tsuei and J.R. Kirtley, *Pairing symmetry in cuprate superconductors*, Rev. Mod. Phys. **72**, 969 (2000).

[12] J. R. Kirtley, C. C. Tsuei, M. Rupp, J. Z. Sun, L. S. Yu-Jahnes, A. Gupta, M. B. Ketchen, K. A. Moler, and M. Bhushan, *Direct Imaging of integer and half-integer Josephson vortices in High-T_c grain boundaries*, Phys. Rev. Lett. **76**, 1336 (1996).

[13] C.C. Tsuei and J.R. Kirtley, *Phase-sensitive evidence for d-wave pairing symmetry in electron-doped cuprate superconductors*, Phys. Rev. Lett. **85**, 182 (2000).

[14] H. Hilgenkamp, Ariando, H.J.H. Smilde, D.H.A. Blank, G. Rijnders, H. Rogalla, J.R. Kirtley and C.C. Tsuei, *Ordering and manipulation of the magnetic moments in large-scale superconducting π-loop arrays*, Nature (London) **422**, 50 (2003).

5

Fractional kink lattices and their bandgap structures

Chapter 5

We consider a modified sine-Gordon equation with phase shifts. At the point of the shifts, fractional kinks can be created. In the particular case of periodic phase shifts, there is a chain of fractional kinks. Here, we introduce and study numerically fractional kink lattices and their energy bands. Analytical calculations are presented for the particular case of chains of integer (anti)kinks and kinks-antikinks in the absence of an applied bias current. Knowledge of band-structure is important for the design of devices that are based on fractional vortices. Because such a system can be realized in experiments and has a wide range of controllability properties, we also propose it as an artificial vortex crystal with controllable energy bands.

5.1 Introduction

A sine-Gordon equation is known to be an important model with application in many branches of modern physics, extending from condensed matter systems, liquid crystals, to quantum field theory. For a rather complete review see [1] and the references therein. A crucial property of the equation is its integrability that permits an analytic determination of the corresponding physical quantities. In condensed matter systems, sine-Gordon equations appear in the theory of long Josephson junction that describe the tunneling of Cooper pairs across a barrier between two superconductors [2]. In the study of Josephson junctions, the sine-Gordon phase represents the phase difference between two neighboring superconductors and the fundamental topological kink solution expresses one magnetic flux quantum $\Phi_0 \approx 2.07 \times 10^{-15}$ Wb.

Bulaevskii, Kuzii, and Sobyanin [3] proposed a Josephson system with a phase-shift of π in the sine-Gordon phase due to the presence of magnetic impurities. The system can admit a half of magnetic flux quantum or semifluxon attached to the point of the phase jump. Recent technological advances can introduce this phase shift in a long Josephson junction using, e.g., superconductors with unconventional pairing symmetry [4, 5], Superconductor-Ferromagnet-Superconductor (SFS) π-junctions [6], and Superconductor-Normal metal-Superconductor (SNS) junctions [7]. A recent work reports a successful experiment on artificial phase shift in Josephson junctions made of standard superconductors [8]. In this experiment, the phase shift can be tuned to be of any value and, hence, one can obtain an arbitrary fractional magnetic flux quantum.

Here, we consider a particular case of Josephson junctions with periodic phase shifts. We study fractional kink lattices and their energy bands that correspond to the oscillations of the chains.

It is of interest to consider and understand such a system because it can be proposed as an artificial periodic structure. This is due to its great degree of control over its electronic properties either at the design time by choosing the distance between vortices or, during experiment, by varying the bias current or the topological charge of the vortices. It can be a useful utility in understanding crystals, while the study of crystals is known to be a central theme of solid state physics [9, 10, 11].

Besides the motivation mentioned above, the present study is also of importance because knowledge of band structures is a key element in designing classical and quantum devices based on fractional vortices. In the classical domain this can help either to avoid resonance phenomena or even to exploit them (e.g. in filters and detectors). In the quantum domain, the absence of an acoustic branch can be a crucial obstacle for thermal excitation of plasma oscillations.

This chapter is organized as follows. In Sec. 5.2, we explain the considered mathematical model and the numerics that we use. This section will give also an introduction to the aforementioned arbitrary fractional kinks, before further discussions on fractional kink lattices. We consider two fundamental arrangements of periodic phase shifts that admit two particular solutions existing also in the ordinary sine-Gordon equation, namely rotating and oscillating solutions. We overview analytical results that have been established for the particular case $\kappa = 2\pi$ and $\gamma = 0$ in Sec. 5.3. Some numerical results for the general value of phase shift κ are discussed in Sec. 5.4. Conclusions of the present study are given in Sec. 5.5.

5.2 Mathematical model and numerical methods

5.2.1 Fractional kinks in a junction with a single phase shift

First, we consider the problem of Josephson junctions with a single κ phase shift, which is usually called as a 0-κ Josephson junction. This is the building block for a more general description.

The dynamics of the Josephson phase $\phi(x,t)$ in a 0-κ long junction is described by

$$\phi_{xx} - \phi_{tt} = \sin(\phi + \theta(x)) - \gamma, \tag{5.2.1}$$

with

$$\theta(x) = \begin{cases} 0, & x < 0, \\ -\kappa, & x > 0. \end{cases} \tag{5.2.2}$$

All variables and parameters are in dimensionless form. Without loss of generality, we can assume that $0 \leq \kappa \leq 2\pi$.

The boundary conditions at $x = 0$ are given by the continuity conditions

$$\begin{aligned} \lim_{x\to 0^-} \phi(x) &= \lim_{x\to 0^+} \phi(x), \\ \lim_{x\to 0^-} \phi_x(x) &= \lim_{x\to 0^+} \phi_x(x). \end{aligned} \tag{5.2.3}$$

The presence of this κ discontinuity can result in the formation of a fractional vortex pinned at $x = 0$, as is confirmed experimentally and reported in, for instance, [5, 8]. This spontaneous formation is to compensate the $-\kappa$ phase jump. A kink solution of (5.2.1) and (5.2.2) that represents a fractional vortex with topological charge κ is given by

$$\phi^{\kappa}(x) = \begin{cases} 4\arctan e^{x+x_0}, & x < 0, \\ \kappa - 4\arctan e^{-x+x_0}, & x > 0, \end{cases} \tag{5.2.4}$$

with

$$x_0 = \ln\tan\frac{\kappa}{8}. \tag{5.2.5}$$

The kink solution (5.2.4) is stable. The eigenvalue of that $\phi^{\kappa}(x)$ can be calculated analytically[1]. The eigenvalue problem of the solution is obtained by substituting the spectral ansatz $\phi = \phi^{\kappa} + e^{i\omega t}\epsilon(x)$ into Eq. (5.2.1) and linearizing about the solution $\phi^{\kappa}(x)$. We will then obtain

$$\epsilon_{xx} - \left[\cos(\phi^{\kappa} + \theta) - \omega^2\right]\epsilon = 0. \tag{5.2.6}$$

The solution of the above eigenvalue problem that corresponds to the smallest eigenvalue of ϕ^{κ} is given by

$$\epsilon(x) = \begin{cases} \epsilon^{-}(x) = e^{\sqrt{1-\omega^2}(x+x_0)}\left(\tanh(x+x_0) - \sqrt{1-\omega^2}\right), & x < 0, \\ \epsilon^{+}(x) = \epsilon^{-}(-x), & x > 0, \end{cases} \tag{5.2.7}$$

with the smallest eigenvalue ω is

$$\omega^2 = \frac{1}{2}\cos\frac{\kappa}{4}\left(\cos\frac{\kappa}{4} + \sqrt{4 - 3\cos^2\frac{\kappa}{4}}\right). \tag{5.2.8}$$

Plot of this eigenvalue as a function of κ is shown in Fig. 5.1. For the particular case of $\kappa = \pi$, the eigenvalue of a semifluxon is $\omega(\pi) = \frac{1}{2}\sqrt{1 + \sqrt{5}} \approx 0.899$.

The fact that a stable fractional kink does not move in space and is attached to the point of the phase shift is shown by its nonzero eigenvalue. The spectral parameter ω can be zero if and only if $\kappa = 2\pi$ because at this value of κ, we have an ordinary 2π kink that is translational invariant in space.

5.2.2 Fractional kink lattices in a junction with periodic phase shift

After briefly considering a Josephson junction with a single phase shift, we consider the problem of Josephson junctions with periodic phase shift. Here, we consider

1 The procedure of calculating the smallest eigenvalue of the solution can be exactly following the steps presented in Chapter 3 of this thesis.

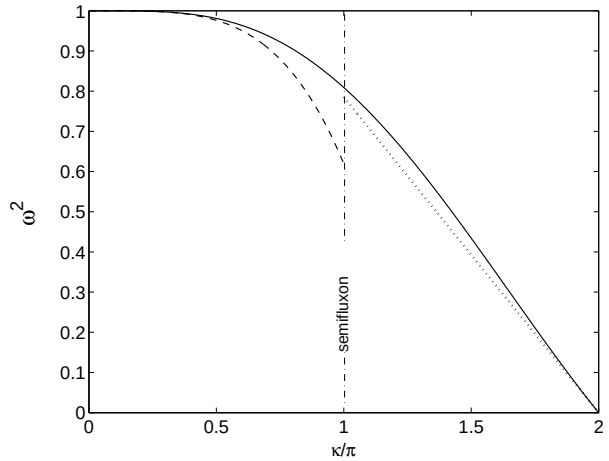

Figure 5.1: *Plot of the eigenvalue ω of a single κ-vortex given by Eq. (5.2.8) versus κ [continuous line] and its approximations for $\kappa \to 0$: $\omega(\kappa) \approx 1 - \kappa^4/256$ [dashed line] and for $\kappa \to 2\pi$: $\omega(\kappa) \approx \frac{1}{4}(2\pi - \kappa)$ [dotted line].*

two basic periodic arrangements that support solutions existing up to $\kappa = 2\pi$. Those two arrangements are represented by

$$\theta(x) = \begin{cases} \ldots, & \ldots, \\ -\kappa, & -a < x < 0, \\ 0, & 0 < x < a, \\ \kappa, & a < x < 2a, \\ 2\kappa, & 2a < x < 3a, \\ \ldots, & \ldots, \end{cases} \tag{5.2.9}$$

and

$$\theta(x) = \begin{cases} -\kappa, & \ldots, -a < x < 0, a < x < 2a, \ldots, \\ 0, & \ldots, 0 < x < a,\ 2a < x < 3a, \ldots, \end{cases} \tag{5.2.10}$$

where a is the distance between two consecutive discontinuities.

There are many static solutions of (5.2.1) combined with $\theta(x)$ defined by either (5.2.9) or (5.2.10) for $\kappa \neq 0,\ 2\pi$. But in this work, we only consider a particular solution of the equation that can be continued up to $\kappa = 2\pi$.

For Eq. (5.2.1) with $\theta(x)$ defined by (5.2.9), we consider a solution representing a lattice of fractional kinks with uniform topological charge that is ordered ferromagnetically. In the time-independent sine-Gordon equation, it corresponds to a rotating

solution. While for $\theta(x)$ given by (5.2.10), the solution we consider is antiferromagnetically ordered fractional kinks that corresponds in the ordinary sine-Gordon equation to an oscillating solution.

Considering only those two particular solutions, the two above periodic arrangements of $\theta(x)$ with periodic boundary conditions correspond respectively to

$$\theta(x) = 0, \quad 0 < x < a, \tag{5.2.11}$$

with boundary conditions

$$\begin{aligned} \lim_{x\to 0} \phi(x) &= \kappa + \lim_{x\to a} \phi(x), \\ \lim_{x\to 0} \phi_x(x) &= \lim_{x\to a} \phi_x(x), \end{aligned} \tag{5.2.12}$$

and

$$\theta(x) = \begin{cases} 0, & 0 < x < a, \\ -\kappa, & a < x < 2a, \end{cases} \tag{5.2.13}$$

with boundary conditions

$$\begin{aligned} \lim_{x\to\{0,a^-\}} \phi(x) &= \lim_{x\to\{2a,a^+\}} \phi(x), \\ \lim_{x\to\{0,a^-\}} \phi_x(x) &= \lim_{x\to\{2a,a^+\}} \phi_x(x). \end{aligned} \tag{5.2.14}$$

Note that our infinite domain in the original system becomes finite with length $L = a$ for (5.2.11)-(5.2.12) and $L = 2a$ for (5.2.13)-(5.2.14). Both systems can be realized in experiments using an annular Josephson junction with couple pair-injectors as explained in [8, 12, 13].

5.2.3 Numerical methods

To calculate numerically the oscillatory energy bands of a chain of fractional vortices, we use a transfer matrix approach approximated by the Euler-forward method that will be briefly reviewed below. The reader interested in the numerics is referred to, e.g., [14] for more complex and delicate methods.

Suppose we want to study the band structure of a static solution $\phi^0(x)$ satisfying Eq. (5.2.1) for a given arrangement of $\theta(x)$ and given values of κ, a, and γ.

Written as a system of first order equations, the eigenvalue problem (5.2.6) takes the form

$$\vec{\epsilon}_x = A\vec{\epsilon}, \tag{5.2.15}$$

with

$$\vec{\epsilon} = \begin{pmatrix} \epsilon \\ \epsilon_x \end{pmatrix} \quad \text{and} \quad A(x) = \begin{pmatrix} 0 & 1 \\ \cos\left[\phi^0(x) + \theta(x)\right] - \omega^2 & 0 \end{pmatrix}. \tag{5.2.16}$$

As a consequence of the Floquet-Bloch theorem, a periodic solution of Eq. (5.2.15) will satisfy

$$\vec{\epsilon}(x+L) = C\vec{\epsilon}(x),$$

with C is a constant matrix and L is the periodicity of the lattice.

We approximate $A(x)$ with a constant matrix A_n given by Eq. (5.2.16) with $x = x_n = n\Delta x$ on interval Δx from x_n to x_{n+1}. We use several spatial discretization steps to compare results obtained from the numerics, i.e. $\Delta x = 0.1, 0.05, 0.02$. The so-called principal matrix C is then approximated by the following transfer matrix discretization

$$C = \prod_{n=1}^{N} \exp(\Delta x A_n), \tag{5.2.17}$$

where $N = L/\Delta x$ is the number of discretization in the computational domain.

The transfer matrix C has two eigenvalues. The product of the eigenvalues satisfies the relation

$$\lambda_1\lambda_2 = \det C = \prod_{n=1}^{N} \det\, e^{\Delta x A_n} = \prod_{n=1}^{N} e^{\mathrm{Tr}(\Delta x A_n)} = 1,$$

where we have used an identity $\det[\exp(M)] = \exp[\mathrm{Tr}(M)]$ and the fact that $\mathrm{Tr}(A) = 0$ (see Eq. (5.2.16)). The spectral parameter ω lies within the energy band if and only if $\lambda_{1,2}$ is a pair of complex-conjugate roots laying on the unit circle in the complex plane, i.e. $|\lambda_1| = |\lambda_2| = 1$.

5.3 Analytical calculations for the case of $\kappa = 2\pi$ and $\gamma = 0$

Before discussing band-gap structures of a periodic solution with general value of κ, we will make an overview over band-gap structures of periodic solutions for the limiting case $\kappa = 2\pi$ and $\gamma = 0$ that have been well-established analytically. A rather complete discussion of the results presented here can be found in [15, 16].

The simplest stable solution of the sine-Gordon equation is the even multiple of π. The band structure of this constant background consists of a forbidden band that ranges in the region $0 < \omega^2 < 1$ and an allowed band $\omega^2 > 1$. A 2π-kink solution (5.2.4) also has the same band structure but with an isolated eigenvalues at $\omega^2 = 0$ and $\omega^2 = 1$. When we have an infinite array of periodic 2π-kinks supported by the time-independent equation of (5.2.1), calculations of the band structure are not trivial, as will be shown below.

5.3.1 Ferromagnetically ordered fractional kinks

First, let us consider a lattice of ferromagnetically ordered integer kinks. A rotating solution that corresponds to it of the first integral of Eq. (5.2.1)

$$\frac{1}{2}\left(\frac{\partial\phi}{\partial x}\right)^2 = 1 - \cos\phi + A \tag{5.3.1}$$

is given by $A > 0$. The solution can be expressed analytically as

$$\phi(x) \;=\; \pi + 2\,\mathrm{am}\left(\frac{(x - x^0)}{k}, k\right) , \qquad k^2 \;=\; \frac{2}{2 + A} \;, \tag{5.3.2}$$

where the period of the kink lattice a is related to k by

$$a \;=\; 2\,k\,\mathbf{K}\left(k^2\right) \;. \tag{5.3.3}$$

$\mathbf{K}(k^2)$ denotes the complete elliptic integral of the first kind (see the Appendix). The parameter x^0 in (5.3.2) can be of any constant value here.

For a periodic array of kinks (5.3.2), the eigenvalue problem (5.2.6) then takes the form

$$\left\{\frac{d^2}{d\bar{x}^2} + k^2\left(\omega^2 + 1\right) - 2k^2\,\mathrm{sn}^2(\bar{x}, k^2)\right\}\epsilon(\bar{x}) \;=\; 0 \;, \tag{5.3.4}$$

with $\bar{x} \;=\; x/k$ and $\mathrm{sn}(\bar{x}, k^2)$ is the Jacobi elliptic function defined in the Appendix. The boundary conditions for $\epsilon(x)$ are given by

$$\epsilon\left(\bar{x} + \frac{a}{k}\right) \;=\; \epsilon(\bar{x}) \;. \tag{5.3.5}$$

Equation (5.3.4) is a Lamé-type equation that admits two linearly independent solutions given by

$$\epsilon_{\pm\eta}(\bar{x}) \;=\; \frac{\sigma(\bar{x} + i\mathbf{K}' \pm \eta)}{\sigma(\bar{x} + i\mathbf{K}')}\; e^{\mp\,\bar{x}\,\zeta(\eta)} \;, \tag{5.3.6}$$

where η is defined as a root of

$$\mathcal{P}(\eta) \;=\; \frac{2 - k^2}{3} - k^2\omega^2 \;. \tag{5.3.7}$$

The Weierstrass functions $\mathcal{P}(u)$, $\zeta(u)$ and $\sigma(u)$ are defined in the Appendix.

Because of the periodic potential, we have the Floquet-Bloch theorem which says that

$$\epsilon_{\pm\eta}(\bar{x} + 2\mathbf{K}) \;=\; e^{\pm iF(\eta)}\,\epsilon_{\pm\eta}(\bar{x}) \;,$$

with

$$F(\eta) \;=\; 2i\left[\mathbf{K}\,\zeta(\eta) - \eta\,\zeta(\mathbf{K})\right] . \tag{5.3.8}$$

The allowed band is given by the value of ω where $F(\eta) \in \mathbb{R}$, i.e.

$$0 < \omega^2 < \frac{1}{k^2} - 1 \quad \text{and} \quad \omega^2 > \frac{1}{k^2} \;. \tag{5.3.9}$$

In this region, $F(\eta)$ goes from 0 to π with $\eta = \mathbf{K} + iy$ and y ranges between 0 and $\mathbf{K}'$.

Correspondingly, the forbidden bands are given by those values of η for which $F(\eta)$ has a non vanishing imaginary part, i.e.

$$\omega^2 < 0 \quad \text{and} \quad \frac{1}{k^2} - 1 < \omega^2 < \frac{1}{k^2} \;. \tag{5.3.10}$$

In this region, $\eta = iy$ with $F(\eta)$ has a purely imaginary value from π to infinity.

After calculating the continuous band-gap structures, one can also impose the periodicity of the boundary conditions (5.3.5) on $\epsilon(x)$ to obtain the eigenvalues of the kink structures. In this case, $F(\eta)$ is then an even multiple of π. The eigenvalues are given by $\omega_0^2 = 0$ with multiplicity one which is associated to the translational invariance property of the solution, and the infinite series of points with multiplicity two

$$\omega_n^2 \equiv \frac{1}{k^2}\left[\frac{2-k^2}{3} - \mathcal{P}(iy_n)\right] \tag{5.3.11}$$

where y_n determined by

$$F(iy_n) = 2\mathbf{K}\, i\,\zeta(iy_n) + 2y_n\,\zeta(\mathbf{K}) = 2n\pi\,, \qquad n = 1, 2, \ldots \tag{5.3.12}$$

These eigenvalues lie in the band $\omega^2 > \frac{1}{k^2}$

In the limit $a \to \infty$, the above band structure goes to the one of a 2π-kink. The allowed band $0 < \omega^2 < \frac{1}{k^2} - 1$ shrinks to the isolated eigenvalue $\omega_0^2 = 0$ and the other allowed band $\omega^2 > \frac{1}{k^2}$ becomes the continuous spectrum $\omega^2 > 1$.

5.3.2 Antiferromagnetically ordered fractional kinks

An oscillating solution that corresponds to an antiferromagnetically ordered kinks of the first integral (5.3.1) is given by $-2 < A < 0$. The solution can be expressed analytically as

$$\phi(x) = 2\arccos[k\,\mathrm{sn}\left(x - x^0, k\right)]\,, \qquad k^2 = 1 + \frac{A}{2}\,, \tag{5.3.13}$$

where the facet length a is related to k by

$$a = 2\,\mathbf{K}\left(k^2\right)\,. \tag{5.3.14}$$

For this periodic (antiferromagnetically ordered) kink-antikink (5.3.13), the eigenvalue problem will take the form

$$\left\{\frac{d^2}{dx^2} + \omega^2 + 1 - 2k^2\,\mathrm{sn}^2(x, k^2)\right\}\epsilon(x) = 0\,. \tag{5.3.15}$$

The solutions of this eigenvalue problem are almost the same to the ones of the eigenvalue problem for ferromagnetically ordered kinks. The difference between the solutions is presented in the Appendix.

Following the same steps as above, one will obtain the allowed band of the periodic solution, i.e.

$$k^2 - 1 < \omega^2 < 0 \quad \text{and} \quad \omega^2 > k^2. \tag{5.3.16}$$

The presence of negative ω^2 informs us that a periodic integer kink-antikink solution is unstable. A similar calculation for the forbidden band will give

$$k^2 - 1 > \omega^2 \quad \text{and} \quad 0 < \omega^2 < k^2. \tag{5.3.17}$$

Imposing the boundary conditions to the eigenfunction $\epsilon(x)$, i.e. selecting the values of ω^2 for which the Floquet exponent is an even multiple of π, we obtain the simple eigenvalues $\omega_0^2 = 0$ and

$$\omega_1^2 = k\ , \tag{5.3.18}$$

and the infinite series of double eigenvalues

$$\omega_n^2 \equiv \frac{2k^2 - 1}{3} - \mathcal{P}(iy_n) \tag{5.3.19}$$

in the band $\omega^2 > k^2$, with y_n defined by

$$F = 2\mathbf{K}\, i\,\zeta(iy_n) + 2y_n\,\zeta(\mathbf{K}) = 2n\pi\ , \qquad n = 2, 3, \ldots . \tag{5.3.20}$$

5.4 Numerical results on the band-gap calculation

After considering the limiting case $\kappa = 2\pi$, a natural question is then how the band structure of a periodic lattice of κ-kinks for a general value of $\kappa \neq 2\pi$. Below we present some numerical results using the numerical scheme explained in Sec. 5.2.3 above.

5.4.1 Ferromagnetically ordered fractional kinks

First, let us consider ferromagnetically ordered fractional kinks of the Josephson system (5.2.1) with periodicity (5.2.9) in the absence of bias current γ. When $\kappa = 2\pi$, this state corresponds to the so-called flux-flow regime (in a moving coordinate) [17]. This particular state has received considerable interest in view of practical applications of Josephson transmission lines as submilimeter band oscillators.

Band structures as a function of κ calculated numerically for some values of a, i.e. $a = 1, 2, 5$ are shown in Fig. 5.2. In all plots one can see that in the absence of discontinuities ($\kappa = 0$) the junction has a band gap for $0 < \omega < 1$ and a single infinite plasma band for $\omega > 1$ as is calculated analytically. As κ increases, fractional vortices appear. Each vortex when isolated ($a \to \infty$) has an eigenvalue $\omega(\kappa) < 1$ (5.2.8). But when the vortices are coupled (a is finite), the eigenvalues form a band. Interestingly, periodic fractional kinks with $\kappa \neq 0, 2\pi$ have band gaps that do not exist in the limit $\kappa = 0,\ 2\pi$. As the distance a decreases, the allowed bands broaden, while the gaps shrink and shift to higher frequencies, as can be seen in consecutive Figs. 5.2(a)–(c).

As has been calculated analytically in the previous section, there are only two forbidden bands when $\kappa = 2\pi$ for a given value of facet length a. For a general value of

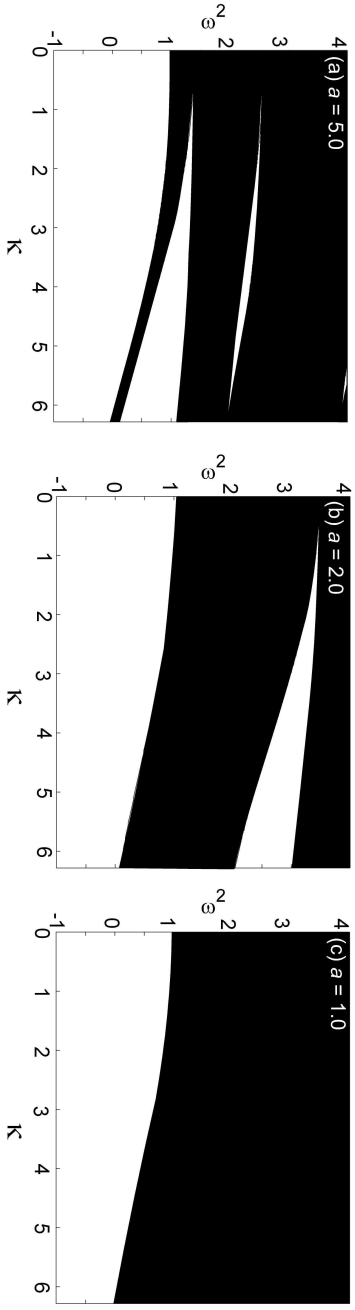

Figure 5.2: *Numerically calculated band structure of ferromagnetically ordered fractional kinks as a function of* κ *for* $a = 5, 2, 1$ *shown in (a)–(c), respectively.*

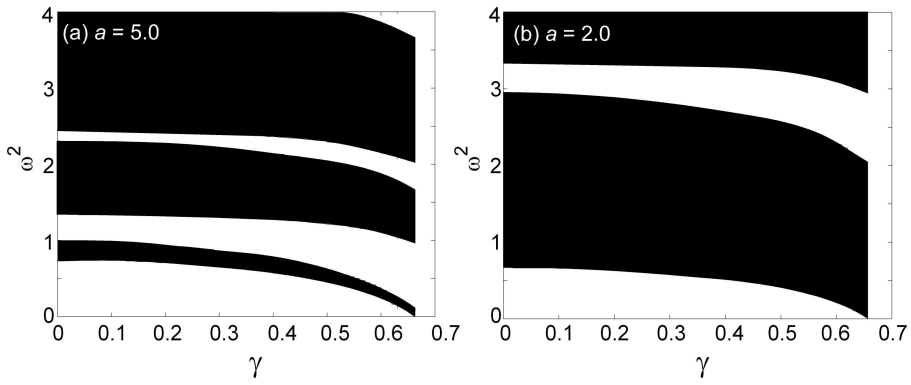

Figure 5.3: *Numerically calculated band structure of ferromagnetically ordered fractional kinks as a function of the applied bias current γ for $\kappa = \pi$ and (a) $a = 5$ and (b) $a = 2$. There is a critical value of $\gamma = \gamma_c(a, \kappa)$ above which the static crystal becomes unstable.*

$\kappa \neq 2\pi$, our numerical results show that a solution might have an infinitely many band gaps.

We also have considered the influence of bias current to the band structure at various fixed values of a and $\kappa = \pi$. This case is interesting for a Josephson system with discontinuities that cannot be controlled during experiment, e.g. a ramp-type 0-π long Josephson junction. In Fig. 5.3, we present the band structure of a periodic π-kink lattice with $a = 5$ and $a = 2$.

For a given a, there is a critical value of $\gamma_c(a)$ at which the static solution becomes unstable. The lowest edge of the first band tends to 0 when $\gamma \to \gamma_c(a)$. For $\gamma > \gamma_c(a)$, there is no static lattice fractional kinks. The system will switch to a finite voltage state.

5.4.2 Antiferromagnetically ordered fractional kinks

After considering the case of ferromagnetically ordered fractional kinks, we now study antiferromagnetically ordered fractional kinks of the Josephson junction system (5.2.1) with periodic phase shift (5.2.10).

In Fig. 5.4, the bands of a fractional kink-antikink lattice are traced from $\kappa = 0$ to $\kappa = 2\pi$. There is a critical value of $\kappa = \kappa_c(a)$ at which the lowest edge of the first allowed band touches zero, i.e. $\omega \to 0$ when $\kappa \to \kappa_c$. At that value of κ, the antiferromagnetically state is unstable and in the time-dependent equation, it will turn into a complimentary state [18].

The band structure of the complimentary state is the mirror reflection of the one shown in Fig. 5.4 with respect to the line $\kappa = \pi$. Therefore, in the interval $2\pi - \kappa_c(a) < \kappa <$

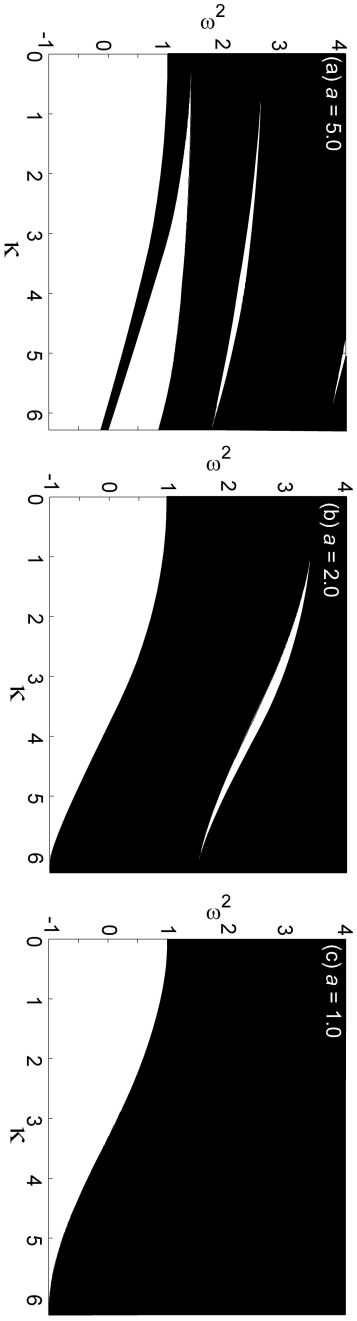

Figure 5.4: *The same as Fig. 5.2 but for antiferromagnetically ordered fractional kinks. For a given value of the facet length a, there is $\kappa_c(a)$ at which the boundary of the lowest branch touches zero. For $\kappa > \kappa_c(a)$ the antiferromagnetically ordered crystal is unstable. In the time-dependent equation, the system switches to resistive states.*

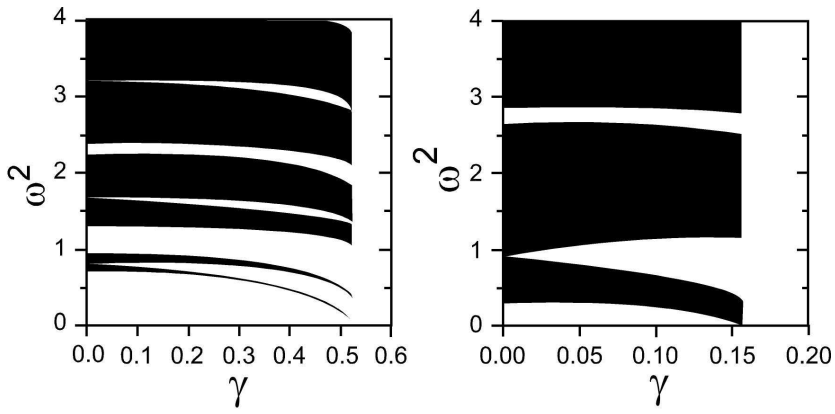

Figure 5.5: *The same as Fig. 5.3 but for antiferromagnetically ordered fractional kinks.*

$\kappa_c(a)$, there are two stable solutions: an antiferromagnetically chain of direct vortices and its complementary solution.

The value of $\kappa_c(a)$ decreases as the coupling increases with $\kappa_c \to \pi$ when $a \to 0$. This is in agreement with the known result [19, 20] that the infinite antiferromagnetically ordered semifluxon chain is stable for any $a \to 0$.

We also have done numerical calculations on the band structures of a chain of fractional kinks under the influence of an applied bias current. We present the results in Fig. 5.5. By applying a bias current, an additional gap can open within each band.

5.5 Conclusions

To conclude, we have calculated the energy bands corresponding to small oscillations of the 1-dimensional periodic fractional vortex crystal as a function of the discontinuity κ, the bias current γ, and the distance between two neighboring discontinuity points a. Such a 1-dimensional vortex crystal has an optical branch and no acoustic one in the dispersion relation, which is a direct consequence of the vortex pinning $\kappa \not\equiv 2\pi$. Our numerical results show that the bands of a periodic lattice of fractional kinks have more structures than a lattice of periodic integer kinks.

We have shown numerically that band structures can be controlled by changing κ. In the case of discontinuities created artificially by injectors, one can make a wiring such that the value κ for all discontinuities can be changed at the same time by using a single control current. It thus provides the possibility to change the band structure "on-the-fly". For natural 0-π long Josephson junctions (see, e.g., [5]) with a fixed the discontinuity $\kappa = \pi$, the band structure can also be smoothly controlled during experiment by an applied bias current.

Here, we only considered the spectrum of a mirror symmetric crystal. However,

unusual properties can be expected from systems with broken reflection symmetry (ratchets) [21, 22], such as crystals of ferroelectrics or of some superconductors [23]. From this point of view, the transport in such systems is not well studied. Using an array of discontinuities with different strengths and distances, one might realize controllable fractional vortex crystals without reflection symmetry and study its nonequilibrium transport. In this case, the eigenvalue problem (5.2.6) corresponds to the motion of a continuous plane wave in a ratchet potential.

Appendix: Hypergeometric functions and Lamé equation

The complete elliptic integrals of the first and second kind used in this report are defined respectively as

$$\mathbf{K}(k^2) \;=\; \int_0^{\pi/2} \frac{d\alpha}{\sqrt{1-k^2\sin^2\alpha}}\,, \qquad \mathbf{E}(k^2) \;=\; \int_0^{\pi/2} d\alpha\,\sqrt{1-k^2\sin^2\alpha}\,. \tag{A-1}$$

The parameter k, $k^2 < 1$, is called elliptic modulus. These elliptic integrals are nothing else but specific hypergeometric functions.

The complementary elliptic integral of the first kind is defined as

$$\mathbf{K}'(k^2) \;=\; \mathbf{K}(k'^2)\,, \tag{A-2}$$

with the complementary modulus $k' \;=\; \sqrt{1-k^2}$.

The function $\mathrm{am}(u,k^2)$ which is called Jacobi's elliptic amplitude is defined through the first order differential equation

$$\left(\frac{d\,\mathrm{am}(u)}{du}\right)^2 \;=\; 1-k^2\sin^2\left[\mathrm{am}(u)\right]\,. \tag{A-3}$$

It has the following quasi-periodic property in u:

$$\mathrm{am}\left(u+2n\mathbf{K}+2i\mathbf{K}'\right) \;=\; n\pi+\mathrm{am}(u)\,.$$

The Jacobi's elliptic function $\mathrm{sn}(u,k^2)$ is defined through the equation

$$\left(\frac{d\,\mathrm{sn}u}{du}\right)^2 \;=\; \left(1-\mathrm{sn}^2u\right)\left(1-k^2\mathrm{sn}^2u\right)\,, \tag{A-4}$$

and is related to the amplitude by $\mathrm{sn}\,u = \sin(\mathrm{am}\,u)$. Its periodic property is given by

$$\mathrm{sn}\left(u+4n\mathbf{K}+2i\mathbf{K}'\right) \;=\; \mathrm{sn}(u)\,.$$

The second order differential equation, which is known as the Nth Lamé equation, is given by

$$\left\{\frac{d^2}{du^2}-E-N(N+1)\mathcal{P}(u)\right\}f(u) \;=\; 0\,, \tag{A-5}$$

with E is a real quantity, N is a positive integer and $\mathcal{P}(u)$ denotes the Weierstrass function. The function $\mathcal{P}(u)$ is a periodic solution of the first order equation (see [24])

$$\left(\frac{d\mathcal{P}}{du}\right)^2 = 4\,(\mathcal{P}-e_1)\,(\mathcal{P}-e_2)\,(\mathcal{P}-e_3)\ , \tag{A-6}$$

with e_1, e_2, e_3 are the characteristic roots that uniquely determine ω and ω':

$$\mathcal{P}\,(u+2n\omega+2m\omega') = \mathcal{P}(u)\ .$$

The stability equation (5.3.4) can be identified with eq. (A-5) with $N=1$, $u=\bar{x}+i\mathbf{K}'$, and $E=\frac{2-k^2}{3}-k^2\omega^2$ in virtue of the relation between $\mathcal{P}(u)$ and the Jacobi elliptic function $\mathrm{sn}(u,k)$ (see formulas 8.151 and 8.169 of [24]):

$$k^2\mathrm{sn}^2(\bar{x},k) = \mathcal{P}(\bar{x}+i\mathbf{K}')+\frac{k^2+1}{3}\ . \tag{A-7}$$

Relation (A-7) holds if the characteristic roots of $\mathcal{P}(u)$ are expressed in terms of k^2 as

$$e_1 = \frac{2-k^2}{3}\ ,\qquad e_2 = \frac{2k^2-1}{3}\ ,\qquad e_3 = -\frac{1+k^2}{3}\ , \tag{A-8}$$

and the real and imaginary half periods of $\mathcal{P}(u)$ are then given by the elliptic integrals of the first kind

$$\omega = \mathbf{K}(k)\ ,\qquad \omega' = i\mathbf{K}'(k)\ . \tag{A-9}$$

The stability equation (5.3.15) can be identified similarly as above only now with $u=x+i\mathbf{K}'$ and $E=\frac{2-k^2}{3}-\omega^2$.

When $N=1$, the two linearly independent solutions of (A-5) are given by (see, e.g., [24, 25, 26, 27])

$$f_{\pm\eta}(u) = \frac{\sigma(u\pm\eta)}{\sigma(u)}\,e^{\mp u\,\zeta(\eta)}\ , \tag{A-10}$$

where η is an auxiliary parameter defined through $\mathcal{P}(\eta)=E$, and $\sigma(u)$ and $\zeta(u)$ are other Weierstrass functions which are defined as

$$\frac{d\,\zeta(u)}{du} = -\mathcal{P}(u)\ ,\qquad \frac{d\,\log\sigma(u)}{du} = \zeta(u)\ , \tag{A-11}$$

with the properties

$$\begin{aligned}\zeta(u+2\mathbf{K}) &= \zeta(u)+2\zeta(\mathbf{K})\ ,\\ \sigma(u+2\mathbf{K}) &= -e^{2(u+\mathbf{K})\zeta(\mathbf{K})}\sigma(u)\ .\end{aligned} \tag{A-12}$$

As a consequence of Eq. (A-12), we can obtain the Floquet exponent of $f_{\pm\eta}(u)$ which is defined as

$$f(u+2\mathbf{K}) = f(u)e^{iF(\eta)}\ , \tag{A-13}$$

with

$$F(\pm\eta) = \pm 2i\,[\mathbf{K}\,\zeta(\eta)-\eta\,\zeta(\mathbf{K})]\ . \tag{A-14}$$

Bibliography

[1] Yu. S. Kivshar and B. A. Malomed, *Dynamics of solitons in nearly integrable systems*, Rev. Mod. Phys. **61**, 763 (1989); *ibid.* **63**, 211 (Addendum) (1991).

[2] B. D. Josephson, *Possible new effects in superconductive tunnelling*, Phys. Letts. **62**, 251 (1962).

[3] L. N. Bulaevskii, V. V. Kuzii, and A. A. Sobyanin, *Superconducting system with weak coupling to the current in the ground state*, JETP Lett. **25**, 290 (1977); L.N. Bulaevskii, V.V. Kuzii, A. A. Sobyanin, and P.N. Lebedev, *On possibility of the spontaneous magnetic flux in a Josephson junction containing magnetic impurities*, Solid State Comm. **25**, 1053 (1978).

[4] C. C. Tsuei and J. R. Kirtley, *Pairing symmetry in cuprate superconductors*, Rev. Mod. Phys. **72**, 969 (2000).

[5] H. Hilgenkamp, Ariando, H. J. H. Smilde, D. H. A. Blank, G. Rijnders, H. Rogalla, J. R. Kirtley, and C. C. Tsuei, *Ordering and manipulation of the magnetic moments in large-scale superconducting π-loop arrays*, Nature (London) **422**, 50 (2003).

[6] V. V. Ryazanov, V. A. Oboznov, A. Yu. Rusanov, A. V. Veretennikov, A. A. Golubov, and J. Aarts, *Coupling of two superconductors through a ferromagnet: Evidence for a π junction*, Phys. Rev Lett. **86**, 2427 (2001).

[7] J. J. A. Baselmans, A. F. Morpurgo, B. J. van Wees, and T. M. Klapwijk, *Reversing the direction of the supercurrent in a controllable Josephson junction*, Nature **397** 43 (1999).

[8] E. Goldobin, A. Sterck, T. Gaber, D. Koelle, and R. Kleiner, *Dynamics of semi-fluxons in Nb long Josephson 0-π junctions*, Phys. Rev. Lett. **92**, 057005 (2004).

[9] C. Kittel, *Introduction to Solid State Physics*, 7th ed. (Wiley, New York, 1996).

[10] N. W. Ashcroft and N. D. Mermin, *Solid State Physics*, (Saunders College, Philadelphia, 1976).

[11] C. Giacovazzo, H.L. Monaco, G. Artioli, D. Viterbo, G. Ferraris, G. Gilli, G. Zanotti, and M. Catti, *Fundamentals of Crystallography*, Vol. 2 of International Union of Crystallography Texts on Crystallography, 2nd ed. (Oxford University Press, Oxford, 2002).

[12] A. Ustinov, *Fluxon insertion into annnular Josephson junction*, Appl. Phys. Letts. **80**, 3153 (2002).

[13] B. A. Malomed and A. Ustinov, *Creation of classical and quantum fluxons by a current dipole in a long Josephson junction*, Phys. Rev. B. **69**, 69502 (2004).

[14] J. M. Thijssen, *Computational Physics*, (Cambridge University Press, Cambridge, 1999).

[15] G. Mussardo, V. Riva, G. Sotkov, and G. Delfino, *Kink scaling functions in 2D non–integrable quantum field theories*, hep-th/0510102.

[16] G. Mussardo, V. Riva and G. Sotkov, *Semiclassical scaling functions of sine-Gordon model*, Nucl. Phys. B **699**, 545 (2004).

[17] A. V. Ustinov, *Solitons in Josephson junctions*, Physica D **123**, 315 (1998) and references therein.

[18] E. Goldobin, D. Koelle, and R. Kleiner, *Ground states of one and two fractional vortices in long Josephson 0-π kappa junctions*, Phys. Rev. B **70**, 174519 (2004).

[19] E. Goldobin, D. Koelle, and R. Kleiner, *Ground states and bias-current-induced rearrangement of semifluxons in 0-π long Josephson junctions*, Phys. Rev. B **67**, 224515 (2003).

[20] A. Zenchuk and E. Goldobin, *Analysis of ground states of 0-π long Josephson junctions*, Phys. Rev. B **69**, 024515 (2004).

[21] H. Linke, *Ratchets and Brownian motors: Basics, experiments and applications*, Appl. Phys. A **75**, 167 (2002).

[22] P. Reimann, *Brownian motors: noisy transport far from equilibrium*, Phys. Rep. **361**, 57 (2002).

[23] L. Bulaevskii, A. A. Guseinov, and A. I. Rusinov, *Superconductivity in crystals without symmetry centers*, Zh. Eksp. Teor. Fiz. **71**, 2356 (1976) [Sov. Phys. JETP **44**, 1243 (1976)].

[24] I. S. Gradshteyn and I. M. Ryzhik, *Table of integrals, series, and products*, (Academic Press, New York, 1980).

[25] E. T. Whittaker and G. N. Watson, *A course of modern analysis*, (Cambridge University Press, Cambridge, 1927).

[26] P. F. Byrd and M. D. Friedman, *Handbook of Elliptic Integrals*, 2nd ed. (Springer, Berlin, 1971).

[27] H. Hancock, *Lectures on the theory of elliptic functions*, (Dover, New York, 1958).

Summary

In this thesis, the stability of fractional Josephson vortices in Josephson junctions with phase shifts is investigated analytically and numerically. A Josephson junction which is made of two superconductors separated by a thin insulator can have phase shifts in its phase difference due to, e.g., the unconventional symmetry of the superconductors or a pair of current-injectors. In such a system, a magnetic field can be spontaneously generated at the discontinuity points that characterize the position of the phase shifts.

The phase difference of a Josephson junction is described by a sine-Gordon equation. Phase shifts make the equation nonautonomous. Because the nonautonomicity takes a special form, the existence of spontaneously generated fractional fluxons can be analyzed and studied simply using phase plane analysis.

Using this very basic procedure, some important questions, such as the presence of critical bias current above which a voltage is created across the junction, and the presence of a minimum distance between two consecutive phase shifts needed for fractional fluxons, already can be answered. It is also shown that there exists some solutions representing fractional fluxons which are proven to be unstable.

An array of short Josephson junctions with a phase shift of π is also discussed. In this array, a lattice π-kink can be generated spontaneously. The unstable solutions representing fractional fluxons found in the long junction might have a stable corresponding solution in the short junction arrays. It is because a long Josephson junction can be seen as a continuous limit of short junction arrays. Yet, it is shown that they are still unstable even in the weak coupling limit.

In this thesis, the so-called tricrystal junctions that have promising applications, e.g., as logic device based on the Josephson effect for high-performance computers are also studied. An infinite long 0-π Josephson junction can be considered as a combination of two semi-infinite 0- and π-junctions. A tricrystal junction is then a combination of three semi-infinite long Josephson junctions having one common point. In a tricrystal junction system, a fluxon coming toward the common point can be trapped. Combinations of the Josephson characteristic lengths of the individual junctions that support trapped fluxons are analyzed. If one of the junctions is a π-junction, it is shown that a semifluxon is stable for any combination of the Josephson characteristics and it is analyzed whether the system supports a multiple-semifluxons state. The minimum number of Josephson junctions forming a multicrystal junction that supports a multiple-semifluxons state is also discussed.

The last part of the thesis deals with a Josephson junction system with phase shifts of κ, with κ is not necessarily π. This system is not as trivial as it might look especially because a fractional kink can have different topological charge from the corresponding fractional antikink. A Josephson junction with one single phase shift and with periodical phase shifts is studied. The stability of fractional kinks supported by the system

is analyzed in both cases. We claim that the knowledge of the band-gap structures for periodic phase shifts is of importance also from an application point of view.

Samenvatting

In dit proefschrift zal de stabiliteit van fractionele Josephson vortices in Josephson juncties met fase verschuivingen zowel analytisch als numeriek onderzocht worden. Een Josephson junctie gemaakt uit twee supergeleiders en gescheiden door een dunne isolator laag kan verschuivingen in zijn fase-verschil hebben vanwege, bijvoorbeeld, de onconventionele symmetrie van de supergeleiders of door een paar stroominjectors. In zo'n systeem kan een magnetisch veld spontaan gegenereerd worden bij de discontinuiteits punten die de positie van de fase verschuivingen karakteriseren.

Het fase verschil van een Josephson junctie word beschreven door een sine-Gordon vergelijking. Fase verschuivingen leiden ertoe dat de vergelijking niet-autonoom is. Vanwege de speciale vorm van de niet-autonomiciteit, kan de existentie van spontaan gegenereerde fractionele fluxons derondanks geanalyseerd en bestudeerd worden door gebruik te maken van fase vlak analyse.

Gebruikmakend van deze basis procedure, kunnen sommige belangrijke vragen, zoals de aanwezigheid van een kritische bias-stroom boven welke een voltage gecreeerd wordt over de junctie, en het bestaan van een minimale afstand tussen twee opeenvolgende fase verschuivingen nodig voor het genereren van fractionele fluxons, beantwoord worden. Ook zullen we bewijzen dat er instabiele oplosingen bestaan die fractionele fluxons representeren.

Een array van korte Josephson juncties met een fase verschuiving van π zal bekeken worden. In dit array kan een lattice π-kink spontaan gegenereerd worden. De instabiele oplossingen, die fractional fluxons representeren, die voorkomen in de lange junctie hebben misschien stabiele corresponderende oplossingen in de korte junctie arrays. Dit komt doordat een lange Josephson junctie gezien kan worden als een continue limiet van korte junctie arrays. Wij laten echter zien dat deze oplossingen nog steeds instabiel zijn, zelfs in de zwakke gekoppeld limiet.

In dit proefschrift worden ook zogenaamde tricrystal juncties onderzocht. Deze juncties hebben veelbelovende applicaties, bijvoorbeeld als logic device gebaseerd op het Josephson effect voor high-performance computers. Een oneindig lange 0-π Josephson junctie kan beschouwd worden als een combintie van twee semi-oneindige 0- en π-juncties. Een tricrystal junctie is dan een combinatie van drie semi-oneindige lange Josephson juncties die één gemeenschappelijk punt hebben. In een tricrystal junctie systeem zal een fluxon gevangen worden als deze in de buurt van het gemeenschappelijk punt komt. Combinaties van Josephson karakteristieke lengtes of van individuele juncties die gevangen fluxons ondersteunen worden geanalyseerd. Als één van de juncties een π-junctie is, dan zullen we laten zien dat een semifluxon stabiel is voor iedere combinatie van Josephson karakteristieken en wordt onderzocht of het systeem een meervoudig-semifluxon toestand ondersteunt. Ook wordt het minimale aantal Josephson juncties die een multicrystal junctie vormen die een meervoudig-semifluxon toestand ondersteunt behandeld.

Het laatste gedeelte van het proefschrift behandelt een Josephson junctie systeem met fase verschuivingen van κ waarbij κ niet persé gelijk is aan π. Dit systeem is niet zo triviaal als het lijkt, omdat een fractionele kink een andere topologische lading kan hebben dan de corresponderende fractionele antikink. Een Josephson junctie met één enkele fase verschuiving en met periodieke fase verschuivingen wordt bestudeerd. De stabiliteit van fractionele kinks ondersteund door het systeem wordt geanalyseerd in beide gevallen. Wij beweren dat kennis van de band-gap structuur voor periodieke fase verschuivingen belangrijk is, ook gezien vanuit de toepassing.

Acknowledgment

"No one who achieves success does so without the help of others.
The wise and confident acknowledge this help with gratitude."
-Alfred North Whitehead.

Many people have contributed in one way or another in accomplishing my study. Therefore, it is a must for me to thank and to express my gratitudes to them. Unfortunately, I will not be able to list them all here. Even though so, those who are not mentioned surely are not forgotten.

Certainly I would like to start off by thanking Stephan van Gils. He is not only my teacher and supervisor, but also a friend to whom I complain, and even share my personal problems. He let me go to any direction of research that I want. Stephan, your visit to Lumajang will always be an unforgettable moment for us!

I am indebted to Brenny van Groesen for the opportunity he gave me to work in his group. My stay in the Netherlands was started from an invitation that was arranged and set by him and Pak Edy Soewono when I was an undergraduate student at ITB.

Next I want to thank the committee members: Arjen Doelman (for his mathematical lessons on perturbation theory), Edward Goldobin (for the fruitful discussions, exchange ideas, and answering my questions on physics), Hans Hilgenkamp (for sharing informations), Bernard Geurts (for sharing experiences and advices), Sasha Golubov, and Niels Pedersen (for their willingness to be committee members).

Discussions with my co-workers are also appreciated. In this regard, those who have not been mentioned before are Gianne Derks, Panos Kevrekidis, Magnus Johansson, and Pak Darminto.

Further, I would like to thank colleagues and ex-colleagues at the Applied Mathematics, in particular Manfred, Frits, Timco (ex-senior who introduced Josephson stuffs to me in the beginning), Barbera, Natan (no more copying your homeworks, I think ☺), Sena, Helena, Kiran, Debby, Jaqueline, Davit, Vita, Pak Agus Suryanto, Arnold, Sander (who translated the summary in Dutch), Johan Simonetti, Marielle Plekenpol, and Diana Dalenoord.

Not to forget, I also want to thank Luuk Hoevenaars for the LaTeXof his thesis, and Pak Trias for the cover design and Mbak Diana for the hospitality.

A thankful greeting goes to the *Enschedese hujjaj*, all members of the Islamic Society of the University of Twente (ISUT), Indonesian Muslim in Enschede Association (IMEA), and Perhimpunan Pelajar Indonesia di Enschede (PPI-E) for making a warm Enschede.

Special thanks go to Pak Tris Probolinggo, Paklik Abas Karno, Pakpuh Sabil, and all *paklik*s and *bulik*s in the family of our grandfathers Mbah Chusnun Suhud and Mbah Karnawi Kebonan for their mental and spiritual supports.

Finally all the words go to Ibu and Bapak Moch. Chozin and my younger brother Iwan Sakhroni for all their constant and intense love and prayers.